Dominik Sulzner, BSc

Inverse Source Reconstruction for the Helmholtz Equation

MASTER'S THESIS

to achieve the university degree of
Diplom-Ingenieur

Master's degree programme:
Mathematics

submitted to

Graz University of Technology

Supervisor

Univ.-Prof. Dipl.-Math. Dr.rer.nat. Olaf Steinbach

Institute of Applied Mathematics

Co-Supervisor

Dipl.-Ing. Dr.techn. Richard Löscher, BSc

Institute of Applied Mathematics

Graz, February 2026

Acknowledgement

First, I would like to thank my supervisor, Univ.-Prof. Dipl.-Math. Dr.rer.nat. Olaf Steinbach, for his valuable input and support. I am also grateful to Dipl.-Ing. Dr.techn. BSc Richard Löscher for his guidance throughout the work on this thesis. His feedback and the many helpful discussions during the development of the thesis were greatly appreciated.
Moreover, I would like to express my sincere gratitude to my family for their continuous support and encouragement. Without you, completing these studies would not have been possible. My sister Natalie deserves special thanks for always having an open ear and for believing in me. I am also deeply grateful to my parents for their unwavering guidance, constant moral support, and ongoing motivation. My partner Therese has shown remarkable patience, understanding, and empathy throughout this thesis, for which I am truly thankful. Finally, my sincere thanks go to my friend Peter for his valuable help with the formatting.
In addition, I acknowledge the use of ChatGPT [23] for assisting with language refinement and grammatical improvements during the writing process.

Abstract

Inverse problems for partial differential equations, especially the Helmholtz equation, arise in a variety of practical applications such as computed tomography, electrical impedance tomography and magnetometric methods in geophysics. In this thesis, we study the inverse problem of reconstructing the source of the Helmholtz equation from Cauchy data, at both a single wave number and multiple wave numbers, in a bounded domain with Lipschitz boundary. The main objective is to establish uniqueness of the reconstruction. The source can be determined uniquely from boundary data at a single wave number if suitable a priori information about the source term is available. By introducing operators mapping the source onto the Neumann datum and the Dirichlet datum, respectively, we derive uniqueness results for sources in subspaces of $L^2(\Omega)$. In contrast, if the boundary data are known for multiple wave numbers, uniqueness is guaranteed in the L^2–sense without any a priori information. Numerical methods as well as numerical examples are provided for both, the reconstruction from boundary data at a single wave number and at multiple wave numbers.

Kurzfassung

Inverse Probleme für partielle Differentialgleichungen, insbesondere für die Helmholtz–Gleichung, sind in zahlreichen praxisrelevanten Anwendungen von Bedeutung, etwa in der Computertomographie, der elektrischen Impedanztomographie und bei magnetometrischen Messverfahren in der Geophysik. In dieser Arbeit wird das inverse Problem der Helmholtz–Gleichung zur Rekonstruktion der Quelle ausgehend von Cauchy–Daten, sowohl für eine Wellenzahl als auch für mehrere Wellenzahlen, in einem beschränkten Gebiet mit Lipschitz–Rand untersucht. Der Fokus liegt darauf, die Eindeutigkeit der Rekonstruktion zu zeigen. Die Quelle kann aus den Randdaten zu einer Wellenzahl eindeutig bestimmt werden, wenn geeignete a priori Informationen über den Quellterm bekannt sind. Durch die Definition zweier Operatoren, welche den Quellterm jeweils auf das Neumann Datum bzw. das Dirichlet Datum abbilden, werden Eindeutigkeitsresultate für Quellen in Teilräumen von $L^2(\Omega)$ bewiesen. Falls die Randdaten allerdings für mehrere Wellenzahlen bekannt sind, ist die Eindeutigkeit

der Rekonstruktion im L^2–Sinne ohne jegliche a priori Informationen gegeben. Numerische Methoden sowie numerische Beispiele werden sowohl für die Rekonstruktion aus Cauchy–Daten zu einer Wellenzahl als auch zu mehreren Wellenzahlen präsentiert.

Contents

Introduction **9**

1 Preliminaries **13**
1.1 Hilbert spaces 13
1.2 Abstract operator theory 15
1.3 Sobolev spaces on Lipschitz domains and some properties 15
1.4 Auxiliary Definitions and Results 20

2 The Helmholtz equation **21**
2.1 Dirichlet boundary value problem 21
2.2 Neumann boundary value problem 24
2.3 A Bi–Helmholtz–type equation 27

3 Source reconstruction from Cauchy data for the Helmholtz equation **31**
3.1 Uniqueness from boundary measurements at a single wave number . . . 32
3.1.1 Uniqueness results for different types of sources 33
3.1.2 Operator mapping the source onto the Neumann trace 40
3.1.3 Operator mapping the source onto the Dirichlet trace 46
3.1.4 Method via a Bi–Helmholtz–type equation 50
3.2 Uniqueness from boundary data at several wave numbers 51

4 Numerical illustration **53**
4.1 Numerical method for the reconstruction at a single wave number . . . 53
4.2 Numerical method for the reconstruction at several wave numbers . . . 67

5 Conclusions and outlook **93**

Bibliography **95**

Introduction

In practical applications the reconstruction of sources from boundary data measurements for partial differential equations is of interest. It is an essential tool in several scientific and engineering fields because one can often measure the boundary data and wants to derive the source term. The task to reconstruct the source from boundary data measurements leads to a classical inverse problem. Some fields, where this is of importance, are medicine and geophysics [8, 17]. In [17] Isakov presents a good overview of applications of inverse problems. For example, in medicine source reconstruction from boundary data measurements is used for medical imaging. Modern medical applications, where source reconstruction is needed, are computed tomography and electrical impedance tomography. In computed tomography x-ray measurements are given and the goal is to derive the density inside the human body. The aim in electrical impedance tomography is to reconstruct the conductivity and permittivity distribution of the body. A time harmonic voltage distribution is applied and the current distribution is measured via electrodes at the surface. Therefore, the boundary data are given [17]. An application in geophysics is the geophysical exploration. Here one wants to reconstruct underground sources such as mineral deposits or oil reservoirs from boundary data measurements on the surface of the earth [20]. More details regarding applications can be found in [8, 17].
One specific inverse problem, which is of interest, is the source reconstruction from boundary data measurements for the Helmholtz equation. As the Helmholtz equation describes the propagation of waves, such as acoustic or electromagnetic waves, the inverse problem of it is commonly used in areas where wave interference and deflection are studied [8]. The mentioned applications above are specific examples for the source reconstruction from boundary data measurements for the inverse problem of the Helmholtz equation.
Existing literature has addressed the reconstruction of sources of the inverse problem of the Helmholtz equation. In [8] Colton and Kress focus on inverse scattering problems, where the Cauchy data are given by far field measurements. Their work gives an overview of fundamental tools and different methods for solving such inverse problems. A difficulty which arises when dealing with inverse problems is, that in general it is not possible to reconstruct the source of an inverse problem only from Cauchy data [3]. El Badia and Ha Duong investigate in [9] the standard inverse problem with the Poisson equation, which is commonly used in the literature. They prove that a source in L^2 can be reconstructed from the boundary data. However, only the harmonic part of the source can be reconstructed uniquely. Furthermore, they show if one knows a priori,

that the source can be represented as a product of two functions, where one is known, then the source can be determined completely. In cases, where a priori information is available, there are more contributions in the literature. Isakov considers in [17] the Poisson equation in $\mathbb{R}^3$ with a characteristic function as source. He demonstrates that the inverse problem is uniquely solvable if the support of the right hand side is either star shaped or convex in one direction. It is shown in [10] that the inverse problem for a diffusion equation admits a unique solution if the source is a linear combination of point or dipolar sources. This is motivated by the practical application of detecting electrostatic dipoles in the human head. Moreover, this work states that a source given by a characteristic function supported on a finite union of balls with distinct centers can be uniquely reconstructed by determining the number, midpoints and radii of the balls. The class of sources, which can be reconstructed, is expanded in [2] to sources, which additionally satisfy a differential equation. El Badia and Nara investigate in [11] unique solvability of the inverse problem of the Helmholtz equation if the source is given as a linear combination of Dirac distributions supported on spheres in $\mathbb{R}^3$. A different perspective arises when the Helmholtz equation is considered, with boundary data available for multiple wave numbers. In [3] Alves et al. establish that in this setting the source can be determined uniquely in the L^2–sense. If no a priori information is known at all, Porter and Devaney demonstrate in [24], that the inverse problem of the Helmholtz equation is still uniquely solvable, if the solution minimises the source energy and satisfies additionally a corresponding integral equation.
Furthermore, various numerical methods are presented in the literature. Alves et al. apply a method depending on the reciprocity gap functional in [3]. El Badia and Nara are interested in reconstructing linear combinations of point sources in [11]. Therefore, an algebraic approach is derived in order to determine the number, locations and intensities of the point sources. A method based on fundamental solutions is employed in [2] to solve inverse problems numerically.
This thesis is organised as follows. In Section 1 we recall several fundamental concepts from functional analysis, Sobolev space theory and Fourier analysis. These tools provide the necessary framework for establishing uniqueness of the source reconstruction. Afterwards, the unique solvability of the Dirichlet and Neumann boundary value problem for the Helmholtz equation and the boundary value problem for a Bi–Helmholtz–type equation are considered in Section 2. In Section 3 we show that the reconstruction of the source from a single pair of Cauchy data is in general not possible. Hence, we discuss the unique solvability of the inverse problem from boundary data at a single wave number for sources, where suitable a priori information is known. More precisely, we consider point sources, Dirac distributions supported on spheres and characteristic functions on hollow or solid balls. This is done in Section 3.1.1. Then we analyse uniqueness of the source reconstruction using a splitting of the problem and introducing an operator, that maps the source onto the Neumann trace. We will compute the kernel and the range of this operator to derive a result for a unique source reconstruction in a subspace of $L^2(\Omega)$ in Section 3.1.2. This will be followed by

an analogous approach, where we introduce an operator, mapping the source onto the Dirichlet trace in Section 3.1.3. Both approaches lead to a restriction on the boundary data, where either the Dirichlet datum or the Neumann datum has to vanish. In Section 3.1.4 we overcome this obstacle by using a Bi–Helmholtz–type equation. In contrast to the case of a single wave number, we receive unique solvability of the inverse problem in the L^2–sense without any a priori information provided that the boundary data are known for multiple wave numbers in Section 3.2. To illustrate the theoretical results from Section 3 we discuss numerical methods in Section 4. We start with an algebraic method to reconstruct point sources in Section 4.1. Finally, the reconstruction of sources $z \in L^2(\Omega)$ from boundary data at multiple wave numbers is investigated in Section 4.2. Both numerical methods are complemented by numerical examples.

1 Preliminaries

In this section we briefly present the fundamental concepts and definitions that will be required throughout this thesis. First, we introduce Banach and Hilbert spaces, followed by the notion of Gelfand triples. Next, we give an overview of abstract operator theory, including compactness and coercivity. Afterwards, we introduce Lipschitz domains and Sobolev spaces defined over such domains and summarise some well–established results in Sobolev theory. Finally, we collect some additional tools, including results from Fourier analysis and complex analysis, that will be used throughout the thesis.

1.1 Hilbert spaces

To start with, we denote the underlying field as $\mathbb{K} \in \{\mathbb{R}, \mathbb{C}\}$. In order to define a Hilbert space, we first recall the definition of a Banach space and an inner product.

Definition 1.1 ([1, Def. 1.8])**.** A normed vector space $(X, \|\cdot\|_X)$ is called complete if every Cauchy sequence converges to a limit in X with respect to the norm $\|\cdot\|_X$. A complete normed space is called a Banach space.

Definition 1.2 ([28, Def. V.1.1])**.** Let H be a vector space over the field $\mathbb{K}$. A mapping $(\cdot,\cdot) : H \times H \to \mathbb{K}$ is called an inner product if

- $(\alpha u_1 + \beta u_2, v) = \alpha(u_1, v) + \beta(u_2, v) \quad \forall u_1, u_2, v \in H,\ \alpha, \beta \in \mathbb{K}$,
- $(u_1, u_2) = \overline{(u_2, u_1)} \quad \forall u_1, u_2 \in H$,
- $(u, u) \geq 0 \quad \forall u \in H$,
- $(u, u) = 0 \iff u = 0$.

Any inner product induces a norm by setting $\|u\|_H := \sqrt{(u, u)}$.

Definition 1.3 ([1, p.5])**.** A Banach space $(H, \|\cdot\|_H)$ with a norm induced by an inner product is called a Hilbert space.

Next, we introduce the dual space of a normed space X.

Definition 1.4 ([28, Def. II.2.1])**.** The dual space of a normed space X over the field $\mathbb{K}$ is defined as $X' := \mathcal{L}(X, \mathbb{K})$, which denotes the space of all linear and continuous

functionals on X. The norm on X' is given by

$$\|\alpha'\|_{X'} := \sup_{0 \neq u \in X} \frac{|\alpha'(u)|}{\|u\|_X}.$$

In addition, we define the duality pairing between $\alpha' \in X'$ and $u \in X$ by

$$\langle \alpha', u \rangle_{X' \times X} := \alpha'(u).$$

A well–established result for Hilbert spaces is the Theorem of Fréchet–Riesz.

Theorem 1.1 ([28, Thm. V.3.6])**.** *Let H be a Hilbert space and let H' denote its dual space. For each $\alpha' \in H'$ there exists a unique $u \in H$ such that $\alpha'(v) = (v, u)$ for all $v \in H$. Moreover, it holds that $\|\alpha'\|_{H'} = \|u\|_H$.*

In the next step, the Gelfand triple, which was originally defined in [12, Sec.4] is outlined. For our setting we take a more general definition from [28].

Definition 1.5 ([28, cf. p.468])**.** Let H be a Hilbert space and let X be a Banach space with the dual space X'. Moreover, let $X \subset H$ be a dense subspace and the embedding

$$\begin{aligned} \iota : X &\to H, \\ u &\mapsto u, \end{aligned}$$

is assumed to be continuous. Consequently, the adjoint operator $\iota' : H' \to X'$ is continuous as well. By Theorem 1.1 we can identify the Hilbert space H with its dual H', i.e., $H \simeq H'$. Altogether, the Gelfand triple is defined as

$$X \subset H \subset X'.$$

For $\alpha' \in H \subset X'$ it holds

$$\|\alpha'\|_{X'} = \sup_{0 \neq u \in X} \frac{|(\alpha', u)|}{\|u\|_X}.$$

In this framework we are able to extend the notion of eigenvalues to operators, mapping from X to X'.

Definition 1.6. A scalar $\lambda \in \mathbb{C}$ is an eigenvalue of an operator $A : X \to X'$ if and only if there exists $u \in X \setminus \{0\}$ such that $Au = \lambda \iota' \iota u$ in X'. In the variational setting this is formulated as

$$\langle Au, v \rangle_{X' \times X} = \lambda \langle \iota' \iota u, v \rangle_{X' \times X} = \lambda \langle \iota u, \iota v \rangle_{H \times H} = \lambda (u, v)_H \quad \forall v \in X.$$

1.2 Abstract operator theory

We consider the general abstract setting, where H is a Hilbert space with inner product $(\cdot,\cdot)$ and H' denotes its dual space. For ease of notation we abbreviate the duality pairing $\langle\cdot,\cdot\rangle_{H'\times H}$ by $\langle\cdot,\cdot\rangle$. We begin by defining compactness and coercivity of an operator.

Definition 1.7 ([28, p.66])**.** A linear operator $C : H \to H'$ is compact if and only if it maps bounded sets to relatively compact sets or if it maps bounded sequences in H to sequences in H', which have a convergent subsequence.

Definition 1.8 ([26, p.57])**.** An operator $A : H \to H'$ is coercive if there exists a compact operator $C : H \to H'$ such that

$$\langle (A + C)u, u\rangle \geq c_1^A \|u\|_H^2 \quad \forall u \in H.$$

This condition is called Gårdings inequality. With these two definitions we can formulate the following abstract theorem.

Theorem 1.2 ([26, Thm. 3.15])**.** *Let $A : H \to H'$ be a linear, bounded, coercive operator and let A be injective, i.e., $Au = 0$ implies $u = 0$. Then the operator equation $Au = z$ has a unique solution $u \in H$ satisfying*

$$\|u\|_H \leq c\|z\|_{H'}.$$

1.3 Sobolev spaces on Lipschitz domains and some properties

In this section we introduce the function spaces required in this thesis and state some key results regarding their properties. This section is mostly based on [26]. First, we start by defining Lipschitz hypographs and consequently Lipschitz domains. Therefore, we consider an open set $\Omega \subset \mathbb{R}^d$ with $d \in \mathbb{N}$.

Definition 1.9 ([26, p.20])**.** Let $\zeta : \mathbb{R}^{d-1} \to \mathbb{R}$ be a Lipschitz continuous function such that

$$\Omega = \{x \in \mathbb{R}^d : x_d < \zeta(\tilde{x}) \text{ for all } \tilde{x} = (x_1, x_2, ..., x_{d-1}) \in \mathbb{R}^{d-1}\}.$$

Then Ω is said to be a Lipschitz hypograph with the boundary

$$\partial\Omega = \{x \in \mathbb{R}^d : x_d = \zeta(\tilde{x}) \text{ for all } \tilde{x} = (x_1, x_2, ..., x_{d-1}) \in \mathbb{R}^{d-1}\}.$$

Definition 1.10 ([26, Def. 2.1])**.** An open set $\Omega \subset \mathbb{R}^d$ is a Lipschitz domain if its boundary $\partial\Omega$ is compact and if there exist finite families $\{W_j\}$ and $\{\Omega_j\}$ satisfying the following properties:

- The family $\{W_j\}$ is a finite open cover of $\partial\Omega$, i.e., each W_j is an open subset of $\mathbb{R}^d$ and $\partial\Omega \subseteq \bigcup_j W_j$.
- Each Ω_j can be transformed to a Lipschitz hypograph by a rigid motion, i.e., by rotations and translations.
- For all j the equality $W_j \cap \Omega = W_j \cap \Omega_j$ is satisfied.

Remark 1.1. If the boundary parametrisation satisfies $\zeta \in \mathcal{C}^{k,r}(\mathbb{R}^{d-1})$ for $k \in \mathbb{N}_0$ and $r \in (0,1]$, we call the boundary k–times Hölder continuous. For the precise definition of $\mathcal{C}^{k,r}(\mathbb{R}^{d-1})$ see, e.g. [26, p.20].

For the notation of partial derivatives we use a multiindex $\alpha = (\alpha_1, ..., \alpha_d) \in \mathbb{N}_0^d$ of order $|\alpha| := \alpha_1 + ... + \alpha_d$. For a sufficiently smooth and real valued function u we denote the partial derivative as

$$D^\alpha u = (\partial_{x_1})^{\alpha_1} \cdots (\partial_{x_d})^{\alpha_d} u.$$

Moreover, $\mathcal{C}(\Omega)$ denotes the space of all continuous functions $u : \Omega \to \mathbb{R}$ and we define the spaces

$$\mathcal{C}^\infty(\Omega) := \{u \in \mathcal{C}(\Omega) : D^\alpha u \in \mathcal{C}(\Omega) \text{ for every } \alpha \in \mathbb{N}_0^d\},$$
$$\mathcal{C}_0^\infty(\Omega) := \{u \in \mathcal{C}^\infty(\Omega) : \operatorname{supp} u \subset\subset \Omega\},$$

where the support of a function is defined as $\operatorname{supp} u := \overline{\{x \in \Omega : u(x) \neq 0\}}$. Furthermore, recall that the Hilbert space $L^2(\Omega)$ is the space of all equivalence classes of measurable, square integrable functions endowed with the inner product

$$(u, v)_{L^2(\Omega)} := \int_\Omega u(x)v(x)\,\mathrm{d}x \quad \forall u, v \in L^2(\Omega).$$

The induced norm is given by

$$\|u\|_{L^2(\Omega)} = \left(\int_\Omega |u(x)|^2\,\mathrm{d}x\right)^{1/2} \quad \forall u \in L^2(\Omega).$$

To define Sobolev spaces properly, we begin by recalling the concept of weak derivatives.

Definition 1.11 ([26, p.23])**.** For

$$u \in L^1_{\mathrm{loc}}(\Omega) := \{u : \Omega \to \mathbb{R} : |u| \text{ is integrable for any compact set } K \subset\subset \Omega\},$$

the weak partial derivative $D^\alpha u \in L^1_{\mathrm{loc}}(\Omega)$ is defined by

$$\int_\Omega [D^\alpha u(x)]\varphi(x)\,\mathrm{d}x = (-1)^{|\alpha|} \int_\Omega u(x) D^\alpha \varphi(x)\,\mathrm{d}x \quad \forall \varphi \in \mathcal{C}_0^\infty(\Omega).$$

For $k \in \mathbb{N}$ we consider the norm

$$\|u\|_{H^k(\Omega)} := \left(\sum_{|\alpha| \leq k} \|D^\alpha u\|^2_{L^2(\Omega)} \right)^{1/2}.$$

The closure of $\mathcal{C}^\infty(\Omega)$ and $\mathcal{C}_0^\infty(\Omega)$, with respect to the norm $\|\cdot\|_{H^k(\Omega)}$, lead to the following Sobolev spaces.

Definition 1.12 ([26, p.24])**.** Let $k \in \mathbb{N}$ and $\Omega \subset \mathbb{R}^d$ be a Lipschitz domain. The Sobolev spaces are defined by

$$H^k(\Omega) := \overline{\mathcal{C}^\infty(\Omega)}^{\|\cdot\|_{H^k(\Omega)}} \quad \text{and} \quad H_0^k(\Omega) := \overline{\mathcal{C}_0^\infty(\Omega)}^{\|\cdot\|_{H^k(\Omega)}}.$$

This can be extended for any arbitrary $0 < s \in \mathbb{R} \setminus \mathbb{N}$. We can write $s = k + \kappa$, where $k \in \mathbb{N}_0$ and $\kappa \in (0, 1)$. Then the Sobolev–Slobodeckii norm is defined as

$$\|u\|_{H^s(\Omega)} := \left(\|u\|^2_{H^k(\Omega)} + |u|^2_{H^s(\Omega)} \right)^{1/2},$$

where

$$|u|^2_{H^s(\Omega)} := \sum_{|\alpha|=k} \int_\Omega \int_\Omega \frac{|D^\alpha u(x) - D^\alpha u(y)|^2}{|x-y|^{d+2\kappa}} \, \mathrm{d}x \, \mathrm{d}y.$$

Therefore, for arbitrary $s \in \mathbb{R}^+$ the Sobolev spaces are again given by

$$H^s(\Omega) := \overline{\mathcal{C}^\infty(\Omega)}^{\|\cdot\|_{H^s(\Omega)}} \quad \text{and} \quad H_0^s(\Omega) := \overline{\mathcal{C}_0^\infty(\Omega)}^{\|\cdot\|_{H^s(\Omega)}}.$$

It holds that $H^s(\Omega)$ is a Hilbert space. For $s > 0$ the space $H^{-s}(\Omega)$ is defined as the dual space of $H_0^s(\Omega)$ with the corresponding dual norm

$$\|f\|_{H^{-s}(\Omega)} := \sup_{0 \neq u \in H_0^s(\Omega)} \frac{\langle f, u \rangle_\Omega}{\|u\|_{H^s(\Omega)}}.$$

Another space that will be used often consists of elements in $H^1(\Omega)$ solving the homogeneous Helmholtz equation. This space is denoted as

$$\mathcal{H}^1_{\Delta+\kappa^2}(\Omega) := \{u \in H^1(\Omega) : \Delta u + \kappa^2 u = 0 \text{ in } L^2(\Omega)\}. \tag{1.1}$$

In the remaining part of this section we state some properties for Sobolev spaces, which will be applied later in the analysis of this thesis. We begin with the Poincaré inequality.

Theorem 1.3 ([21, Thm. A.6])**.** *Let $\Omega \subset \mathbb{R}^d$ be a bounded domain. Then there exists a constant $c_p = c_p(\Omega)$ such that*

$$\|u\|_{L^2(\Omega)} \leq c_p \|\nabla u\|_{L^2(\Omega)} \quad \forall u \in H_0^1(\Omega).$$

Remark 1.2 ([21, p.238]). As a consequence, the norms $\|\cdot\|_{H^1(\Omega)}$ and $\|\nabla(\cdot)\|_{L^2(\Omega)}$ are equivalent on $H_0^1(\Omega)$.

In the next step we recall some trace theorems.

Theorem 1.4 ([26, cf. Thm. 2.21])**.** *Let $\Omega \subset \mathbb{R}^d$ be a Lipschitz domain. Then for $s \in (1/2, 3/2)$ the trace operator $\widetilde{\gamma}_0 : H^s(\Omega) \to H^{s-1/2}(\partial\Omega)$ is bounded satisfying*

$$\|\widetilde{\gamma}_0 u\|_{H^{s-1/2}(\partial\Omega)} \leq c_T \|u\|_{H^s(\Omega)} \quad \forall u \in H^s(\Omega).$$

Theorem 1.5 ([26, cf. Thm. 2.22])**.** *Let $\Omega \subset \mathbb{R}^d$ be a Lipschitz domain. Then for $s \in (1/2, 3/2)$ the trace operator $\widetilde{\gamma}_0 : H^s(\Omega) \to H^{s-1/2}(\partial\Omega)$ has a continuous right inverse operator*

$$\mathcal{E} : H^{s-1/2}(\partial\Omega) \to H^s(\Omega),$$

satisfying $\widetilde{\gamma}_0 \mathcal{E} w = w$ for all $w \in H^{s-1/2}(\partial\Omega)$. Furthermore, the operator is bounded with

$$\|\mathcal{E} w\|_{H^s(\Omega)} \leq c_{IT} \|w\|_{H^{s-1/2}(\partial\Omega)} \quad \forall w \in H^{s-1/2}(\partial\Omega).$$

For boundary value problems with given Dirichlet and Neumann data, we will use the following theorem.

Theorem 1.6 ([14, cf. Thm. 1.5.1.2])**.** *Let $\Omega \subset \mathbb{R}^d$ be a bounded domain with a $\mathcal{C}^{1,1}$–boundary $\partial\Omega$ and let γ denote the operator defined by $\gamma u = u|_{\partial\Omega}$ for $u \in \mathcal{C}^\infty(\overline{\Omega})$. Furthermore, $\underline{n}$ is the outward pointing normal vector with respect to Ω. Then the mapping*

$$u \mapsto \left\{ \gamma u, \gamma \frac{\partial u}{\partial \underline{n}} \right\},$$

which is defined for $u \in \mathcal{C}^\infty(\overline{\Omega})$ has a unique continuous extension as an operator from

$$H^2(\Omega) \to H^{3/2}(\partial\Omega) \times H^{1/2}(\partial\Omega).$$

In addition, this operator has a right continuous inverse.

Remark 1.3 ([14, Thm. 1.5.2.1]). The unique continuous extension of the operator in Theorem 1.6 holds for bounded domains $\Omega \subset \mathbb{R}^2$ with polygonal boundary as well.

If we assume additional regularity of the Laplacian we can extend the trace operators to the endpoints $s = 1/2$ and $s = 3/2$. Therefore, the space

$$H^s_\Delta(\Omega) := \{u \in H^s(\Omega) : \Delta u \in L^2(\Omega)\}, \quad \mathrm{s} \geq 0,$$

has to be introduced.

Lemma 1.7 ([5, Cor. 3.7])**.** *Suppose $\Omega \subset \mathbb{R}^d$ is a bounded Lipschitz domain. The restriction of $\widetilde{\gamma_0}$ to the space $H^s_\Delta(\Omega)$ induces a well–defined, linear and continuous operator*

$$\gamma_0 : H^s_\Delta(\Omega) \to H^{s-1/2}(\partial\Omega) \qquad \forall s \in \left[\frac{1}{2}, \frac{3}{2}\right],$$

and it holds that

$$\ker(\gamma_0) \subseteq H^{3/2}(\Omega).$$

Lemma 1.8 ([5, Cor. 5.7])**.** *Let Ω be a bounded Lipschitz domain and let $\underline{n}$ denote the outward pointing normal vector. The Neumann trace map defined as $u \mapsto \frac{\partial u}{\partial \underline{n}}|_{\partial\Omega}$ for $u \in C^\infty(\overline{\Omega})$ can be uniquely extended to a linear and continuous operator*

$$\gamma_1 : H^s_\Delta(\Omega) \to H^{s-3/2}(\partial\Omega) \qquad \forall s \in \left[\frac{1}{2}, \frac{3}{2}\right],$$

and it holds that

$$\ker(\gamma_1) \subseteq H^{3/2}(\Omega).$$

Furthermore, we introduce the space

$$H^2_0(\Omega) := \{u \in H^2(\Omega) : \gamma_0 u = 0, \gamma_1 u = 0 \text{ on } \partial\Omega\}, \tag{1.2}$$

which will be equipped with the norm $\|\Delta(\cdot)\|_{L^2(\Omega)}$.

Remark 1.4. The norm $\|\Delta(\cdot)\|_{L^2(\Omega)}$ is an equivalent norm on $H^2_0(\Omega)$ since it holds that

$$\|u\|^2_{H^2(\Omega)} = \|u\|^2_{L^2(\Omega)} + \|\nabla u\|^2_{L^2(\Omega)} + \|\Delta u\|^2_{L^2(\Omega)} \leq (c_p^2 + c_p + 1)\|\Delta u\|^2_{L^2(\Omega)},$$

where c_p is the Poincaré constant from Theorem 1.3.

In the next theorem we recall the Rellich–Kondrachov theorem for the space $H^s(\Omega)$.

Theorem 1.9 ([1, cf. Thm. 6.2])**.** *Let $\Omega \subset \mathbb{R}^d$ be a bounded Lipschitz domain. For integers $s \geq 1$ and $\tilde{s} \geq 0$ with $s > \tilde{s}$, the embedding*

$$H^s(\Omega) \hookrightarrow H^{\tilde{s}}(\Omega),$$

is compact.

We will employ this theorem for $\tilde{s} = 0$ and obtain that the embeddings

$$H^2(\Omega) \hookrightarrow L^2(\Omega) \quad \text{and} \quad H^1(\Omega) \hookrightarrow L^2(\Omega),$$

are compact.

1.4 Auxiliary Definitions and Results

In this section we gather some auxiliary tools as well as some properties. First of all we define the Fourier transform.

Definition 1.13 (cf. [25, IX.1])**.** Let $f \in L^2(\mathbb{R}^d)$ and $\xi \in \mathbb{R}^d$. The Fourier transform of f in ξ is defined as

$$(\mathcal{F}f)(\xi) = \hat{f}(\xi) = \frac{1}{(2\pi)^{d/2}} \int_{\mathbb{R}^d} f(x) e^{-ix\cdot\xi} \, \mathrm{d}x.$$

Moreover, there holds the Plancherel formula

$$\|\mathcal{F}f\|_{L^2(\mathbb{R}^d)} = \|f\|_{L^2(\mathbb{R}^d)}. \tag{1.3}$$

The subsequent lemma is an important property of the Fourier transform.

Lemma 1.10 ([25, Thm. IX.12])**.** *The Fourier transform of a compactly supported function $f \in L^2(\mathbb{R}^d)$ is analytic.*

In addition, we formulate a theorem from complex analysis, which is called identity theorem.

Lemma 1.11 ([4, Cor. 6.10])**.** *Let f and g be two analytic functions defined on a domain $U \neq \emptyset$. If the set $\{x \in U : f(x) = g(x)\}$ has an accumulation point in U, then $f = g$ on U.*

Finally, Holmgren's theorem, which is a unique continuation result, is stated.

Theorem 1.12 ([16, Thm. 5.3.1])**.** *Let $P = \sum_{|\alpha|\leq m} a_\alpha(x) D^\alpha$ be a linear differential operator of order m with real analytic coefficients a_α defined on an open set $\Omega \subset \mathbb{R}^d$. Moreover, let $\varphi \in \mathcal{C}^1(\Omega)$ be a real valued function and $x_0 \in \Omega$ such that*

$$p_m(x_0, \nabla\varphi(x_0)) \neq 0,$$

where $p_m(x,\xi) := \sum_{|\alpha|=m} a_\alpha(x)\xi^\alpha$ is the principal symbol of P. Then there exists a neighbourhood $\Omega' \subset \Omega$ of the point x_0 such that any distribution u satisfying

- *$Pu = 0$ in Ω,*
- *$u = 0$ for all $x \in \Omega$ with $\varphi(x) > \varphi(x_0)$,*

vanishes in Ω'.

2 The Helmholtz equation

One of the most important partial differential equations of second order is the Helmholtz equation, which describes the propagation of waves, such as acoustic or electromagnetic waves [8]. It can be derived from the scalar wave equation using a time harmonic wave with frequency ω [22]. In our framework the inhomogeneous Helmholtz equation will be given on a bounded Lipschitz domain $\Omega \subset \mathbb{R}^d$ with $d = 2, 3$, as

$$-\Delta u(x) - \kappa^2 u(x) = z(x) \quad \text{for } x \in \Omega,$$

where $\kappa \geq 0$ is the wave number and the right hand side satisfies $z \in L^2(\Omega)$. Furthermore, we consider a Bi–Helmholtz–type equation, which is given by

$$\Delta^2 u(x) - \kappa^4 u(x) = z(x) \quad \text{for } x \in \Omega.$$

In the following subsections we study the Dirichlet and Neumann boundary value problem for the Helmholtz equation as well as the boundary value problem for the Bi–Helmholtz–type equation with Dirichlet and Neumann data. Our aim is to derive unique solvability for these boundary value problems, which is crucial in order to understand the inverse problem discussed afterwards in Section 3.

2.1 Dirichlet boundary value problem

The subsequent assumptions are imposed throughout this section.

Assumptions 2.1.

(A1) The source satisfies $z \in L^2(\Omega)$.

(A2) The Dirichlet datum fulfils $g \in H^{1/2}(\partial\Omega)$.

(A3) The wave number $\kappa \geq 0$ satisfies that κ^2 is not an eigenvalue of the Dirichlet Laplacian, i.e.,

$$\begin{aligned} -\Delta u(x) &= \kappa^2 u(x) && \text{for } x \in \Omega, \\ u(x) &= 0 && \text{for } x \in \partial\Omega, \end{aligned} \tag{2.1}$$

has only the trivial solution $u = 0$.

We consider the Dirichlet boundary value problem for the Helmholtz equation, given by

$$\begin{aligned} -\Delta u(x) - \kappa^2 u(x) &= z(x) && \text{for } x \in \Omega, \\ u(x) &= g(x) && \text{for } x \in \partial\Omega. \end{aligned} \tag{2.2}$$

The following theorem establishes unique solvability of the Dirichlet boundary value problem for the Helmholtz equation.

Theorem 2.1. *Let $g \in H^{1/2}(\partial\Omega)$ and $z \in L^2(\Omega)$ be given. Under the Assumptions 2.1 there exists a unique weak solution $u \in H^1(\Omega)$ of the Dirichlet boundary value problem (2.2), satisfying*

$$\|u\|_{H^1(\Omega)} \leq c \left(\|z\|_{L^2(\Omega)} + \|g\|_{H^{1/2}(\partial\Omega)} \right).$$

Proof. We first rewrite the Dirichlet boundary value problem (2.2) as a variational formulation. To do so, we consider the Hilbert space $X = H_0^1(\Omega)$ with the equivalent norm $\|\nabla(\cdot)\|_{L^2(\Omega)}$ (cf. Remark 1.2). Furthermore, we define the manifold

$$V_g := \{v \in H^1(\Omega) : \widetilde{\gamma}_0 v = g \text{ on } \partial\Omega\},$$

where $\widetilde{\gamma}_0 : H^1(\Omega) \to H^{1/2}(\partial\Omega)$ denotes the Dirichlet trace operator as defined in Theorem 1.4. Multiplying the partial differential equation in (2.2) with a test function $v \in H_0^1(\Omega)$, integrating over Ω and applying integration by parts leads to

$$\begin{aligned}
\int_\Omega z(x)v(x)\,\mathrm{d}x &= \int_\Omega [-\Delta u(x) - \kappa^2 u(x)]v(x)\,\mathrm{d}x \\
&= \int_\Omega \nabla u(x) \cdot \nabla v(x) - \kappa^2 u(x)v(x)\,\mathrm{d}x - \int_{\partial\Omega} \frac{\partial}{\partial \underline{n}} u(x) \widetilde{\gamma}_0 v(x)\,\mathrm{d}s_x \\
&= \int_\Omega \nabla u(x) \cdot \nabla v(x) - \kappa^2 u(x)v(x)\,\mathrm{d}x,
\end{aligned}$$

where $\underline{n} \in \mathbb{R}^d$ denotes the outward pointing normal vector with respect to Ω. Then the variational formulation is: find $u \in V_g$ such that

$$\int_\Omega \nabla u(x) \cdot \nabla v(x) - \kappa^2 u(x)v(x)\,\mathrm{d}x = \int_\Omega z(x)v(x)\,\mathrm{d}x \qquad \forall v \in H_0^1(\Omega).$$

Applying the inverse trace theorem (Theorem 1.5) we obtain for the Dirichlet datum $g \in H^{1/2}(\partial\Omega)$ a bounded extension $u_g \in H^1(\Omega)$ satisfying $\widetilde{\gamma}_0 u_g = g$ on $\partial\Omega$. Hence, the variational formulation can be rewritten as: find $u_0 := u - u_g \in H_0^1(\Omega)$ such that

$$a_{-\kappa^2}(u_0, v) = \int_\Omega z(x)v(x)\,\mathrm{d}x - a_{-\kappa^2}(u_g, v) \qquad \forall v \in H_0^1(\Omega),$$

where for any $\mu \in \mathbb{R}$

$$\begin{aligned}
&a_\mu(\cdot,\cdot) : H^1(\Omega) \times H^1(\Omega) \to \mathbb{R} \\
&(u, v) \to \int_\Omega \nabla u(x) \nabla v(x) + \mu u(x)v(x)\,\mathrm{d}x.
\end{aligned} \tag{2.3}$$

For the following analysis we use the Gelfand triple (cf. Def. 1.5)

$$H_0^1(\Omega) \subset L^2(\Omega) \subset H^{-1}(\Omega).$$

In the next step we have to verify the properties of Theorem 1.2 for the operator $A_{-\kappa^2} : H_0^1(\Omega) \to H^{-1}(\Omega)$ induced by the bilinear form $a_{-\kappa^2}(\cdot,\cdot)$. The operator is given by $\langle A_{-\kappa^2} u_0, v\rangle_\Omega = a_{-\kappa^2}(u_0, v)$. It is linear by definition and the boundedness is a consequence of the Cauchy–Schwarz–inequality. It remains to show coercivity and injectivity of $A_{-\kappa^2}$. In order to do so, we rewrite $a_{-\kappa^2}(u_0, v)$ as

$$a_{-\kappa^2}(u_0, v) = a_0(u_0, v) - \kappa^2 c(u_0, v),$$

where $a_0(\cdot,\cdot)$ is the bilinear form of the Dirichlet Laplacian. This bilinear form is bounded, symmetric and $H_0^1(\Omega)$–elliptic, which follows from the Poincaré inequality (cf. Theorem 1.3). Moreover,

$$c(u_0, v) = \int_\Omega u_0(x)v(x)\,\mathrm{d}x = \langle Cu_0, v\rangle_\Omega,$$

induces an operator $C : H_0^1(\Omega) \to H^{-1}(\Omega)$. To show compactness of the operator C let $(u_n)_n \subset H_0^1(\Omega)$ be a bounded sequence. By the Rellich–Kondrachov embedding theorem (Theorem 1.9) $H_0^1(\Omega)$ embeds compactly into $L^2(\Omega)$, i.e., there exists a subsequence u_{n_k} such that $u_{n_k} \to u$ in $L^2(\Omega)$. Moreover, we get

$$\langle Cu_{n_k}, v\rangle_\Omega = \int_\Omega u_{n_k} v\,\mathrm{d}x \to \int_\Omega uv\,\mathrm{d}x = \langle Cu, v\rangle_\Omega \qquad \forall v \in H_0^1(\Omega),$$

which shows that $Cu_{n_k} \to Cu$ in $H^{-1}(\Omega)$. Therefore, C is a compact operator. We can now establish coercivity and injectivity of $A_{-\kappa^2}$.

- $A_{-\kappa^2}$ is coercive:
  Adding the compact operator C scaled with κ^2 ensures coercivity. This is shown by

  $$\begin{aligned}\langle (A_{-\kappa^2} + \kappa^2 C)u_0, u_0\rangle_\Omega &= a_{-\kappa^2}(u_0, u_0) + \kappa^2 c(u_0, u_0) = a_0(u_0, u_0)\\ &= \int_\Omega |\nabla u_0(x)|^2\,\mathrm{d}x = \|u_0\|^2_{H_0^1(\Omega)}.\end{aligned}$$

  Therefore, Gårdings inequality is satisfied, which implies that $A_{-\kappa^2}$ is coercive.

- $A_{-\kappa^2}$ is injective:
  In order to prove that the operator $A_{-\kappa^2}$ is injective, we consider $A_{-\kappa^2} u_0 = 0$ in $H^{-1}(\Omega)$. This implies that

  $$a_{-\kappa^2}(u_0, v) = 0 \qquad \forall v \in H_0^1(\Omega),$$

  which is exactly the weak formulation of the Dirichlet eigenvalue problem of the Laplacian (2.1). Since κ^2 is not an eigenvalue of the Dirichlet Laplacian by Assumption (A3), the only solution is $u_0 = 0$, which shows that $A_{-\kappa^2}$ is injective.

As a result, $A_{-\kappa^2} : H_0^1(\Omega) \to H^{-1}(\Omega)$ is linear, bounded, coercive and injective. In the next step we define the right hand side of the variational formulation as

$$\ell(v) := \int_\Omega zv \,\mathrm{d}x - \langle A_{-\kappa^2} u_g, v\rangle_\Omega \quad \text{for } v \in H_0^1(\Omega).$$

If $\ell \in H^{-1}(\Omega)$, then Theorem 1.2 provides unique solvability of the variational formulation and the bound

$$\|u_0\|_{H^1(\Omega)} \leq c\|\ell\|_{H^{-1}(\Omega)}.$$

Therefore, we estimate the dual norm by using the Cauchy–Schwarz–inequality, the Poincaré inequality, the boundedness of $A_{-\kappa^2}$ and the trace theorem (Theorem 1.4). Hence, we obtain

$$\|\ell\|_{H^{-1}(\Omega)} = \sup_{0\neq v\in H_0^1(\Omega)} \frac{|\langle \ell, v\rangle_\Omega|}{\|v\|_{H^1(\Omega)}} \leq c\left(\|z\|_{L^2(\Omega)} + \|g\|_{H^{1/2}(\partial\Omega)}\right),$$

where c is a generic constant. So far we have

$$\|u_0\|_{H^1(\Omega)} \leq c\left(\|z\|_{L^2(\Omega)} + \|g\|_{H^{1/2}(\partial\Omega)}\right).$$

Adding $\|u_g\|_{H^1(\Omega)}$, using the triangle inequality on the left hand side and the trace theorem (Theorem 1.4) on the right hand side leads to the estimate

$$\|u\|_{H^1(\Omega)} \leq c\left(\|z\|_{L^2(\Omega)} + \|g\|_{H^{1/2}(\partial\Omega)}\right),$$

which completes the proof. □

2.2 Neumann boundary value problem

Now we want to take a closer look at the Neumann boundary value problem for the Helmholtz equation. First, we formulate the assumptions for this section.

Assumptions 2.2.

(B1) The source satisfies $z \in L^2(\Omega)$.

(B2) The Neumann datum fulfils $f \in H^{-1/2}(\partial\Omega)$.

(B3) The wave number $\kappa \geq 0$ satisfies that κ^2 is not an eigenvalue of the Neumann Laplacian, i.e.,

$$\begin{aligned} -\Delta u(x) &= \kappa^2 u(x) && \text{for } x \in \Omega, \\ \frac{\partial u}{\partial \underline{n}}(x) &= 0 && \text{for } x \in \partial\Omega, \end{aligned} \tag{2.4}$$

where $\underline{n}$ is the outward pointing normal vector with respect to Ω, has only the trivial solution $u = 0$.

Let us consider the Neumann boundary value problem for the Helmholtz equation, given by

$$\begin{aligned} -\Delta u(x) - \kappa^2 u(x) &= z(x) \qquad \text{for } x \in \Omega, \\ \frac{\partial u}{\partial \underline{n}}(x) &= f(x) \qquad \text{for } x \in \partial\Omega. \end{aligned} \tag{2.5}$$

Unique solvability of problem (2.5) is stated in the following theorem.

Theorem 2.2. *Let $f \in H^{-1/2}(\partial\Omega)$ and $z \in L^2(\Omega)$ be given. Under the Assumptions 2.2 there exists a unique weak solution $u \in H^1(\Omega)$ of the Neumann boundary value problem* (2.5)*, satisfying*

$$\|u\|_{H^1(\Omega)} \leq c \left(\|z\|_{L^2(\Omega)} + \|f\|_{H^{-1/2}(\partial\Omega)} \right).$$

Proof. We start by rewriting the Neumann boundary value problem (2.5) as a variational formulation. To do so, we use the Hilbert space $X = H^1(\Omega)$ endowed with the norm $\|\cdot\|_{H^1(\Omega)}$. Multiplying the partial differential equation in (2.5) with a test function $v \in H^1(\Omega)$, integrating over Ω and applying integration by parts leads to

$$\begin{aligned} \int_\Omega z(x)v(x)\,\mathrm{d}x &= \int_\Omega [-\Delta u(x) - \kappa^2 u(x)]v(x)\,\mathrm{d}x \\ &= \int_\Omega \nabla u(x) \cdot \nabla v(x) - \kappa^2 u(x)v(x)\,\mathrm{d}x - \int_{\partial\Omega} f(x)\widetilde{\gamma}_0 v(x)\,\mathrm{d}s_x. \end{aligned}$$

Using the notation of (2.3) the variational formulation is: find $u \in H^1(\Omega)$ such that

$$a_{-\kappa^2}(u,v) = \int_\Omega z(x)v(x)\,\mathrm{d}x + \int_{\partial\Omega} f(x)\widetilde{\gamma}_0 v(x)\,\mathrm{d}s_x \qquad \forall v \in H^1(\Omega).$$

For the following analysis we use the Gelfand triple (cf. Def. 1.5)

$$H^1(\Omega) \subset L^2(\Omega) \subset H^{-1}(\Omega).$$

In the next step we will verify the assumptions of Theorem 1.2. Hence, we introduce the operator $A_{-\kappa^2} : H^1(\Omega) \to H^{-1}(\Omega)$. This operator is induced by the bilinear form $a_{-\kappa^2}(\cdot,\cdot)$ and given by $\langle A_{-\kappa^2}u, v\rangle_\Omega = a_{-\kappa^2}(u,v)$. The operator $A_{-\kappa^2}$ is linear and bounded. In order to show coercivity of $A_{-\kappa^2}$ we use a different splitting of the bilinear form compared to the Dirichlet boundary value problem in Section 2.1. The bilinear form $a_{-\kappa^2}(u,v)$ can be rewritten as

$$a_{-\kappa^2}(u,v) = a_{\kappa^2}(u,v) - 2\kappa^2 c(u,v),$$

where $a_{\kappa^2}(\cdot,\cdot)$ is bounded, symmetric and $H^1(\Omega)$–elliptic if $\kappa^2 \neq 0$. This condition is satisfied because $\kappa^2 = 0$ is excluded by Assumption (B3) as it would be an eigenvalue of the homogeneous Neumann Laplacian with a constant solution u. The bilinear form

$$c(u,v) = \int_\Omega u(x)v(x)\,\mathrm{d}x = \langle Cu, v\rangle_\Omega,$$

induces an operator $C : H^1(\Omega) \to H^{-1}(\Omega)$. Compactness of the operator C is shown as in Section 2.1 but using $H^1(\Omega)$ instead of $H^1_0(\Omega)$. With this compact operator C we can now show that $A_{-\kappa^2}$ is coercive and then that it is injective.

- $A_{-\kappa^2}$ is coercive:
  Adding the compact operator C scaled with $2\kappa^2$ ensures coercivity. This is shown by

$$\begin{aligned}\langle (A_{-\kappa^2} + 2\kappa^2 C)u, u\rangle_\Omega &= a_{-\kappa^2}(u,u) + 2\kappa^2 c(u,u) = a_{\kappa^2}(u,u)\\ &= \int_\Omega |\nabla u(x)|^2 \,\mathrm{d}x + \kappa^2 \int_\Omega |u(x)|^2 \,\mathrm{d}x\\ &= \|\nabla u\|^2_{L^2(\Omega)} + \kappa^2 \|u\|^2_{L^2(\Omega)} \geq \min\{1,\kappa^2\}\|u\|^2_{H^1(\Omega)}.\end{aligned}$$

  Since $\kappa^2 > 0$ by Assumption (B3) the constant $\min\{1,\kappa^2\} > 0$ and hence, we have shown that $A_{-\kappa^2}$ is coercive.

- $A_{-\kappa^2}$ is injective:
  In order to prove that the operator $A_{-\kappa^2}$ is injective, we consider $A_{-\kappa^2}u = 0$ in $H^{-1}(\Omega)$. This implies that

$$a_{-\kappa^2}(u,v) = 0 \qquad \forall v \in H^1(\Omega),$$

  which is exactly the weak formulation of the Neumann eigenvalue problem of the Laplacian (2.4) with homogeneous Neumann datum. Since κ^2 is not an eigenvalue of this problem by Assumption (B3), the only solution is $u = 0$, which shows that $A_{-\kappa^2}$ is injective.

Altogether, the operator $A_{-\kappa^2} : H^1(\Omega) \to H^{-1}(\Omega)$ is linear, bounded, coercive and injective. In the next step we define the right hand side of the variational formulation as

$$\ell(v) := \int_\Omega zv \,\mathrm{d}x + \langle f, \widetilde{\gamma}_0 v\rangle_{\partial\Omega} \quad \text{for } v \in H^1(\Omega).$$

If $\ell \in H^{-1}(\Omega)$, then Theorem 1.2 provides unique solvability of the variational formulation and an additional bound

$$\|u\|_{H^1(\Omega)} \leq c\|\ell\|_{H^{-1}(\Omega)}.$$

We can estimate the dual norm by using the Cauchy–Schwarz–inequality and the trace theorem (Theorem 1.4). Hence, we obtain

$$\|\ell\|_{H^{-1}(\Omega)} = \sup_{0\neq v\in H^1(\Omega)} \frac{|\langle \ell, v\rangle_\Omega|}{\|v\|_{H^1(\Omega)}} \leq c\left(\|z\|_{L^2(\Omega)} + \|f\|_{H^{-1/2}(\partial\Omega)}\right),$$

where c is a generic constant. Altogether, we get the estimate

$$\|u\|_{H^1(\Omega)} \leq c\left(\|z\|_{L^2(\Omega)} + \|f\|_{H^{-1/2}(\partial\Omega)}\right),$$

which completes the proof. □

We have shown unique solvability of the Dirichlet and Neumann boundary value problem for the Helmholtz equation. In the next section we focus on the boundary value problem with Dirichlet and Neumann data for the Bi–Helmholtz–type equation.

2.3 A Bi–Helmholtz–type equation

In this section we assume the following.

Assumptions 2.3.

(C1) The source satisfies $z \in L^2(\Omega)$, where $\Omega \subset \mathbb{R}^d$, $d = 2, 3$, is a bounded domain with $\mathcal{C}^{1,1}$–boundary.

(C2) The Cauchy data satisfy $g \in H^{3/2}(\partial\Omega)$ and $f \in H^{1/2}(\partial\Omega)$.

(C3) The wave number $\kappa \geq 0$ satisfies that κ^4 is not an eigenvalue of the Bi–Laplacian with homogeneous Dirichlet and Neumann datum, i.e.,

$$\begin{aligned} \Delta^2 u(x) &= \kappa^4 u(x) && \text{for } x \in \Omega, \\ u(x) &= 0 && \text{for } x \in \partial\Omega, \\ \frac{\partial u}{\partial \underline{n}}(x) &= 0 && \text{for } x \in \partial\Omega, \end{aligned} \tag{2.6}$$

where $\underline{n}$ is the outward pointing normal vector with respect to Ω, has only the trivial solution $u = 0$.

In this section we consider the boundary value problem for the Bi–Helmholtz–type equation, given by

$$\begin{aligned} \Delta^2 u(x) - \kappa^4 u(x) &= z(x) && \text{for } x \in \Omega, \\ u(x) &= g(x) && \text{for } x \in \partial\Omega, \\ \frac{\partial u}{\partial \underline{n}}(x) &= f(x) && \text{for } x \in \partial\Omega. \end{aligned} \tag{2.7}$$

Unique solvability of the boundary value problem (2.7) is stated in the next theorem.

Theorem 2.3. *Let $g \in H^{3/2}(\partial\Omega)$, $f \in H^{1/2}(\partial\Omega)$ and $z \in L^2(\Omega)$ be given. Under the Assumptions 2.3 there exists a unique weak solution $u \in H^2(\Omega)$ of the boundary value problem* (2.7)*, satisfying*

$$\|u\|_{H^2(\Omega)} \leq c \left(\|z\|_{L^2(\Omega)} + \|g\|_{H^{3/2}(\partial\Omega)} + \|f\|_{H^{1/2}(\partial\Omega)} \right).$$

Proof. We start by rewriting the boundary value problem (2.7) as a variational formulation. To do so, we use the Hilbert space $X = H_0^2(\Omega)$ with the norm $\|\Delta(\cdot)\|_{L^2(\Omega)}$ (cf. Remark 1.4). For the weak formulation we introduce additionally the manifold

$$V_{g,f} := \{v \in H^2(\Omega) : \gamma_0 v = g, \gamma_1 v = f \text{ on } \partial\Omega\}.$$

Multiplying the partial differential equation in (2.7) with a test function $v \in H_0^2(\Omega)$, integrating over Ω and applying integration by parts twice leads to

$$\begin{aligned}\int_\Omega z(x)v(x)\,\mathrm{d}x &= \int_\Omega [\Delta^2 u(x) - \kappa^4 u(x)]v(x)\,\mathrm{d}x \\ &= -\int_\Omega \nabla(\Delta u(x))\cdot\nabla v(x)\,\mathrm{d}x + \int_{\partial\Omega}\frac{\partial}{\partial \underline{n}}(\Delta u(x))\gamma_0 v(x)\,\mathrm{d}s_x \\ &\quad - \kappa^4\int_\Omega u(x)v(x)\,\mathrm{d}x \\ &= \int_\Omega \Delta u(x)\Delta v(x)\,\mathrm{d}x - \int_{\partial\Omega}\Delta u(x)\frac{\partial}{\partial \underline{n}}v(x)\,\mathrm{d}s_x - \kappa^4\int_\Omega u(x)v(x)\,\mathrm{d}x \\ &= \int_\Omega \Delta u(x)\Delta v(x)\,\mathrm{d}x - \kappa^4\int_\Omega u(x)v(x)\,\mathrm{d}x.\end{aligned}$$

We obtain the following variational formulation: find $u \in V_{g,f}$ such that

$$\int_\Omega \Delta u(x)\Delta v(x) - \kappa^4 u(x)v(x)\,\mathrm{d}x = \int_\Omega z(x)v(x)\,\mathrm{d}x \qquad \forall v \in H_0^2(\Omega).$$

By the generalised inverse trace theorem (Theorem 1.6) there exists an extension $\tilde{u} \in H^2(\Omega)$ of the Cauchy data such that $\gamma_0\tilde{u} = g$ and $\gamma_1\tilde{u} = f$ on $\partial\Omega$. Hence, the variational formulation can be rewritten as: find $u_0 := u - \tilde{u} \in H_0^2(\Omega)$ such that

$$\tilde{a}_{-\kappa^4}(u_0, v) = \int_\Omega z(x)v(x)\,\mathrm{d}x - \tilde{a}_{-\kappa^4}(\tilde{u}, v) \qquad \forall v \in H_0^2(\Omega),$$

where for any $\mu \in \mathbb{R}$

$$\begin{aligned}&\tilde{a}_\mu(\cdot,\cdot) : H^2(\Omega)\times H^2(\Omega) \to \mathbb{R} \\ &(u, v) \to \int_\Omega \Delta u(x)\Delta v(x) + \mu u(x)v(x)\,\mathrm{d}x.\end{aligned}$$

For the following analysis we use the Gelfand triple (cf. Def. 1.5)

$$H_0^2(\Omega) \subset L^2(\Omega) \subset H^{-2}(\Omega).$$

Next, we want to apply Theorem 1.2 for the operator $\tilde{A}_{-\kappa^4} : H_0^2(\Omega) \to H^{-2}(\Omega)$ induced by the bilinear form $\tilde{a}_{-\kappa^4}(\cdot,\cdot)$. The operator is given by $\langle \tilde{A}_{-\kappa^4}u_0, v\rangle_\Omega = \tilde{a}_{-\kappa^4}(u_0, v)$ which is linear by definition. It remains to show boundedness, coercivity and injectivity of $\tilde{A}_{-\kappa^4}$. Therefore, we rewrite the bilinear form as

$$\tilde{a}_{-\kappa^4}(u_0, v) = \tilde{a}_0(u_0, v) - \kappa^4 c(u_0, v),$$

where

$$c(u_0, v) = \int_\Omega u_0(x)v(x)\,\mathrm{d}x = \langle Cu_0, v\rangle_\Omega,$$

induces an operator $C : H_0^2(\Omega) \to H^{-2}(\Omega)$. Compactness of C can be shown analogously to Section 2.1 since $H_0^2(\Omega)$ embeds compactly into $L^2(\Omega)$ by the Rellich–Kondrachov embedding theorem (Theorem 1.9). Now we can prove the remaining assumptions of Theorem 1.2.

- $\tilde{A}_{-\kappa^4}$ is bounded:
  First, we estimate the duality pairing $\langle \tilde{A}_{-\kappa^4} u_0, v\rangle_\Omega$ by

$$\begin{aligned}\langle \tilde{A}_{-\kappa^4} u_0, v\rangle_\Omega = \tilde{a}_{-\kappa^4}(u_0, v) &= \int_\Omega \Delta u_0(x)\Delta v(x)\,\mathrm{d}x - \kappa^4 \int_\Omega u_0(x)v(x)\,\mathrm{d}x \\ &\le \|\Delta u_0\|_{L^2(\Omega)}\|\Delta v\|_{L^2(\Omega)} + \kappa^4 \|u_0\|_{L^2(\Omega)}\|v\|_{L^2(\Omega)} \\ &\le (1+\kappa^4)\|u_0\|_{H^2(\Omega)}\|v\|_{H^2(\Omega)}.\end{aligned}$$

  Hence, we obtain

$$\|\tilde{A}_{-\kappa^4} u_0\|_{H^{-2}(\Omega)} = \sup_{0\neq v\in H_0^2(\Omega)} \frac{|\langle \tilde{A}_{-\kappa^4} u_0, v\rangle_\Omega|}{\|v\|_{H^2(\Omega)}} \le (1+\kappa^4)\|u_0\|_{H^2(\Omega)},$$

  which proves the boundedness of the operator $\tilde{A}_{-\kappa^4}$.

- $\tilde{A}_{-\kappa^4}$ is coercive:
  Coercivity is shown by adding the compact operator C scaled with κ^4 and using the estimate in Remark 1.4. This is shown by

$$\begin{aligned}\langle (\tilde{A}_{-\kappa^4} + \kappa^4 C)u_0, u_0\rangle_\Omega = \tilde{a}_{-\kappa^4}(u_0,u_0) + \kappa^4 c(u_0,u_0) &= \tilde{a}_0(u_0,u_0) \\ &= \int_\Omega |\Delta u_0(x)|^2\,\mathrm{d}x \ge (c_p^2 + c_p + 1)^{-1}\|u_0\|_{H^2(\Omega)}^2,\end{aligned}$$

  which shows that $\tilde{A}_{-\kappa^4}$ is coercive.

- $\tilde{A}_{-\kappa^4}$ is injective:
  In order to prove that the operator $\tilde{A}_{-\kappa^4}$ is injective, we consider $\tilde{A}_{-\kappa^4} u_0 = 0$ in $H^{-2}(\Omega)$. This implies that

$$\tilde{a}_{-\kappa^4}(u_0, v) = 0 \qquad \forall v \in H_0^2(\Omega),$$

  which is exactly the weak formulation of the eigenvalue problem of the Bi–Laplacian (2.6). Since κ^4 is not an eigenvalue of the Bi–Laplacian by Assumption (C3), the only solution is $u_0 = 0$, which shows that $\tilde{A}_{-\kappa^4}$ is injective.

Now we have shown that $\tilde{A}_{-\kappa^4} : H_0^2(\Omega) \to H^{-2}(\Omega)$ is linear, bounded, coercive and injective. In the next step we define the right hand side of the variational formulation as

$$\ell(v) := \int_\Omega zv\,\mathrm{d}x - \langle \tilde{A}_{-\kappa^4}\tilde{u}, v\rangle_\Omega \quad \text{for } v \in H_0^2(\Omega).$$

If $\ell \in H^{-2}(\Omega)$, then Theorem 1.2 provides unique solvability of the variational formulation and the bound

$$\|u_0\|_{H^2(\Omega)} \leq c\|\ell\|_{H^{-2}(\Omega)}.$$

We can estimate the dual norm by using the Cauchy–Schwarz–inequality and the boundedness of $\tilde{A}_{-\kappa^4}$. Hence, we obtain

$$\|\ell\|_{H^{-2}(\Omega)} = \sup_{0\neq v\in H_0^2(\Omega)} \frac{|\langle \ell, v\rangle_\Omega|}{\|v\|_{H^2(\Omega)}} \leq c\left(\|z\|_{L^2(\Omega)} + \|\tilde{u}\|_{H^2(\Omega)}\right),$$

where c is a generic constant. So far we have

$$\|u_0\|_{H^2(\Omega)} \leq c\left(\|z\|_{L^2(\Omega)} + \|\tilde{u}\|_{H^2(\Omega)}\right).$$

Next, we add $\|\tilde{u}\|_{H^2(\Omega)}$ and use the triangle inequality on the left hand side. On the right hand side we apply Theorem 1.6, which yields the estimate

$$\|\tilde{u}\|_{H^2(\Omega)} \leq c\left(\|g\|_{H^{3/2}(\partial\Omega)} + \|f\|_{H^{1/2}(\partial\Omega)}\right).$$

Altogether, we receive

$$\|u\|_{H^2(\Omega)} \leq c\left(\|z\|_{L^2(\Omega)} + \|g\|_{H^{3/2}(\partial\Omega)} + \|f\|_{H^{1/2}(\partial\Omega)}\right),$$

which completes the proof. □

In summary, we have established unique solvability of the Dirichlet and Neumann boundary problem for the Helmholtz equation (2.2),(2.5), as well as of the boundary value problem for the Bi–Helmholtz–type equation (2.7).

3 Source reconstruction from Cauchy data for the Helmholtz equation

We start by formulating the assumptions for this section.

Assumptions 3.1.

(D1) Let $\Omega \subset \mathbb{R}^d, d = 2, 3$, be a bounded Lipschitz domain with boundary $\partial\Omega$.

(D2) The Cauchy data $g \in H^{1/2}(\partial\Omega)$ and $f \in H^{-1/2}(\partial\Omega)$ are given.

(D3) The wave number $\kappa \geq 0$ satisfies that κ^2 is neither an eigenvalue of the Dirichlet Laplacian (2.1) nor an eigenvalue of the Neumann Laplacian (2.4). Additionally, κ^4 is not an eigenvalue of the Bi–Laplacian (2.6).

Under Assumptions 3.1 we consider the inverse problem of reconstructing the source z in the Helmholtz equation as a model problem. The objective is to find the right hand side z of the partial differential equation

$$\begin{aligned} \Delta u(x) + \kappa^2 u(x) &= z(x) && \text{for } x \in \Omega, \\ u(x) &= g(x) && \text{for } x \in \partial\Omega, \\ \frac{\partial u}{\partial \underline{n}}(x) &= f(x) && \text{for } x \in \partial\Omega, \end{aligned} \tag{3.1}$$

where $\underline{n}$ denotes the outward pointing normal vector with respect to the domain Ω. As the functional setting varies throughout this section, the space for the source z is not fixed a priori. The appropriate space for z will be stated explicitly in the subsequent sections.

So far we have established unique solvability of the forward problems in Section 2. Now we are interested in deriving unique solvability for the source z of our model problem (3.1). This has already been discussed in [3, 11]. While Alves et al. analyse in [3] the unique solvability for a homogeneous Dirichlet datum in domains with $\mathcal{C}^1$–boundaries, El Badia and Nara study in [11] the unique solvability for different types of sources in $\mathbb{R}^3$. In the latter, point sources, Dirac distributions supported on spheres as well as characteristic functions on hollow and solid balls are considered.

In this section we will start with an example which demonstrates that it is in general not possible to reconstruct the right hand side z of the inverse problem from boundary data measurements at a single wave number. After Example 3.1 the unique solvability of the inverse problem (3.1) is shown for point sources in Section 3.1.1. Moreover, we

prove for Dirac distributions supported on spheres and for characteristic sources on a finite union of (hollow) balls, that we can retrieve some quantities of the source but not the complete source. In Section 3.1.2 and 3.1.3 we define operators, mapping the source onto boundary traces. Analysing the mapping properties of these operators leads on the one hand to constraints regarding the boundary data. On the other hand we obtain unique solvability of the inverse problem (3.1) if some a priori information is known about the source z. In Section 3.1.4 a method using a Bi–Helmholtz–type equation is employed to get rid of the assumptions on the boundary data and to obtain a more general uniqueness result. Finally, unique solvability of the inverse problem (3.1) from boundary data at multiple wave numbers is discussed in Section 3.2.

3.1 Uniqueness from boundary measurements at a single wave number

As mentioned, we now start with an example in order to show, that the inverse problem is in general not uniquely solvable. We consider $\kappa = 1$ and the Helmholtz equation in $\Omega \subset \mathbb{R}^2$.

Example 3.1 ([3, cf. p.3])**.** Let $\Omega = B(0,1) = \{x \in \mathbb{R}^2 : \|x\| < 1\}$ be the open unit ball in $\mathbb{R}^2$. We consider the function

$$u(x) := -\|x\|^4 + 2\|x\|^2 - 1.$$

In the first step we calculate the gradient of u. This leads to

$$\nabla u(x) = 4(1 - \|x\|^2) \begin{pmatrix} x_1 \\ x_2 \end{pmatrix}.$$

For all $x \in \partial\Omega = \{x \in \mathbb{R}^2 : \|x\| = 1\}$ we get that $u(x) = 0$ and $\partial_{\underline{n}} u(x) = 0$. Furthermore, we compute

$$\Delta u(x) + u(x) = -\|x\|^4 - 14\|x\|^2 + 7.$$

We consider the inverse problem (3.1) for $\kappa = 1$, $g = 0$ and $f = 0$, where the aim is to find $z \in L^2(\Omega)$ such that

$$\begin{aligned} \Delta u(x) + u(x) &= z(x) && \text{for } x \in \Omega, \\ u(x) &= 0 && \text{for } x \in \partial\Omega, \\ \frac{\partial u}{\partial \underline{n}}(x) &= 0 && \text{for } x \in \partial\Omega. \end{aligned}$$

Obviously $z = 0$ is a solution. As a matter of fact, our calculation above shows that $z = -\|x\|^4 - 14\|x\|^2 + 7$ is another solution. Hence, it is impossible to identify the source from one pair of boundary data measurements.

Example 3.1 illustrates, that it is in general not possible to reconstruct the right hand side z from the boundary data measurements. Therefore, in the following sections we investigate the unique solvability of the inverse problem (3.1) for different types of sources and for boundary data given at a single wave number.

3.1.1 Uniqueness results for different types of sources

In this section we investigate uniqueness results for different types of sources from the Cauchy data at a single wave number. We consider point sources, Dirac distributions supported on spheres and finally characteristic sources on a finite union of hollow or solid balls. This analysis is based on [11].

Assumptions 3.2. In addition to Assumptions 3.1 we restrict ourselves to the three-dimensional case, i.e., $\Omega \subset \mathbb{R}^3$. Moreover, the points y_j for $j = 1, ..., n$ considered in this section are pairwise distinct.

We study the model problem (3.1), where the source term is a linear combination of point sources. Therefore, the source z can be represented as

$$z = \sum_{j=1}^{n} \lambda_j \delta_{y_j} \qquad \text{for } n \in \mathbb{N}, \lambda_j \in \mathbb{C} \setminus \{0\}, y_j \in \Omega, \tag{3.2}$$

where δ_{y_j} denotes the Dirac distribution in $y_j \in \Omega$.
The following theorem establishes uniqueness of the inverse problem (3.1) if it is known a priori, that the source is a linear combination of point sources as in (3.2).

Theorem 3.1 ([11, Thm. 1])**.** *Let Assumptions 3.1–3.2 be satisfied and let z_1 and z_2 be two point sources given as*

$$z_i = \sum_{j=1}^{n_i} \lambda_{j,i} \delta_{y_{j,i}} \qquad \textit{for } n_i \in \mathbb{N}, \lambda_{j,i} \in \mathbb{C} \setminus \{0\}, y_{j,i} \in \Omega \textit{ and } i = 1, 2,$$

with pairwise distinct points $y_{j,i}$. Furthermore, let z_1 and z_2 be solutions of the inverse problem (3.1) *such that the corresponding functions are u_1 and u_2, i.e., $\gamma_0 u_1 = \gamma_0 u_2$ and $\gamma_1 u_1 = \gamma_1 u_2$ on $\partial\Omega$. Then*

$$n := n_1 = n_2, \qquad \lambda_{j,1} = \lambda_{j,2}, \qquad y_{j,1} = y_{j,2}, \qquad \textit{for } j = 1, ..., n,$$

and hence $z_1 = z_2$.

Proof. In the first step of the proof we deal with the Sobolev regularity of the sources z_i and the corresponding elements u_i for $i = 1, 2$. Since $\Omega \subset \mathbb{R}^3$, the point sources satisfy $z_i \in H^{-s}(\Omega)$ for all $s > 3/2$ (cf.[1, p.56]). Furthermore, by [22, Thm. 6.1] the solutions satisfy $u_i \in H^r(\Omega)$ for all $r < 1/2$ and are smooth away from the source

locations $y_{j,i}$. Next, we briefly argue that each $u_i \in H^r(\Omega)$ for all $r < 1/2$ and $i = 1, 2$ is unique. Suppose that u_i and $\tilde{u}_i$ solve the same forward problem with source z_i and Dirichlet datum g. Then the difference $\bar{u}_i := u_i - \tilde{u}_i$ solves

$$\begin{aligned} \Delta \bar{u}_i(x) + \kappa^2 \bar{u}_i(x) &= 0 \qquad \text{for } x \in \Omega, \\ \bar{u}_i(x) &= 0 \qquad \text{for } x \in \partial\Omega, \end{aligned}$$

for $i = 1, 2$. By Assumption (D3) κ^2 is not an eigenvalue of this problem. Hence, $\bar{u}_i = 0$, which implies the uniqueness of the elements u_i for $i = 1, 2$.
We can now prove the main part of the theorem. The functions u_1 and u_2 solve the Helmholtz equation with Cauchy data g and f but with different right hand sides z_1 and z_2. Thus, we consider the difference $\bar{u} := u_2 - u_1$ and obtain by linearity of the problem immediately that $\bar{u}$ satisfies the boundary value problem

$$\begin{aligned} \Delta \bar{u}(x) + \kappa^2 \bar{u}(x) &= \sum_{j=1}^{n_2} \lambda_{j,2} \delta_{y_{j,2}}(x) - \sum_{j=1}^{n_1} \lambda_{j,1} \delta_{y_{j,1}}(x) \qquad \text{for } x \in \Omega, \\ \bar{u}(x) &= 0 \qquad \text{for } x \in \partial\Omega, \\ \frac{\partial \bar{u}}{\partial \underline{n}}(x) &= 0 \qquad \text{for } x \in \partial\Omega. \end{aligned}$$

We will denote the source as $z := \sum_{j=1}^{n_2} \lambda_{j,2} \delta_{y_{j,2}} - \sum_{j=1}^{n_1} \lambda_{j,1} \delta_{y_{j,1}}$. In the next step we apply Holmgren's theorem (Theorem 1.12) and verify its assumptions. Our differential operator is linear and has constant coefficients, which are in particular real and analytic. Since the principal symbol of the Helmholtz operator is given by

$$p_2(x, \xi) = \|\xi\|_2^2 \qquad \text{for } \xi \in \mathbb{R}^d,$$

which vanishes only for $\xi = 0$, the operator has no real characteristics. Hence, the boundary $\partial\Omega$ is a non–characteristic surface. Thus, by Holmgren's theorem, the solution of the differential equation vanishes on the domain without the point sources $y_{j,i}$, i.e.,

$$\bar{u} = 0 \quad \text{on } \Omega \setminus \left[\left(\bigcup_{j=1}^{n_1} y_{j,1} \right) \cup \left(\bigcup_{j=1}^{n_2} y_{j,2} \right) \right].$$

We can conclude, that on the one hand $\bar{u}$ itself is now a linear combination of Dirac distributions. On the other hand $\bar{u}$ solves the Helmholtz equation, where the source term z is the difference of point sources. By the regularity results discussed at the beginning of the proof we know that $z \in H^{-s}(\Omega)$ for all $s > 3/2$ and $\bar{u} \in H^r(\Omega)$ for all $r < 1/2$. However, since $\bar{u}$ is a linear combination of Dirac distributions, it can not belong to the space $H^r(\Omega)$ for all $r < 1/2$. Hence, it can only hold that $\bar{u} = 0$ in Ω, which implies $z_1 = z_2$ as distributions. In the last step we recall that the Dirac

distributions are linearly independent since the locations $y_{j,i}$ are pairwise distinct. Therefore, we receive that the coefficients and the locations of our point sources are identical, which completes the proof. □

As shown in Theorem 3.1 we obtain uniqueness of the inverse problem (3.1) if the source is a linear combination of point sources. The corresponding numerical analysis and numerical examples will be presented in Section 4.1.
In the next step we consider the inverse problem (3.1), where the source is a linear combination of Dirac distributions supported on spheres. Our source z can now be written as

$$z = \sum_{j=1}^{n} \lambda_j \delta_{\partial B(y_j, r_j)} \qquad \text{for } n \in \mathbb{N}, \lambda_j \in \mathbb{C} \setminus \{0\}, y_j \in \Omega,$$

where $\partial B(y_j, r_j)$ denotes the sphere with center y_j and radius r_j. Such sources satisfy $z \in H^{-s}$ for all $s > 1/2$. This can be shown by using the characterisation of Sobolev spaces via the Fourier transformation as defined in [1, p.75 f.].
In order to prove the following statements regarding uniqueness we need an auxiliary lemma and an essential relation between the source and the Cauchy data. This relation will then be formulated as a definition. We start with the auxiliary lemma, which is the mean value theorem for the Helmholtz equation. This theorem occurs first in Weber [27, p.224 (4.)] for a three dimensional domain, see also [19] for a more recent publication and the results in arbitrary dimensions.

Lemma 3.2 ([19, Thm. 2.1])**.** *Let $\partial B(y, r) \subset \Omega \subset \mathbb{R}^3$ be a sphere with midpoint y and radius r. Furthermore, let u solve the homogeneous Helmholtz equation*

$$\Delta u + \kappa^2 u = 0 \qquad \text{in } \Omega,$$

with $\kappa \in \mathbb{R} \setminus \{0\}$. Then

$$u(y)\frac{\sin(\kappa r)}{\kappa r} = \frac{1}{4\pi r^2} \int_{\partial B(y,r)} u(x) \, \mathrm{d}s_x.$$

Now we want to determine the relation between the source z of the inverse problem (3.1) and the Cauchy data. Therefore, we use a test function $v \in \mathcal{H}^1_{\Delta+\kappa^2}(\Omega)$, as introduced in (1.1), and integrate by parts twice, which leads to

$$\begin{aligned} \int_\Omega zv \, \mathrm{d}x &= \int_\Omega (\Delta + \kappa^2) uv \, \mathrm{d}x \\ &= -\int_\Omega \nabla u \cdot \nabla v \, \mathrm{d}x + \kappa^2 \int_\Omega uv \, \mathrm{d}x + \int_{\partial\Omega} \gamma_1 u \gamma_0 v \, \mathrm{d}s_x \\ &= \int_\Omega \underbrace{(\Delta + \kappa^2) v}_{=0} u \, \mathrm{d}x - \int_{\partial\Omega} \gamma_0 u \gamma_1 v \, \mathrm{d}s_x + \int_{\partial\Omega} \gamma_1 u \gamma_0 v \, \mathrm{d}s_x \\ &= \int_{\partial\Omega} f \gamma_0 v \, \mathrm{d}s_x - \int_{\partial\Omega} g \gamma_1 v \, \mathrm{d}s_x =: R(v). \end{aligned} \tag{3.3}$$

As this equation is essential for the subsequent analysis the following definition formalises this relation.

Definition 3.1 ([10, cf. p.656])**.** For any $v \in \mathcal{H}^1_{\Delta+\kappa^2}(\Omega)$ the reciprocity gap functional is defined by

$$R(v) := \int_{\partial\Omega} (f\gamma_0 v - g\gamma_1 v)\,\mathrm{d}s_x,$$

where f is the Neumann datum and g is the Dirichlet datum of the inverse problem (3.1).

With these two considerations we can now formulate the following theorem. It states that the intensities and radii of a source distributed on spheres cannot be determined separately. However, the number n of such sources and the centers y_j of the spheres can be uniquely recovered from boundary data at a single wave number κ.

Theorem 3.3 ([11, Thm. 3])**.** *Let Assumptions 3.1–3.2 be fulfilled. Then the following statements hold.*

1. *If $z = \lambda\delta_{\partial B(y,r)}$ is the source of the inverse problem (3.1), it is not possible to uniquely determine both the intensity λ and the domain $\partial B(y,r)$ from boundary data measurements at a single wave number κ.*
2. *If $z = \sum_{j=1}^n \lambda_j \delta_{\partial B(y_j,r_j)}$ with $n \in \mathbb{N}$ is the source of the inverse problem (3.1), then the number n, the centers y_j of $\partial B(y_j,r_j)$ and the expressions $\lambda_j r_j^2 \frac{\sin(\kappa r_j)}{\kappa r_j}$ can be uniquely determined from the Cauchy data at a single wave number κ.*

Proof. We start by proving the first statement. Therefore, we have to construct two different sources $z_i = \lambda_i \delta_{\partial B(y,r_i)}$ for $i = 1, 2$ such that the corresponding functions u_i satisfy

$$\Delta u_i + \kappa^2 u_i = z_i \qquad \text{in } \Omega,$$

and $\gamma_0 u_1 = \gamma_0 u_2$ and $\gamma_1 u_1 = \gamma_1 u_2$ on $\partial\Omega$. We choose the same center y but different radii for our spheres. Hence, our sources differ. Let us consider u_i solving the Helmholtz equation with the right hand side z_i for $i = 1, 2$ and $\gamma_0 u_1 = \gamma_0 u_2$. The difference $\bar{u} := u_2 - u_1$ solves by linearity

$$\Delta\bar{u} + \kappa^2\bar{u} = z_2 - z_1 \qquad \text{in } \Omega, \tag{3.4a}$$

$$\gamma_0\bar{u} = 0 \qquad \text{on } \partial\Omega. \tag{3.4b}$$

We multiply the right hand side in (3.4a) with a test function $v \in \mathcal{H}^1_{\Delta+\kappa^2}(\Omega)$, use (3.3) and apply $\gamma_0\bar{u} = 0$ on $\partial\Omega$. This leads to

$$\begin{aligned}\int_\Omega (z_2 - z_1)v\,\mathrm{d}x &= \int_\Omega (\Delta\bar{u} + \kappa^2\bar{u})v\,\mathrm{d}x \\ &= \int_{\partial\Omega} \gamma_1\bar{u}\gamma_0 v\,\mathrm{d}s_x - \int_{\partial\Omega} \gamma_0\bar{u}\gamma_1 v\,\mathrm{d}s_x = \int_{\partial\Omega} \gamma_1\bar{u}\gamma_0 v\,\mathrm{d}s_x.\end{aligned}$$

Our aim is now to obtain a vanishing left hand side in this equation by choosing the scalars λ_1 and λ_2 as explained in the following. Therefore, we multiply the right hand side in (3.4a) with a test function $v \in \mathcal{H}^1_{\Delta+\kappa^2}(\Omega)$, use the representation of the sources z_1 and z_2 and apply Lemma 3.2. This leads to

$$\begin{aligned}\int_\Omega (z_2 - z_1)v \,\mathrm{d}x &= \lambda_2 \int_{\partial B(y,r_2)} v \,\mathrm{d}x - \lambda_1 \int_{\partial B(y,r_1)} v \,\mathrm{d}x \\ &= 4\pi \left(\lambda_2 r_2^2 \frac{\sin(\kappa r_2)}{\kappa r_2} - \lambda_1 r_1^2 \frac{\sin(\kappa r_1)}{\kappa r_1} \right) v(y).\end{aligned}$$

Since the radii r_1 and r_2 are distinct, we can choose the intensities λ_1 and λ_2 such that

$$\lambda_1 r_1^2 \frac{\sin(\kappa r_1)}{\kappa r_1} = \lambda_2 r_2^2 \frac{\sin(\kappa r_2)}{\kappa r_2}.$$

This choice ensures that

$$0 = \int_\Omega (z_2 - z_1)v \,\mathrm{d}x = \int_{\partial\Omega} \gamma_1 \bar{u} \gamma_0 v \,\mathrm{d}s_x \qquad \forall v \in \mathcal{H}^1_{\Delta+\kappa^2}(\Omega).$$

In particular, this gives us $z_2 - z_1 \in \mathcal{H}^1_{\Delta+\kappa^2}(\Omega)^\perp$. Furthermore, we obtain that $\int_{\partial\Omega} \gamma_1 \bar{u} \gamma_0 v \,\mathrm{d}s_x = 0$. We note that v solves the homogeneous Helmholtz equation in Ω, but on the boundary v can represent any function. Thus, we can conclude that $\gamma_1 \bar{u} = 0$ on $\partial\Omega$. Since $\bar{u}$ has vanishing Dirichlet and Neumann trace, we have constructed two functions u_1 and u_2 with identical Cauchy data but different sources z_1 and z_2. This completes the proof of the first statement.
To prove the second claim we start by using the reciprocity gap functional as in Definition 3.1. Applying (3.3) and the representation of the source leads to

$$R(v) = \sum_{j=1}^n \lambda_j \int_{\partial B(y_j,r_j)} v(x) \,\mathrm{d}x \qquad \forall v \in \mathcal{H}^1_{\Delta+\kappa^2}(\Omega).$$

The right hand side can be rewritten by making use of Lemma 3.2 as

$$R(v) = \sum_{j=1}^n 4\lambda_j \pi r_j^2 v(y_j) \frac{\sin(\kappa r_j)}{\kappa r_j} \qquad \forall v \in \mathcal{H}^1_{\Delta+\kappa^2}(\Omega). \tag{3.5}$$

We note that for a point source $z = \sum_{j=1}^n \lambda_j \delta_{y_j}$ the reciprocity gap functional is $R(v) = \sum_{j=1}^n \lambda_j v(y_j)$. Since we have proven uniqueness for point sources in Theorem 3.1, we compare the two expressions for the reciprocity gap functional with each other. Consequently, we obtain that the right hand side of (3.5) represents a linear combination of n point sources with centers y_j and intensities $4\lambda_j \pi r_j^2 \frac{\sin(\kappa r_j)}{\kappa r_j}$. Therefore, the number n, the centers y_j and the intensities $4\lambda_j \pi r_j^2 \frac{\sin(\kappa r_j)}{\kappa r_j}$ are uniquely determined. Dividing these intensities by 4π we also have determined the expression $\lambda_j r_j^2 \frac{\sin(\kappa r_j)}{\kappa r_j}$, which completes the proof. □

Finally, we consider the inverse problem (3.1), where the source term is a linear combination of characteristic functions. We denote the source by

$$z = \sum_{j=1}^{n} \lambda_j \chi_{\omega_j} \qquad \text{for } n \in \mathbb{N}, \lambda_j \in \mathbb{C} \setminus \{0\},$$

where χ_{ω_j} is the characteristic function of

$$\omega_j := \{x \in \mathbb{R}^3 : 0 \leq r_0^j < \|x - y_j\| \leq r_1^j\}.$$

Here $y_j \in \Omega$ denotes the center of the ball and r_0^j and r_1^j are radii for $j = 1, ..., n$. If $r_0^j = 0$ we call ω_j a solid ball otherwise a hollow ball. The source satisfies $z \in L^2(\Omega)$. To prove the following theorem we require an auxiliary lemma. This is the mean value theorem for the Helmholtz equation for balls. It is derived from Lemma 3.2 by integrating with respect to the radius over the interval $[r_0, r_1]$.

Corollary 3.4 ([19, Cor. 2.1])**.** *Under the same assumptions as in Lemma 3.2 we obtain*

$$4\pi u(y) \int_{r_0}^{r_1} \frac{r^2 \sin(\kappa r)}{\kappa r} \, \mathrm{d}r = \int_{\omega} u(x) \, \mathrm{d}x,$$

where $\omega := \{x \in \mathbb{R}^3 : 0 \leq r_0 < \|x - y\| \leq r_1\}$.

Now we are able to formulate the following theorem. As in Theorem 3.3 we cannot determine the intensities and the radii of the balls separately. However, the number and the centers of the balls can be uniquely recovered from boundary data at a single wave number κ.

Theorem 3.5 ([11, cf. p. 7 and Thm. 2])**.** *Let Assumptions 3.1–3.2 be fulfilled. Then the following statements hold.*

1. *If $z = \lambda \chi_\omega$ is the source of the inverse problem (3.1), then it is not possible to uniquely determine both the intensity λ and the domain ω from boundary data measurements at a single wave number κ.*
2. *If $z = \sum_{j=1}^{n} \lambda_j \chi_{\omega_j}$ with $n \in \mathbb{N}$ is the source of the inverse problem (3.1), then the number n, the centers y_j of ω_j and the expressions $\lambda_j \int_{r_0^j}^{r_1^j} r^2 \frac{\sin(\kappa r)}{\kappa r} \, \mathrm{d}r$ can be uniquely determined from the Cauchy data at a single wave number κ.*

Proof. We proceed as in the proof of Theorem 3.3 and only highlight the differences. We start by proving the first statement. We have to construct two different sources $z_i = \lambda_i \chi_{\omega_i}$ for $i = 1, 2$ solving (3.1) such that the corresponding functions u_i satisfy

$$\Delta u_i + \kappa^2 u_i = z_i \qquad \text{in } \Omega,$$

and $\gamma_0 u_1 = \gamma_0 u_2$ and $\gamma_1 u_1 = \gamma_1 u_2$ on $\partial\Omega$. Now we choose the supports ω_i to be either two solid balls or two hollow balls, where each of them has the center y but different radii. Since the supports are not identical and the intensities λ_i are non–zero, it follows that $z_1 \neq z_2$. The difference $\bar{u} := u_2 - u_1$ solves by linearity

$$\Delta\bar{u} + \kappa^2\bar{u} = z_2 - z_1 \qquad \text{in } \Omega, \tag{3.6a}$$
$$\gamma_0\bar{u} = 0 \qquad \text{on } \partial\Omega. \tag{3.6b}$$

Multiplying the right hand side (3.6a) with a test function $v \in \mathcal{H}^1_{\Delta+\kappa^2}(\Omega)$ and applying (3.3) as well as $\gamma_0\bar{u} = 0$ on $\partial\Omega$ leads again to

$$\int_\Omega (z_2 - z_1)v \,\mathrm{d}x = \int_{\partial\Omega} \gamma_1\bar{u}\gamma_0 v \,\mathrm{ds}_x.$$

Using the representation of our sources z_i and applying Corollary 3.4, we obtain

$$\int_\Omega (z_2 - z_1)v \,\mathrm{d}x = 4\pi \left(\lambda_2 \int_{r_0^2}^{r_1^2} r^2 \frac{\sin(\kappa r)}{\kappa r} \,\mathrm{d}r - \lambda_1 \int_{r_0^1}^{r_1^1} r^2 \frac{\sin(\kappa r)}{\kappa r} \,\mathrm{d}r \right) v(y).$$

Since the radii of the two domains are distinct we can choose the intensities λ_1 and λ_2 such that

$$\lambda_1 \int_{r_0^1}^{r_1^1} r^2 \frac{\sin(\kappa r)}{\kappa r} \,\mathrm{d}r = \lambda_2 \int_{r_0^2}^{r_1^2} r^2 \frac{\sin(\kappa r)}{\kappa r} \,\mathrm{d}r.$$

This choice ensures that

$$0 = \int_\Omega (z_2 - z_1)v \,\mathrm{d}x = \int_{\partial\Omega} \gamma_1\bar{u}\gamma_0 v \,\mathrm{ds}_x \qquad \forall v \in \mathcal{H}^1_{\Delta+\kappa^2}(\Omega).$$

The remainder of the argument coincides with the proof of Theorem 3.3. Hence, we can conclude that $\bar{u}$ has vanishing Dirichlet and Neumann trace. Therefore, we have constructed two functions u_1 and u_2 having the same Cauchy data but different sources z_1 and z_2. This completes the proof of the first statement.
The proof of the second claim follows analogously. Using the reciprocity gap functional as in Definition 3.1 and Corollary 3.4 we get

$$R(v) = \sum_{j=1}^{n} 4\lambda_j \pi v(y_j) \int_{r_0^j}^{r_1^j} r^2 \frac{\sin(\kappa r)}{\kappa r} \,\mathrm{d}r \qquad \forall v \in \mathcal{H}^1_{\Delta+\kappa^2}(\Omega). \tag{3.7}$$

Comparing (3.7) with the reciprocity gap functional for point sources leads to uniqueness of the number n, the centers y_j as well as the expressions $4\lambda_j\pi \int_{r_0^j}^{r_1^j} r^2 \frac{\sin(\kappa r)}{\kappa r} \,\mathrm{d}r$. Dividing the last quantity by 4π we also have recovered the expressions $\lambda_j \int_{r_0^j}^{r_1^j} r^2 \frac{\sin(\kappa r)}{\kappa r} \,\mathrm{d}r$, which completes the proof. □

In summary, we have shown for the inverse problem (3.1) that point sources can be reconstructed uniquely in a bounded Lipschitz domain $\Omega \subset \mathbb{R}^3$. For sources given by a linear combination of Dirac distributions supported on spheres or by characteristic functions on hollow or solid balls, the number of sources as well as the centers can be uniquely determined. However, we are not able to reconstruct the radii separately from the intensities.

3.1.2 Operator mapping the source onto the Neumann trace

In Section 3.1.1 we have investigated uniqueness results for point sources, Dirac distributions on spheres as well as characteristic functions on hollow or solid balls. However, point sources are mostly of theoretical interest when considering idealised models. For practical applications we will now focus on sources in $L^2(\Omega)$. This section is based on the analysis in [3]. The main difference is that Alves et al. have considered domains with $\mathcal{C}^1$–boundary whereas we will allow domains with lower regularity, i.e., with Lipschitz boundary. Consequently, regularity results from [5, 6] will be applied.
We suppose that Assumptions 3.1 hold and start by considering the model problem

$$\begin{aligned} \Delta u + \kappa^2 u &= z && \text{in } \Omega, \\ u &= g && \text{on } \partial\Omega, \end{aligned}$$

where $g \in H^{1/2}(\partial\Omega)$ and $z \in L^2(\Omega)$. This problem is uniquely solvable by Theorem 2.1 with $u \in H^1(\Omega)$. Since the problem is linear the solution u can be written as $u = u_z + u_g$ with u_z solving

$$\begin{aligned} \Delta u_z + \kappa^2 u_z &= z && \text{in } \Omega, \\ u_z &= 0 && \text{on } \partial\Omega, \end{aligned} \tag{3.8}$$

and u_g solving

$$\begin{aligned} \Delta u_g + \kappa^2 u_g &= 0 && \text{in } \Omega, \\ u_g &= g && \text{on } \partial\Omega. \end{aligned} \tag{3.9}$$

By Theorem 2.1 the problems (3.8) and (3.9) are uniquely solvable with $u_z \in H_0^1(\Omega)$ and $u_g \in H^1(\Omega)$. We define the operator

$$\begin{aligned} \Lambda_\kappa^N : L^2(\Omega) &\to L^2(\partial\Omega) \\ z &\mapsto \partial_{\underline{n}} u_z. \end{aligned}$$

In the inverse problem (3.1) the normal trace satisfies

$$f = \partial_{\underline{n}} u = \partial_{\underline{n}}(u_z + u_g) = \Lambda_\kappa^N(z) + \partial_{\underline{n}} u_g.$$

The Neumann boundary condition in the inverse problem (3.1) can be rewritten as

$$\Lambda_\kappa^N(z) = f - \partial_{\underline{n}} u_g,$$

and hence we can determine the source $z \in L^2(\Omega)$ when solving this operator equation. Thus, we have to characterise the mapping properties of Λ_κ^N, especially the kernel and the range of this operator. With the Dirichlet and Neumann trace operator defined in Lemma 1.7 and Lemma 1.8, respectively, we can formulate the following lemma regarding the mapping properties of the operator Λ_κ^N.

Lemma 3.6. *Let $\kappa \geq 0$ such that κ^2 is not an eigenvalue of the Dirichlet Laplacian. Then*

$$\operatorname{ran}(\Lambda_\kappa^N) = \operatorname{ran}(\gamma_1|_{\ker(\gamma_0)}),$$

is a dense proper linear subspace of $L^2(\partial\Omega)$. Furthermore, for the kernel it holds that

$$\ker(\Lambda_\kappa^N) = (\Delta + \kappa^2)(H_0^2(\Omega)),$$

where $H_0^2(\Omega)$ is defined in (1.2).

Proof. For $z \in L^2(\Omega)$ problem (3.8) admits a unique solution $u_z \in H_\Delta^1(\Omega)$, which has been defined by

$$H_\Delta^1(\Omega) := \{u \in H^1(\Omega) : \Delta u \in L^2(\Omega)\}.$$

Furthermore, u_z satisfies $\gamma_0 u_z = 0$. Therefore, $u_z \in \ker(\gamma_0)$ and by Lemma 1.7 we get that $u_z \in H_\Delta^{3/2}(\Omega)$. So we can write the operator Λ_κ^N as

$$\Lambda_\kappa^N : L^2(\Omega) \overset{(\Delta+\kappa^2)^{-1}}{\to} H_\Delta^{3/2}(\Omega) \cap H_0^1(\Omega) \overset{\gamma_1}{\to} \operatorname{ran}(\gamma_1|_{H_\Delta^{3/2}(\Omega)\cap H_0^1(\Omega)}).$$

Since we can characterise the space to which γ_1 is restricted as $\ker(\gamma_0|_{H_\Delta^{3/2}(\Omega)})$ we get

$$\operatorname{ran}(\Lambda_\kappa^N) = \operatorname{ran}(\gamma_1|_{\ker(\gamma_0)}).$$

By [5, Lem. 8.2] this is a dense proper linear subspace of $L^2(\partial\Omega)$. In the next step we want to characterise the kernel of the operator. It holds that $z \in \ker(\Lambda_\kappa^N)$ if and only if

$$\begin{aligned} u_z = (\Delta + \kappa^2)^{-1} z &\in \ker(\gamma_1|_{H_\Delta^{3/2}(\Omega)\cap H_0^1(\Omega)}) \\ &= \{v \in H_\Delta^{3/2}(\Omega) : \gamma_0 v = \gamma_1 v = 0 \text{ on } \partial\Omega\} \\ &= H_0^2(\Omega), \end{aligned}$$

where the last equality holds due to [6, Cor. 4.2 (i)]. □

For a more regular domain than a Lipschitz domain we get some characterisations for $\operatorname{ran}(\Lambda_\kappa^N)$.

Remark 3.1 ([6, Thm. 4.10 (i)]). Let Ω be a $C^{1,r}$ domain for $r \in (1/2, 1]$ then it holds that

$$\operatorname{ran}(\Lambda_\kappa^N) = \operatorname{ran}(\gamma_1|_{\ker(\gamma_0)}) = H^{1/2}(\partial\Omega).$$

Remark 3.2 ([6, Thm. 4.9 (i)]). In the case that Ω is a quasi convex domain it holds that

$$\operatorname{ran}(\Lambda_\kappa^N) = \operatorname{ran}(\gamma_1|_{\ker(\gamma_0)}) = \{\psi \in L^2(\partial\Omega) : \psi \underline{n} \in H^{1/2}(\partial\Omega)^d\}.$$

As a result, we know the range of Λ_κ^N as well as that $\Lambda_\kappa^N : L^2(\Omega)/\ker(\Lambda_\kappa^N) \to \operatorname{ran}(\Lambda_\kappa^N)$ is an isomorphism. Since $\ker(\Lambda_\kappa^N)$ is a closed subspace we can write $L^2(\Omega)$ as the orthogonal decomposition

$$L^2(\Omega) = \ker(\Lambda_\kappa^N) \oplus \ker(\Lambda_\kappa^N)^\perp.$$

Lemma 3.7 ([3, Rem. 1])**.** *It holds that*

$$\ker(\Lambda_\kappa^N)^\perp = \mathcal{H}_{\Delta+\kappa^2}(\Omega) := \{z \in L^2(\Omega) : \Delta z + \kappa^2 z = 0 \text{ in } L^2(\Omega)\}.$$

Proof. Since $\ker(\Lambda_\kappa^N) = (\Delta + \kappa^2)(H_0^2(\Omega))$ we have to specify the functions $z \in L^2(\Omega)$ such that

$$\langle z, w\rangle_{L^2(\Omega)} = 0 \qquad \forall w \in (\Delta + \kappa^2)(H_0^2(\Omega)).$$

Let $v \in H_0^2(\Omega)$ and write $w = \Delta v + \kappa^2 v$, then integration by parts leads us to

$$\begin{aligned} 0 &= \langle z, \Delta v + \kappa^2 v\rangle_{L^2(\Omega)} \\ &= \langle \Delta z + \kappa^2 z, v\rangle_\Omega + \langle \partial_{\underline{n}} v, z\rangle_{\partial\Omega} - \langle v, \partial_{\underline{n}} z\rangle_{\partial\Omega} \\ &= \langle \Delta z + \kappa^2 z, v\rangle_\Omega, \end{aligned}$$

which means that $\Delta z + \kappa^2 z = 0$ as a distribution on $H_0^2(\Omega)$. Since this would also hold true for $v \in \mathcal{C}_0^\infty(\Omega)$ we get, that $\Delta z + \kappa^2 z = 0$ as a distribution. But the zero distribution is in $L^2(\Omega)$ and therefore it holds that $\Delta z + \kappa^2 z = 0$ in $L^2(\Omega)$, which implies $z \in \mathcal{H}_{\Delta+\kappa^2}(\Omega)$. □

The space $L^2(\Omega)$ can be written as $L^2(\Omega) = \ker(\Lambda_\kappa^N) \oplus \ker(\Lambda_\kappa^N)^\perp$ and restricting Λ_κ^N to the orthogonal complement of its kernel leads to

$$\Lambda_\kappa^N : \ker(\Lambda_\kappa^N)^\perp \to \operatorname{ran}(\Lambda_\kappa^N).$$

This operator is bijective and hence invertible. With this consideration and the previous two lemmata we receive the following theorem.

Theorem 3.8. *Let $\kappa \geq 0$ and κ^2 not be an eigenvalue of the Dirichlet Laplacian. Let $g \in H^{1/2}(\partial\Omega)$ be given such that $\gamma_1 u_g \in \operatorname{ran}(\Lambda_\kappa^N)$ and $f \in \operatorname{ran}(\Lambda_\kappa^N)$. Then the inverse problem* (3.1) *has a unique solution $\bar{z} \in \mathcal{H}_{\Delta+\kappa^2}(\Omega)$. All other solutions are of the form*

$$z = \bar{z} + w \qquad \text{with } w \in (\Delta + \kappa^2)(H_0^2(\Omega)).$$

We know that u_g solves the Dirichlet boundary value problem for the homogeneous Helmholtz equation in (3.9) with Dirichlet datum g. In order to apply Theorem 3.8 the condition

$$\gamma_1 u_g \in \operatorname{ran}(\Lambda_\kappa^N) = \operatorname{ran}(\gamma_1|_{\ker(\gamma_0)}),$$

has to be satisfied. Although this condition is difficult to check in practice, it is fulfilled if $u_g \in \ker(\gamma_0)$, i.e., $\gamma_0 u_g = 0$, which implies that $g = 0$. As a consequence the solution u_g of (3.9) has to be zero and thus, we have an overdetermined system.

Remark 3.3. To ensure unique solvability of the inverse problem (3.1) with this approach, we restrict ourselves to the case where the Dirichlet datum $g = 0$.

Hence, in the following we assume $g = 0$ and that the Neumann datum f is given. In the next step we consider another ansatz, where we will show a different splitting of $L^2(\Omega)$. The idea of this approach is to show at first that the source term z is unique up to elements in $\ker(\Lambda_\kappa^N)$. If we can also identify the element in the kernel uniquely, then our source z is unique. This can be shown if we assume additionally that the source z satisfies $(\Delta - \kappa^2)z = F$ for $F \in L^2(\Omega)$. Hence, we introduce for $F \in L^2(\Omega)$ the space

$$\mathcal{H}_{\Delta-\kappa^2,F}(\Omega) := \{\hat{z} \in L^2(\Omega) : (\Delta - \kappa^2)\hat{z} = F\} \subset L^2(\Omega).$$

For this class of sources the reconstruction by boundary data measurements at a single wave number is unique and the method to reconstruct the source involves solving a Bi–Helmholtz–type equation. Firstly, we start with the splitting of $L^2(\Omega)$.

Lemma 3.9 ([3, Lem. 3.1])**.** *We introduce the following space*

$$\mathcal{H}_{\Delta-\kappa^2}(\Omega) := \{z \in L^2(\Omega) : \Delta z - \kappa^2 z = 0 \text{ in } L^2(\Omega)\}.$$

Now let $\kappa \geq 0$ and κ^4 not be an eigenvalue of the Bilaplacian. Then the splitting

$$L^2(\Omega) = \mathcal{H}_{\Delta-\kappa^2}(\Omega)\dot{+}(\Delta + \kappa^2)(H_0^2(\Omega)),$$

holds and $\dot{+}$ denotes a direct sum in the sense of linear spaces.

Proof. Let $z \in L^2(\Omega)$ be arbitrarily given. For u_z the solution of (3.8) we get that $u_z \in H_\Delta^{3/2}(\Omega) \cap H_0^1(\Omega)$ and $\gamma_1 u_z = \Lambda_\kappa^N(z) \in \operatorname{ran}(\gamma_1|_{\ker(\gamma_0)})$. Furthermore, we have to show that the Bi–Helmholtz–type equation

$$\begin{aligned} \Delta^2 v(x) - \kappa^4 v(x) &= 0 && \text{for } x \in \Omega, \\ v(x) &= 0 && \text{for } x \in \partial\Omega, \\ \frac{\partial v}{\partial \underline{n}}(x) &= \Lambda_\kappa^N(z) && \text{for } x \in \partial\Omega, \end{aligned}$$

is well–posed in $H^{3/2}_{\Delta}(\Omega)$. By Assumption (D3) κ^4 is not an eigenvalue of the Bilaplacian. Therefore, we split the Bi–Helmholtz–type equation as

$$0 = (\Delta^2 - \kappa^4)v = (\Delta - \kappa^2)(\Delta + \kappa^2)v.$$

Now either $(\Delta - \kappa^2)v = 0$ or $(\Delta + \kappa^2)v = 0$ with $\gamma_0 v = 0$ on $\partial\Omega$ has to be satisfied. Since κ^2 is not an eigenvalue of the Dirichlet Laplacian, the operator $(\Delta + \kappa^2)$ with Dirichlet boundary conditions is invertible. Hence, $(\Delta - \kappa^2)v = 0$ and v having homogeneous Dirichlet datum has to be satisfied. This implies $v \in H^{3/2}_{\Delta}(\Omega)$. With $v, u_z \in H^{3/2}_{\Delta}(\Omega)$ we define $w := u_z - v \in H^{3/2}_{\Delta}(\Omega)$. Moreover, it holds that $\gamma_0 w = 0$ and $\gamma_1 w = \gamma_1 u_z - \gamma_1 v = 0$. By [6, Cor. 4.2] we derive that $w \in H^2_0(\Omega)$. We can rewrite z as

$$\begin{aligned} z = (\Delta + \kappa^2)u_z &= (\Delta + \kappa^2)(v + w) \\ &= \underbrace{(\Delta + \kappa^2)v}_{\in \mathcal{H}_{\Delta-\kappa^2}(\Omega)} + \underbrace{(\Delta + \kappa^2)w}_{\in (\Delta+\kappa^2)(H^2_0(\Omega))}, \end{aligned}$$

and obtain that an arbitrary $L^2(\Omega)$ function is the sum of a function in $\mathcal{H}_{\Delta-\kappa^2}(\Omega)$ and a function in $(\Delta + \kappa^2)(H^2_0(\Omega))$. Hence, $L^2(\Omega) = \mathcal{H}_{\Delta-\kappa^2}(\Omega) + (\Delta + \kappa^2)(H^2_0(\Omega))$ and it remains to check that

$$\mathcal{H}_{\Delta-\kappa^2}(\Omega) \cap (\Delta + \kappa^2)(H^2_0(\Omega)) = \{0\}.$$

Let u be an element in this intersection. Then it holds true that

$$\Delta u - \kappa^2 u = 0 \quad \text{and} \quad u = (\Delta + \kappa^2)v \quad \text{for } v \in H^2_0(\Omega).$$

Combining these two properties leads to

$$0 = \Delta u - \kappa^2 u = \Delta(\Delta + \kappa^2)v - \kappa^2(\Delta + \kappa^2)v = \Delta^2 v - \kappa^4 v.$$

Since the Cauchy data of v are given and by Assumption (D3) we know that κ^4 is not an eigenvalue of the Bi–Laplacian, we obtain by Theorem 2.3 that the unique solution is $v = 0$. This implies that $u = 0$, which completes the proof. □

With the splitting from Lemma 3.9 it holds that $L^2(\Omega)/\ker(\Lambda^N_\kappa) = \mathcal{H}_{\Delta-\kappa^2}(\Omega)$. Now we define

$$\Lambda^N_\kappa : \mathcal{H}_{\Delta-\kappa^2}(\Omega) \to \operatorname{ran}(\Lambda^N_\kappa),$$

which is bijective and hence invertible. In this setting we get the same result as in Theorem 3.8 but this time we get a unique solution $z \in \mathcal{H}_{\Delta-\kappa^2}(\Omega)$, which means that our source satisfies

$$(\Delta - \kappa^2)z = 0.$$

Theorem 3.10 ([3, cf. Lem. 2.2])**.** *Let $\kappa \geq 0$ and κ^4 not be an eigenvalue of the Bilaplacian* (2.6)*. Let $g = 0$ and $f \in \operatorname{ran}(\Lambda_\kappa^N)$ be given. Then the inverse problem* (3.1) *has a unique solution $\bar{z} \in \mathcal{H}_{\Delta-\kappa^2}(\Omega)$. All other solutions are of the form*

$$z = \bar{z} + w \qquad \text{with } w \in (\Delta + \kappa^2)(H_0^2(\Omega)).$$

Our goal is now to determine the element in $(\Delta + \kappa^2)(H_0^2(\Omega))$. Hence, we use the additional information that our source satisfies $z \in \mathcal{H}_{\Delta-\kappa^2,F}(\Omega)$ for $F \in L^2(\Omega)$. By Lemma 3.9 we get the decomposition of $L^2(\Omega)$ into

$$L^2(\Omega) = \mathcal{H}_{\Delta-\kappa^2}(\Omega) \dot{+} (\Delta + \kappa^2)(H_0^2(\Omega)).$$

Therefore, taking $h \in \mathcal{H}_{\Delta-\kappa^2}(\Omega)$ and $v_F \in H_0^2(\Omega)$ we can write $z \in L^2(\Omega)$ as

$$z = h + (\Delta + \kappa^2)v_F.$$

Knowing that $z \in \mathcal{H}_{\Delta-\kappa^2,F}(\Omega)$ and $h \in \mathcal{H}_{\Delta-\kappa^2}(\Omega)$ we obtain

$$F = (\Delta - \kappa^2)z = (\Delta^2 - \kappa^4)v_F \quad \text{for } v_F \in H_0^2(\Omega).$$

Since $F \in L^2(\Omega)$ and the boundary data for v_F are known, we can determine v_F uniquely. As a consequence also

$$w_F = (\Delta + \kappa^2)v_F \in L^2(\Omega),$$

is uniquely determined. This implies that z can be written as $z = h + w_F$.

Corollary 3.11 ([3, Thm. 2.3])**.** *Let $g = 0$ and $f \in \operatorname{ran}(\Lambda_\kappa^N)$ be given. The inverse source problem to find $z \in \mathcal{H}_{\Delta-\kappa^2,F}(\Omega)$ such that*

$$\begin{aligned} \Delta u_F(x) + \kappa^2 u_F(x) &= z(x) && \text{for } x \in \Omega, \\ u_F(x) &= 0 && \text{for } x \in \partial\Omega, \\ \frac{\partial u_F}{\partial \underline{n}}(x) &= f(x) && \text{for } x \in \partial\Omega, \end{aligned} \tag{3.10}$$

admits a unique solution.

Proof. We have shown in Theorem 3.10 that z is unique up to elements in $\ker(\Lambda_\kappa^N)$. With $\bar{z} \in \mathcal{H}_{\Delta-\kappa^2}(\Omega)$ uniquely determined, we we can write

$$z = \bar{z} + w \qquad \text{with } w \in (\Delta + \kappa^2)(H_0^2(\Omega)).$$

By the previous discussion, we get that this arbitrary w satisfies $w = w_F$ and is therefore unique. As a consequence, the source z as sum of two uniquely determined functions is unique. □

Let the boundary data measurement $f \in H^{1/2}(\partial\Omega) \subset \operatorname{ran}(\Lambda_\kappa^N)$ be given. If we have the source $z \in \mathcal{H}_{\Delta-\kappa^2,F}(\Omega)$, we can reconstruct it by applying $(\Delta - \kappa^2)$ to our partial differential equation in the inverse problem (3.10). This leads to the following Bi–Helmholtz–type equation with the right hand side F

$$\begin{aligned} \Delta^2 u_F(x) - \kappa^4 u_F(x) &= F(x) && \text{for } x \in \Omega, \\ u_F(x) &= 0 && \text{for } x \in \partial\Omega, \\ \frac{\partial u_F}{\partial \underline{n}}(x) &= f(x) && \text{for } x \in \partial\Omega. \end{aligned}$$

Here we can determine u_F by solving the Bi–Helmholtz–type equation and as a consequence we receive the source z by computing $z = \Delta u_F + \kappa^2 u_F$.

3.1.3 Operator mapping the source onto the Dirichlet trace

As we have seen in Section 3.1.2 we need further information about our source z to ensure unique solvability of the inverse problem (3.1). In addition, the condition from Remark 3.3 requiring the Dirichlet datum $g = 0$ is sufficient. In the following we want to circumvent the constraint $g = 0$. Contrary to the previous approach, where we have only considered the Dirichlet datum for our derivation we now investigate an ansatz, where the Neumann datum is used. Hence, our next step is to do the analysis for this approach. We suppose that Assumptions 3.1 hold and start by considering the model problem

$$\begin{aligned} \Delta u + \kappa^2 u &= z && \text{in } \Omega, \\ \gamma_1 u &= f && \text{on } \partial\Omega, \end{aligned}$$

where $f \in H^{-1/2}(\partial\Omega)$ and $z \in L^2(\Omega)$. This problem is uniquely solvable by Theorem 2.2 with $u \in H^1(\Omega)$. Since the problem is linear the solution u can be written as $u = u_z + u_f$ with u_z solving

$$\begin{aligned} \Delta u_z + \kappa^2 u_z &= z && \text{in } \Omega, \\ \gamma_1 u_z &= 0 && \text{on } \partial\Omega, \end{aligned} \tag{3.11}$$

and u_f solving

$$\begin{aligned} \Delta u_f + \kappa^2 u_f &= 0 && \text{in } \Omega, \\ \gamma_1 u_f &= f && \text{on } \partial\Omega. \end{aligned} \tag{3.12}$$

The problems (3.11) and (3.12) are uniquely solvable with $u_z, u_f \in H^1(\Omega)$ by Theorem 2.2. Now let us introduce the operator

$$\begin{aligned} \Lambda_\kappa^D : L^2(\Omega) &\to L^2(\partial\Omega) \\ z &\mapsto \gamma_0 u_z. \end{aligned}$$

In the inverse problem (3.1) the Dirichlet trace satisfies

$$g = \gamma_0 u = \gamma_0(u_z + u_f) = \Lambda_\kappa^D(z) + \gamma_0 u_f.$$

The Dirichlet boundary condition in the inverse problem (3.1) can be rewritten as

$$\Lambda_\kappa^D(z) = g - \gamma_0 u_f,$$

and hence we can determine the source $z \in L^2(\Omega)$ when solving this operator equation. Therefore, we have to characterise the mapping properties of Λ_κ^D, especially the kernel and the range of this operator.

Lemma 3.12. *Let $\kappa \geq 0$ such that κ^2 is not an eigenvalue of the Neumann Laplacian. Then*

$$\operatorname{ran}(\Lambda_\kappa^D) = \operatorname{ran}(\gamma_0|_{\ker(\gamma_1)}),$$

is a dense proper linear subspace of $H^1(\partial\Omega)$. Furthermore, for the kernel the same characterisation as in Lemma 3.6 holds, namely

$$\ker(\Lambda_\kappa^D) = (\Delta + \kappa^2)(H_0^2(\Omega)).$$

Proof. For $z \in L^2(\Omega)$ problem (3.11) admits a unique solution $u_z \in H^1_\Delta(\Omega)$ with $\gamma_1 u_z = 0$. Therefore, $u_z \in \ker(\gamma_1)$ and by Lemma 1.8 we get that $u_z \in H^{3/2}_\Delta(\Omega)$. Consequently, we can write the operator Λ_κ^D as

$$\Lambda_\kappa^D : L^2(\Omega) \overset{(\Delta+\kappa^2)^{-1}}{\to} H^{3/2}_\Delta(\Omega) \cap H_{N,0}(\Omega) \overset{\gamma_0}{\to} \operatorname{ran}(\gamma_0|_{H^{3/2}_\Delta(\Omega)\cap H_{N,0}(\Omega)}),$$

where

$$H_{N,0}(\Omega) := \{v \in H^1_\Delta(\Omega) : \gamma_1 v = 0 \text{ on } \partial\Omega\}.$$

Since we can characterise the space to which γ_0 is restricted as $\ker(\gamma_1|_{H^{3/2}_\Delta(\Omega)})$ we get

$$\operatorname{ran}(\Lambda_\kappa^D) = \operatorname{ran}(\gamma_0|_{\ker(\gamma_1)}).$$

By [5, Lem. 8.2] this is a dense proper linear subspace of $H^1(\partial\Omega)$. In the next step we want to characterise the kernel of the operator. It holds that $z \in \ker(\Lambda_\kappa^D)$ if and only if

$$\begin{aligned} u_z = (\Delta + \kappa^2)^{-1} z &\in \ker(\gamma_0|_{H^{3/2}_\Delta(\Omega)\cap H_{N,0}(\Omega)}) \\ &= \{v \in H^{3/2}_\Delta(\Omega) : \gamma_0 v = \gamma_1 v = 0 \text{ on } \partial\Omega\} \\ &= H_0^2(\Omega), \end{aligned}$$

where the last equality holds due to [6, Cor. 4.2 (i)]. □

For a more regular domain than a Lipschitz domain we get some characterisations for $\operatorname{ran}(\Lambda_\kappa^D)$.

Remark 3.4 ([6, Thm. 4.10 (ii)]). Let Ω be a $C^{1,r}$ domain for $r \in (1/2, 1]$ then it holds that

$$\operatorname{ran}(\Lambda_\kappa^D) = \operatorname{ran}(\gamma_0|_{\ker(\gamma_1)}) = H^{3/2}(\partial\Omega).$$

Remark 3.5 ([6, Thm. 4.9 (ii)]). In the case that Ω is a quasi convex domain it holds that

$$\operatorname{ran}(\Lambda_\kappa^D) = \operatorname{ran}(\gamma_0|_{\ker(\gamma_1)}) = \{\varphi \in H^1(\partial\Omega) : \nabla_{\tan}\varphi \in H^{1/2}(\partial\Omega)^d\},$$

where the tangential gradient operator is defined as

$$\begin{aligned} \nabla_{\tan} : H^1(\partial\Omega) &\to L^2(\partial\Omega)^d \\ u &\mapsto \left(\sum_{j=1}^{d} n_j(n_j\partial_k - n_k\partial_j)u\right)_{k=1,\dots,d}^{T}. \end{aligned}$$

So we know the range of Λ_κ^D as well as that $\Lambda_\kappa^D : L^2(\Omega)/\ker(\Lambda_\kappa^D) \to \operatorname{ran}(\Lambda_\kappa^D)$ is an isomorphism. Since $\ker(\Lambda_\kappa^D)$ is a closed subspace we can write $L^2(\Omega)$ as the orthogonal decomposition

$$L^2(\Omega) = \ker(\Lambda_\kappa^D) \oplus \ker(\Lambda_\kappa^D)^\perp.$$

Due to the equality $\ker(\Lambda_\kappa^N) = \ker(\Lambda_\kappa^D)$, we know that their orthogonal complements have to be identical. This means that

$$\ker(\Lambda_\kappa^D)^\perp = \mathcal{H}_{\Delta+\kappa^2}(\Omega).$$

Restricting the operator Λ_κ^D to the orthogonal complement of its kernel leads to

$$\Lambda_\kappa^D : \ker(\Lambda_\kappa^D)^\perp \to \operatorname{ran}(\Lambda_\kappa^D).$$

This operator is bijective and hence invertible. With this consideration and the previous lemma we get the following theorem.

Theorem 3.13. *Let $\kappa \geq 0$ and κ^2 not be an eigenvalue of the Neumann Laplacian. Let $g \in \operatorname{ran}(\Lambda_\kappa^D)$ and $f \in H^{-1/2}(\partial\Omega)$ be given such that $\gamma_0 u_f \in \operatorname{ran}(\Lambda_\kappa^D)$. Then the inverse problem* (3.1) *has a unique solution $\bar{z} \in \mathcal{H}_{\Delta+\kappa^2}(\Omega)$. All other solutions are of the form*

$$z = \bar{z} + w \qquad \text{with } w \in (\Delta + \kappa^2)(H_0^2(\Omega)).$$

We know that u_f is solving the Neumann boundary value problem for the homogeneous Helmholtz equation in (3.12) with Neumann datum f. In order to apply Theorem 3.13 the condition

$$\gamma_0 u_f \in \operatorname{ran}(\Lambda_\kappa^D) = \operatorname{ran}(\gamma_0|_{\ker(\gamma_1)}),$$

has to be satisfied. This condition is difficult to verify in practice. However, it is satisfied if $u_f \in \ker(\gamma_1)$, i.e., $\gamma_1 u_f = 0$, which implies $f = 0$. As a consequence the solution u_f of (3.12) has to be zero and thus, we have an overdetermined system.

Remark 3.6. To ensure unique solvability of the inverse problem (3.1) with this approach, we restrict ourselves to the case where the Neumann datum $f = 0$.

In the following we assume $f = 0$ and that the Dirichlet datum g is given. We now consider the approach using Lemma 3.9 for the splitting of $L^2(\Omega)$, which states $L^2(\Omega) = \mathcal{H}_{\Delta-\kappa^2}(\Omega)\dot{+}(\Delta+\kappa^2)(H_0^2(\Omega))$. In this case $L^2(\Omega)/\ker(\Lambda_\kappa^D) = \mathcal{H}_{\Delta-\kappa^2}(\Omega)$ holds. Now we define

$$\Lambda_\kappa^D : \mathcal{H}_{\Delta-\kappa^2}(\Omega) \to \operatorname{ran}(\Lambda_\kappa^D),$$

which is bijective and hence invertible. In this setting we get the same result as in Theorem 3.13 but this time we get a unique solution $z \in \mathcal{H}_{\Delta-\kappa^2}(\Omega)$.

Theorem 3.14. *Let $\kappa \geq 0$ and κ^4 not be an eigenvalue of the Bilaplacian. Let $g \in \operatorname{ran}(\Lambda_\kappa^D)$ and $f = 0$ be given. Then the inverse problem (3.1) has a unique solution $\bar{z} \in \mathcal{H}_{\Delta-\kappa^2}(\Omega)$. All other solutions are of the form*

$$z = \bar{z} + w \qquad \text{with } w \in (\Delta + \kappa^2)(H_0^2(\Omega)).$$

To get a unique solution our goal is now to determine the element in $(\Delta+\kappa^2)(H_0^2(\Omega))$. Therefore, we make use of the information that our source satisfies $z \in \mathcal{H}_{\Delta-\kappa^2,F}(\Omega)$ for $F \in L^2(\Omega)$. This leads by the same argumentation as before Corollary 3.11 to the following Corollary.

Corollary 3.15. *Let $g \in \operatorname{ran}(\Lambda_\kappa^D)$ and $f = 0$ be given. The inverse source problem to find $z \in \mathcal{H}_{\Delta-\kappa^2,F}(\Omega)$ such that*

$$\begin{aligned} \Delta u_F(x) + \kappa^2 u_F(x) &= z(x) && \text{for } x \in \Omega, \\ u_F(x) &= g(x) && \text{for } x \in \partial\Omega, \\ \frac{\partial u_F}{\partial \underline{n}}(x) &= 0 && \text{for } x \in \partial\Omega, \end{aligned} \tag{3.13}$$

admits a unique solution.

Proof. This can be proven analogously to Corollary 3.11. □

Let the boundary data measurement $g \in H^{3/2}(\partial\Omega) \subset \operatorname{ran}(\Lambda_\kappa^D)$ be given. If the source satisfies $z \in \mathcal{H}_{\Delta-\kappa^2,F}(\Omega)$, we can reconstruct it by applying $(\Delta - \kappa^2)$ to our partial differential equation in the inverse problem (3.13). This leads to the following Bi–Helmholtz–type equation with the right hand side F

$$\begin{aligned} \Delta^2 u_F(x) - \kappa^4 u_F(x) &= F(x) && \text{for } x \in \Omega, \\ u_F(x) &= g(x) && \text{for } x \in \partial\Omega, \\ \frac{\partial u_F}{\partial \underline{n}}(x) &= 0 && \text{for } x \in \partial\Omega. \end{aligned}$$

Here we can determine u_F by solving the Bi–Helmholtz–type equation and as a consequence we receive the source z by computing $z = \Delta u_F + \kappa^2 u_F$.

3.1.4 Method via a Bi–Helmholtz–type equation

In Section 3.1.2 and 3.1.3 we have considered two approaches to show that under the assumption $z \in \mathcal{H}_{\Delta-\kappa^2,F}(\Omega)$ the inverse problem (3.1) admits a unique solution. In the first approach we have imposed the restrictions $g = 0$ (see Remark 3.3) and $f \in \operatorname{ran}(\Lambda_\kappa^N)$. In contrast, in the second ansatz we restrict ourselves to $f = 0$ (see Remark 3.6) and $g \in \operatorname{ran}(\Lambda_\kappa^D)$. The goal of this section is to investigate the inverse problem without imposing $g = 0$ or $f = 0$ by using a Bi–Helmholtz–type equation. For this purpose, additional regularity assumptions on the domain Ω and the boundary data g and f are required. We start by formulating the assumptions for this section.

Assumptions 3.3.

(E1) Let $\Omega \subset \mathbb{R}^d, d = 2, 3$, be a bounded domain with $\mathcal{C}^{1,1}$–boundary $\partial\Omega$.

(E2) The Cauchy data $g \in H^{3/2}(\partial\Omega)$ and $f \in H^{1/2}(\partial\Omega)$ are given.

(E3) The wave number $\kappa \geq 0$ satisfies that κ^2 is neither an eigenvalue of the Dirichlet Laplacian (2.1) nor an eigenvalue of the Neumann Laplacian (2.4). Additionally, κ^4 is not an eigenvalue of the Bi–Laplacian (2.6).

Recall that, for fixed $F \in L^2(\Omega)$, the space $\mathcal{H}_{\Delta-\kappa^2,F}(\Omega)$ is defined by

$$\mathcal{H}_{\Delta-\kappa^2,F}(\Omega) = \{\hat{z} \in L^2(\Omega) : (\Delta - \kappa^2)\hat{z} = F\}.$$

With this notation we can formulate the following Lemma concerning the uniqueness of the source reconstruction.

Lemma 3.16. *Let $g \in H^{3/2}(\partial\Omega)$ and $f \in H^{1/2}(\partial\Omega)$ be given. Under the Assumptions 3.3 the inverse source problem: find $z \in \mathcal{H}_{\Delta-\kappa^2,F}(\Omega)$ such that*

$$\begin{aligned} \Delta u(x) + \kappa^2 u(x) &= z(x) && \text{for } x \in \Omega, \\ u(x) &= g(x) && \text{for } x \in \partial\Omega, \\ \frac{\partial u}{\partial \underline{n}}(x) &= f(x) && \text{for } x \in \partial\Omega, \end{aligned} \tag{3.14}$$

admits a unique solution.

Proof. We apply the operator $(\Delta - \kappa^2)$ to the Helmholtz equation and make use of $z \in \mathcal{H}_{\Delta-\kappa^2,F}(\Omega)$. Hence, we obtain that

$$(\Delta^2 - \kappa^4)u(x) = (\Delta - \kappa^2)z(x) = F(x) \qquad \text{for } x \in \Omega,$$

and u satisfies the boundary conditions $\gamma_0 u = g$ and $\gamma_1 u = f$. The Bi–Helmholtz–type equation for the fixed right hand side $F \in L^2(\Omega)$ and the given boundary data has a unique solution $u \in H^2(\Omega)$ as shown in Theorem 2.3. Hence, the source z is uniquely determined by $z = (\Delta + \kappa^2)u$. □

Contrary to the previous two sections we are now able to solve problem (3.14) without setting the Dirichlet datum or the Neumann datum to zero, i.e., we can solve it now for general boundary data assuming additional regularity on the domain and the Cauchy data.

3.2 Uniqueness from boundary data at several wave numbers

In Section 3.1.1 we have shown that we can determine point sources from the boundary data at a single wave number. However, for Dirac distributions supported on spheres and characteristic functions on hollow and solid balls it is only possible to retrieve the centers and expressions, which include both the intensities and the radii. Hence, we can not recover this type of sources for a single wave number. Afterwards, we have proven in Section 3.1.4 that the inverse problem (3.1) is uniquely solvable from boundary data measurements at a single wave number, provided that some additional information about the source is available. In this section we are interested in whether the source can be determined uniquely from boundary data at multiple wave numbers. The analysis in this section is based on [3, Sec.3].
We assume $z \in L^2(\Omega)$ and $\kappa \in I$, where $I \subset \mathbb{R}^+$ is an open non empty interval. For each $\kappa \in I$ we consider the problem

$$\begin{aligned} \Delta u_z^\kappa + \kappa^2 u_z^\kappa &= z && \text{in } \Omega, \\ u_z^\kappa &= 0 && \text{on } \partial\Omega, \end{aligned} \tag{3.15}$$

and the map $\Lambda_\kappa^N(z) = \gamma_1 u_z^\kappa$ on $\partial\Omega$, which is depending on various wave numbers $\kappa \in I$. For $\kappa \in I$ we further define the map

$$\kappa \mapsto \Lambda_\kappa^N(z).$$

The inverse problem consists of recovering the source term $z \in L^2(\Omega)$ from the knowledge of the boundary data $g_\kappa = 0$ and $f_\kappa \in H^{1/2}(\partial\Omega)$ at multiple wave numbers $\kappa \in I$. The uniqueness result is stated in the following theorem.

Theorem 3.17 ([3, Thm. 3.1])**.** *Let $z \in L^2(\Omega)$ and further let $\kappa \in I$ be in some open, non empty interval $I \subset \mathbb{R}^+$. If the map $\kappa \mapsto \Lambda_\kappa^N(z)$ is known for every $\kappa \in I$, then the source z is uniquely determined in the $L^2(\Omega)$ sense.*

Proof. We show injectivity of the operator Λ_κ^N. Therefore, let z_1, $z_2 \in L^2(\Omega)$ be arbitrary such that

$$\Lambda_\kappa^N(z_1) = \Lambda_\kappa^N(z_2) \qquad \forall \kappa \in I,$$

where $u^{\kappa}_{z_i} \in H^1_0(\Omega)$ for $i = 1, 2$ is the solution of (3.15). Using the reciprocity gap functional from Definition 3.1 for a test function $v \in \mathcal{H}^1_{\Delta+\kappa^2}(\Omega)$ and equation (3.3) leads, for $i = 1, 2$, to

$$\int_\Omega z_i v \,\mathrm{d}x = \int_{\partial\Omega} \Lambda_\kappa(z_i)\gamma_0 v \,\mathrm{d}s_x.$$

Because of the assumption $\Lambda^N_\kappa(z_1) = \Lambda^N_\kappa(z_2)$ we derive

$$\int_\Omega (z_1 - z_2) v \,\mathrm{d}x = 0 \qquad \forall v \in \mathcal{H}^1_{\Delta+\kappa^2}(\Omega).$$

As test functions we choose plane waves, which are defined by

$$v(x) = v_{\kappa,\xi}(x) = e^{-i\kappa x\cdot\xi} \qquad \text{for } \kappa \in I, \xi \in \partial B(0,1). \tag{3.16}$$

We can easily check that $v_{\kappa,\xi} \in \mathcal{H}^1_{\Delta+\kappa^2}(\Omega)$. Using the plane waves as test functions leads immediately to the Fourier transformation as defined in Definition 1.13. For every $\kappa \in I$ and every $\xi \in \partial B(0,1)$ it holds that

$$\begin{aligned} 0 &= \int_\Omega (z_1 - z_2)(x) e^{-i\kappa x\cdot\xi} \,\mathrm{d}x \\ &= \int_{\mathbb{R}^d} \chi_\Omega(x)(z_1 - z_2)(x) e^{-ix\cdot\kappa\xi} \,\mathrm{d}x \\ &= (2\pi)^{d/2} \mathcal{F}[(z_1 - z_2)\chi_\Omega](\kappa\xi), \end{aligned}$$

where χ_Ω denotes the characteristic function of Ω, defined by

$$\chi_\Omega(x) = \begin{cases} 1, & \text{if } x \in \Omega, \\ 0, & \text{if } x \notin \Omega. \end{cases}$$

Hence,

$$\mathcal{F}[(z_1 - z_2)\chi_\Omega](\kappa\xi) = 0 \qquad \text{on } I \times \partial B(0,1),$$

and is analytic on $\mathbb{R}^d$ due to Lemma 1.10. In order to derive equality on $\mathbb{R}^d$ we will apply the identity theorem (Theorem 1.11). Since the set $I \times \partial B(0,1)$ has an accumulation point in $\mathbb{R}^d$ we get

$$\mathcal{F}[(z_1 - z_2)\chi_\Omega] = 0 \qquad \text{on } \mathbb{R}^d.$$

Applying Plancherel's formula (1.3) leads to

$$0 = \|\mathcal{F}[(z_1 - z_2)\chi_\Omega]\|^2_{L^2(\mathbb{R}^d)} = \|(z_1 - z_2)\chi_\Omega\|^2_{L^2(\mathbb{R}^d)} = \|z_1 - z_2\|^2_{L^2(\Omega)},$$

and from this we derive $z_1 = z_2$ almost everywhere. Therefore, the source is determined in the sense of $L^2(\Omega)$, which completes the proof. □

As shown in Theorem 3.17 we obtain uniqueness of the inverse problem (3.1) in the L^2–sense if the boundary data are given for multiple wave numbers $\kappa \in I$. The corresponding numerical analysis and numerical examples will be presented in Section 4.2.

4 Numerical illustration

The results of Section 3 have demonstrated that the reconstruction of a source is unique if we consider point sources at a single wave number or if the boundary data are given for multiple wave numbers. To complement this theoretical analysis we now present numerical methods for both settings. We start by considering the reconstruction of point sources from boundary data measurements at a single wave number in Section 4.1. Afterwards in Section 4.2 a numerical method for reconstructing L^2–sources from the Cauchy data at multiple wave numbers will be discussed. Both sections are complemented by numerical examples.

4.1 Numerical method for the reconstruction at a single wave number

We have shown in Section 3.1.1 that the reconstruction of Dirac distributions on spheres and characteristic functions on balls is not unique since it is not possible to recover the intensities and the radii at the same time. However, Theorem 3.1 demonstrates that point sources solving the inverse problem (3.1) can be identified uniquely. Thus, in the numerical part we discuss an algebraic method to reconstruct point sources from boundary data measurements at a single wave number, based on El Badia and Nara in [11]. As mentioned above, we conclude this section by presenting numerical examples.

Description of the numerical method

We consider the inverse problem of the Helmholtz equation for a bounded Lipschitz domain $\Omega \subset \mathbb{R}^3$ under Assumptions 3.2. The inverse problem is formulated as follows: find the point source $z = \sum_{j=1}^{n} \lambda_j \delta_{y_j}$ such that

$$\begin{aligned} \Delta u(x) + \kappa^2 u(x) &= z(x) && \text{for } x \in \Omega, \\ u(x) &= g(x) && \text{for } x \in \partial\Omega, \\ \frac{\partial u}{\partial \underline{n}}(x) &= f(x) && \text{for } x \in \partial\Omega, \end{aligned} \tag{4.1}$$

where $n \in \mathbb{N}$, $y_j \in \Omega$ and $\lambda_j \in \mathbb{C} \setminus \{0\}$. The goal is to reconstruct the source by determining the number of point sources n, the intensities λ_j and the coordinates of

the point sources $\{y_{j,1}, y_{j,2}, y_{j,3}\}$ for $j = 1, ..., n$ from the Cauchy data g and f at a single wave number $\kappa \in \mathbb{R}^+$. This will be achieved by applying an algebraic method, based on the reciprocity gap functional, which has been defined in Definition 3.1 by

$$R(v) = \int_{\partial\Omega} (f\gamma_0 v - g\gamma_1 v)\,\mathrm{d}s_x, \qquad \forall v \in \mathcal{H}^1_{\Delta+\kappa^2}(\Omega).$$

The starting point of this method is the equation outlined in (3.3), where plugging in the representation of our source leads to

$$\sum_{j=1}^{n} \lambda_j v(y_j) = R(v), \qquad \forall v \in \mathcal{H}^1_{\Delta+\kappa^2}(\Omega). \tag{4.2}$$

In the next step we define two families of test functions in $\mathcal{H}^1_{\Delta+\kappa^2}(\Omega)$ given by

$$v_m := (x + \mathrm{i}y)^m \exp(-\mathrm{i}\kappa z), \quad w_m := (x + \mathrm{i}y)^m \exp(\mathrm{i}\kappa z) \qquad \text{for } m \in \mathbb{N}_0. \tag{4.3}$$

It can easily be checked, that $v_m, w_m \in \mathcal{H}^1_{\Delta+\kappa^2}(\Omega)$ for all $m \in \mathbb{N}_0$. We start by using the test functions v_m. Inserting v_m into (4.2) gives us the following system of equations

$$\sum_{j=1}^{n} \lambda_j (y_{j,1} + \mathrm{i}y_{j,2})^m \exp(-\mathrm{i}\kappa y_{j,3}) = R(v_m), \quad \forall m \in \mathbb{N}_0.$$

Denoting $P_j := y_{j,1} + \mathrm{i}y_{j,2}$, $c_j := \lambda_j \exp(-\mathrm{i}\kappa y_{j,3})$ and $\alpha_m := R(v_m)$ leads to

$$\sum_{j=1}^{n} c_j P_j^m = \alpha_m \quad \forall m \in \mathbb{N}_0. \tag{4.4}$$

The values α_m can be computed numerically for all $m \in \mathbb{N}_0$. The following theorem states that the source can be reconstructed if an upper bound $N \in \mathbb{N}$ is known such that the number of point sources satisfies $n \leq N$.

Theorem 4.1 (cf. [10, Thm. 2])**.** *Suppose, that an upper bound N for the number of point sources n is known. Then the quantities n, λ_j and y_j for $j = 1, ..., n$ are determined by $2N$ numbers α_m for $0 \leq m \leq 2N - 1$.*

The proof of this theorem is omitted and can be found in [10, Sec.4]. Instead, the main steps of the derivation are presented. The first step is to determine the number of sources n. In [10, Lem. 2] it is shown that the Hankel matrix $H \in \mathbb{C}^{N\times N}$ defined by

$$H = \begin{bmatrix} \alpha_0 & \alpha_1 & \alpha_2 & \cdots & \cdots & \alpha_{N-1} \\ \alpha_1 & \alpha_2 & \alpha_3 & \cdots & \cdots & \alpha_N \\ \alpha_2 & \alpha_3 & \alpha_4 & \cdots & \cdots & \alpha_{N+1} \\ \vdots & \vdots & \vdots & \vdots & \vdots & \vdots \\ \alpha_{N-1} & \alpha_N & \alpha_{N+1} & \cdots & \cdots & \alpha_{2N-2} \end{bmatrix},$$

has rank n. As outlined in [10, Rem. 3] computing the rank of H as the number of linearly independent columns is numerically unstable. Hence, this approach is not applicable since the entries of H are computed numerically. However, one can do a singular value decomposition with a numerical threshold $\varepsilon > 0$. The number of singular values greater than ε gives the estimate of n.
With the number of point sources identified we proceed to recover the remaining quantities in (4.4), which are P_j and c_j for $j = 1, ..., n$. Therefore, we have to introduce three auxiliary matrices. Namely the Vandermonde matrix V, which is defined as

$$V = \begin{bmatrix} 1 & 1 & 1 & \cdots & \cdots & 1 \\ P_1 & P_2 & P_3 & \cdots & \cdots & P_n \\ P_1^2 & P_2^2 & P_3^2 & \cdots & \cdots & P_n^2 \\ \vdots & \vdots & \vdots & \vdots & \vdots & \vdots \\ P_1^{n-1} & P_2^{n-1} & P_3^{n-1} & \cdots & \cdots & P_n^{n-1} \end{bmatrix},$$

and the two diagonal matrices, which are given by

$$C = \operatorname{diag}(c_1, ..., c_n) \quad \text{and} \quad D = \operatorname{diag}(P_1, ..., P_n).$$

An essential property is that the Vandermonde matrix V is invertible as our point sources are pairwise distinct. Because only the values α_m for $m \in \mathbb{N}_0$ are known, we have to relate them with these matrices. One can verify that $VCV^T = H_0$ and $VDCV^T = H_1$, where the Hankel matrices $H_0, H_1 \in \mathbb{C}^{n\times n}$ are defined by

$$H_0 = \begin{bmatrix} \alpha_0 & \alpha_1 & \cdots & \alpha_{n-1} \\ \alpha_1 & \alpha_2 & \cdots & \alpha_n \\ \vdots & \vdots & \vdots & \vdots \\ \alpha_{n-1} & \alpha_n & \cdots & \alpha_{2n-2} \end{bmatrix}, \quad H_1 = \begin{bmatrix} \alpha_1 & \alpha_2 & \cdots & \alpha_n \\ \alpha_2 & \alpha_3 & \cdots & \alpha_{n+1} \\ \vdots & \vdots & \vdots & \vdots \\ \alpha_n & \alpha_{n+1} & \cdots & \alpha_{2n-1} \end{bmatrix}.$$

The diagonal matrix C has non–zero entries and is therefore invertible. Thus, the equality $H_0 = VCV^T$ implies that H_0 is invertible. In the next step we compute

$$H_1 H_0^{-1} = (VDCV^T)(VCV^T)^{-1} = VDCV^T V^{-T} C^{-1} V^{-1} = VDV^{-1}.$$

Hence, the computable matrix $H_1H_0^{-1}$ is similar to D and as a consequence it has the same eigenvalues. Therefore, the eigenvalues of $H_1H_0^{-1}$ are P_j for $j = 1, ..., n$. Computing the real and the imaginary part of the eigenvalues leads to the source coordinates $y_{j,1}$ and $y_{j,2}$. Next, we can easily compute the expression c_j by solving the linear system (4.4), which is equivalent to solving

$$V \begin{pmatrix} c_1 \\ c_2 \\ \vdots \\ c_n \end{pmatrix} = \begin{pmatrix} \alpha_0 \\ \alpha_1 \\ \vdots \\ \alpha_{n-1} \end{pmatrix}. \tag{4.5}$$

Since the values $c_j := \lambda_j \exp(-\mathrm{i}\kappa y_{j,3})$ for $j = 1, ..., n$ are now known it remains to determine the intensities λ_j and the coordinates $y_{j,3}$. To do so, we use the test functions w_m defined in (4.3). Plugging w_m into (4.2) leads to

$$\sum_{j=1}^{n} d_j P_j^m = R(w_m) =: \beta_m \quad \forall m \in \mathbb{N}_0,$$

where $d_j := \lambda_j \exp(\mathrm{i}\kappa y_{j,3})$ for $j = 1, ..., n$. The values β_m can be computed numerically for all $m \in \mathbb{N}_0$ and P_j for $j = 1, ..., n$ has been determined previously. Hence, computing the expressions d_j is equivalent to solving the linear system

$$V \begin{pmatrix} d_1 \\ d_2 \\ \vdots \\ d_n \end{pmatrix} = \begin{pmatrix} \beta_0 \\ \beta_1 \\ \vdots \\ \beta_{n-1} \end{pmatrix}. \tag{4.6}$$

At this point we have $2n$ equations

$$c_j = \lambda_j \exp(-\mathrm{i}\kappa y_{j,3}), \qquad d_j = \lambda_j \exp(\mathrm{i}\kappa y_{j,3}),$$

and $2n$ unknowns λ_j and $y_{j,3}$ for $j = 1, ..., n$. A direct computation yields

$$c_j d_j = \lambda_j^2, \qquad \frac{d_j}{c_j} = \exp(2\mathrm{i}\kappa y_{j,3}),$$

for $j = 1, ..., n$. To avoid taking a square root in the computation of λ_j, the missing quantities of the point source are instead determined by

$$y_{j,3} = \Re\left(\frac{\ln(d_j/c_j)}{2\mathrm{i}\kappa}\right), \qquad \lambda_j = d_j \exp(-\mathrm{i}\kappa y_{j,3}) \qquad \text{for } j = 1, ..., n. \tag{4.7}$$

Thus, we are able to reconstruct all the parameters of the linear combination of point sources from the Cauchy data at a single wave number algebraically.

Numerical examples

In this section we apply the algebraic reconstruction method from El Badia and Nara in [11] to different numerical examples. First, we start by reconstructing one point source from the boundary data at a single wave number. Subsequently, we increase the complexity of the numerical examples by considering a higher wave number, multiple point sources and noisy boundary data. This demonstrates the capabilities and limitations of this method.

We consider the domain $\Omega = B(0,1) \subset \mathbb{R}^3$ and recall that the source z of the inverse problem (3.1) can be represented as

$$z(x) = \sum_{j=1}^{n} \lambda_j \delta_{y_j}(x) \quad \text{for } x \in \Omega,$$

where $n \in \mathbb{N}$, $y_j \in \Omega$ and $\lambda_j \in \mathbb{C} \setminus \{0\}$. First, we are interested in the Cauchy data on $\partial\Omega$, which can be computed by using the fundamental solution of the Helmholtz equation. In [22, Thm. 9.4] the fundamental solution in $\mathbb{R}^3$ is given by

$$U_\kappa^*(x,y) = -\frac{1}{4\pi} \frac{\exp(-\mathrm{i}\kappa\|x-y\|)}{\|x-y\|} \quad \text{for } x, y \in \mathbb{R}^3,$$

and satisfies

$$(\Delta_x + \kappa^2) U_\kappa^*(x,y) = \delta_y \quad \text{for } x, y \in \mathbb{R}^3.$$

A short computation gives us the gradient of the fundamental solution $U_\kappa^*(x,y)$ with respect to x as

$$\nabla_x U_\kappa^*(x,y) = \frac{1}{4\pi} \frac{\exp(-\mathrm{i}\kappa\|x-y\|)(\mathrm{i}\kappa\|x-y\|+1)}{\|x-y\|^3}(x-y) \quad \text{for } x, y \in \mathbb{R}^3.$$

Since our source z is a linear combination of point sources and the problem is linear, the Cauchy data can be expressed as

$$g(x) = -\frac{1}{4\pi} \sum_{j=1}^{n} \lambda_j \frac{\exp(-\mathrm{i}\kappa\|x-y_j\|)}{\|x-y_j\|} \quad \text{for } x \in \partial\Omega,$$

$$f(x) = \frac{1}{4\pi} \sum_{j=1}^{n} \lambda_j \frac{\exp(-\mathrm{i}\kappa\|x-y_j\|)(\mathrm{i}\kappa\|x-y_j\|+1)}{\|x-y_j\|^3}(x-y_j)\cdot x \quad \text{for } x \in \partial\Omega,$$

where the outward pointing normal vector for the domain $\Omega = B(0,1)$ is $\underline{n}(x) = x$. For all numerical examples the Cauchy data are given at 361 uniformly distributed boundary points on the sphere obtained from a spherical t–design with $t = 18$ [7], which allows exact integration for all polynomials of degree up to $t = 18$.
We assume that the number of point sources n has an upper bound $N = 6$. Hence, we require the basis functions v_m for $0 \le m \le 11$ defined in (4.3). By determining the singular values of the Hankel matrix $H \in \mathbb{C}^{6\times 6}$ defined by

$$H = \begin{bmatrix} \alpha_0 & \alpha_1 & \alpha_2 & \cdots & \cdots & \alpha_5 \\ \alpha_1 & \alpha_2 & \alpha_3 & \cdots & \cdots & \alpha_6 \\ \alpha_2 & \alpha_3 & \alpha_4 & \cdots & \cdots & \alpha_7 \\ \vdots & \vdots & \vdots & \vdots & \vdots & \vdots \\ \alpha_5 & \alpha_6 & \alpha_7 & \cdots & \cdots & \alpha_{10} \end{bmatrix}, \tag{4.8}$$

we retrieve the number of point sources n with a suitable threshold. This should separate the dominant singular values from the non–dominant ones. For a wave number $\kappa = 1.85$ setting the threshold to $\varepsilon = 0.05$ is appropriate as illustrated in Figure 4.1. The figure shows the singular values of H for $n = 1, ..., 6$ point sources with the chosen threshold marked by a red line.

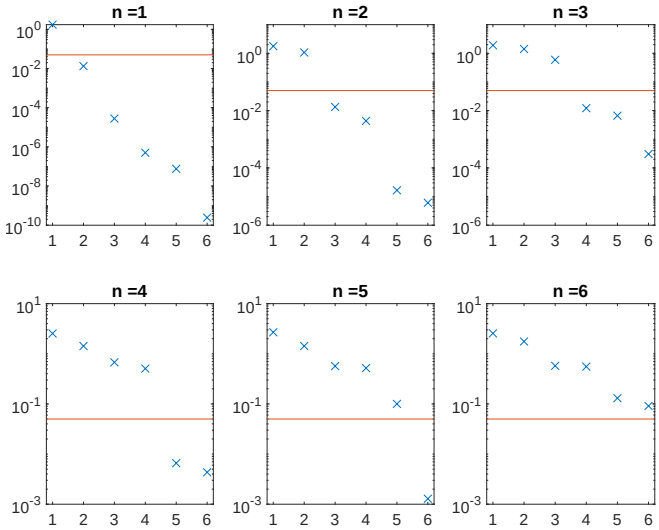

Figure 4.1: Singular values of the matrix H for $N = 6$ and $\kappa = 1.85$ for a varying number n of point sources. The threshold of $\varepsilon = 0.05$ is marked by a red line.

Computing the real and imaginary part of the eigenvalues of

$$H_1 H_0^{-1} = \begin{bmatrix} \alpha_1 & \alpha_2 & \cdots & \alpha_n \\ \alpha_2 & \alpha_3 & \cdots & \alpha_{n+1} \\ \vdots & \vdots & \vdots & \vdots \\ \alpha_n & \alpha_{n+1} & \cdots & \alpha_{2n-1} \end{bmatrix} \begin{bmatrix} \alpha_0 & \alpha_1 & \cdots & \alpha_{n-1} \\ \alpha_1 & \alpha_2 & \cdots & \alpha_n \\ \vdots & \vdots & \vdots & \vdots \\ \alpha_{n-1} & \alpha_n & \cdots & \alpha_{2n-2} \end{bmatrix}^{-1},$$

leads to the coordinates $y_{j,1}$ and $y_{j,2}$ for $j = 1, ..., n$. Moreover, to reconstruct the intensities λ_j and $y_{j,3}$ we additionally use the basis function w_m for $0 \leq m \leq n-1$ defined in (4.3). Finally, we solve the two linear systems (4.5) and (4.6) and compute λ_j and $y_{j,3}$ for $j = 1, ..., n$ according to formula (4.7).
In our numerical examples presented below we consider $n = 1, ..., 6$ point sources. The exact locations of the point sources are given by

$$\begin{aligned} &y_1 = (-0.7, 0.3, -0.2), \quad y_2 = (0.6, -0.3, 0.1), \quad y_3 = (0.5, 0.5, 0.2), \\ &y_4 = (-0.6, -0.4, 0.0), \quad y_5 = (0.0, -0.5, 0.4), \quad y_6 = (0.2, 0.7, -0.5), \end{aligned} \tag{4.9}$$

with corresponding intensities

$$\begin{aligned} &\lambda_1 = 1.0, \quad &&\lambda_2 = \exp(\mathrm{i}\pi/2), \quad &&\lambda_3 = \exp(\mathrm{i}\pi/4), \\ &\lambda_4 = -1.0, \quad &&\lambda_5 = \exp(2\mathrm{i}\pi/3), \quad &&\lambda_6 = \exp(-2\mathrm{i}\pi/5). \end{aligned} \tag{4.10}$$

For a numerical test with n point sources, we will use the first n locations and intensities from (4.9) and (4.10), respectively.

Reconstruction of a single point source at a small wave number

In the first example we consider a single point source, where the location y_1 and the intensity λ_1 are given in (4.9) and (4.10). We want to reconstruct the source from the exact Cauchy data g and f at a single small wave number $\kappa = 1.85$.

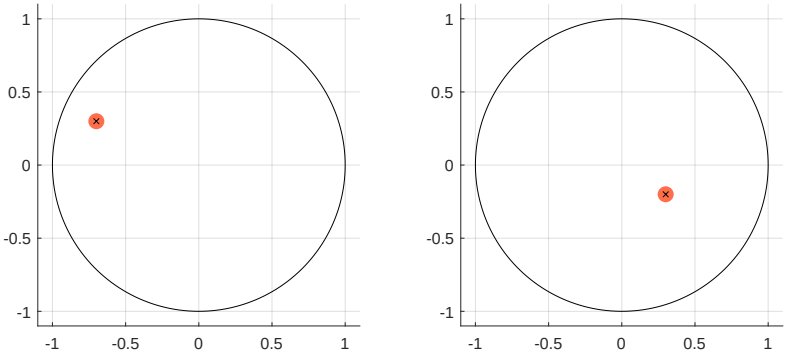

Figure 4.2: Reconstruction of a single point source located in y_1 with the wave number $\kappa = 1.85$ and no noise. On the left the xy-plane is depicted and on the right the yz-plane is shown.

In Figure 4.2 the black cross indicates the exact position of the point source, whereas the red filled circle represents the reconstructed source location obtained from the algebraic method. One can see that the reconstruction is accurate for a single point source and the wave number $\kappa = 1.85$. Furthermore, Table 4.1 presents the absolute error of the exact and the reconstructed intensity. In this and all subsequent tables only the absolute error is depicted since the exact intensities satisfy $|\lambda_j| = 1$ for $j = 1, ..., n$, which implies that the absolute and relative errors coincide. We obtain that the intensity is recovered accurately with an absolute error of the order 10^{-4}.

Table 4.1: Exact and reconstructed intensity for a single point source located in y_1 with the intensity λ_1. The wave number is $\kappa = 1.85$.

Source	Exact intensity	Reconstructed intensity	$\lvert\lambda_{ex} - \lambda_{rec}\rvert$
1	1.0	$0.9998623 - 0.0001032\mathrm{i}$	$1.72e-04$

Reconstruction of a single point source at a high wave number

In the next example we are interested in whether the reconstruction of the same single point source works if we increase the wave number. To do so, we repeat the previous test for a single wave number $\kappa = 18.5$.

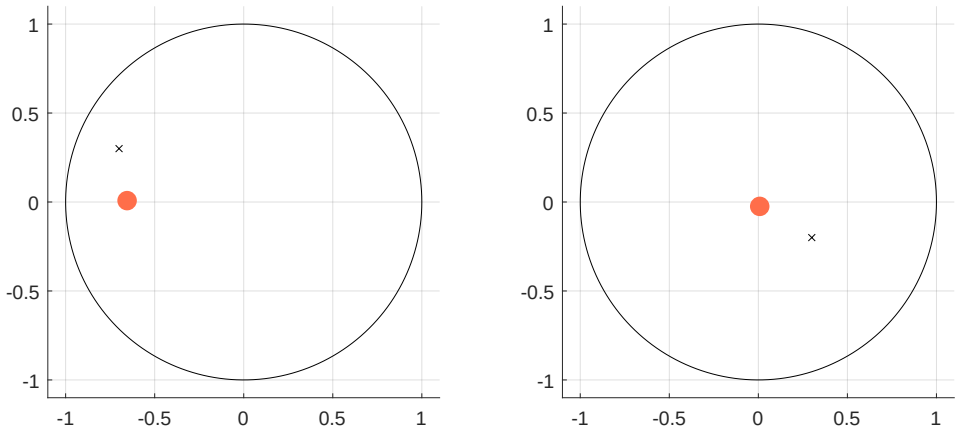

Figure 4.3: Failed reconstruction of a single point source located in y_1 with $\kappa = 18.5$. On the left the xy-plane is depicted and on the right the yz-plane is shown.

In Figure 4.3 the reconstruction of the single point source in y_1 with intensity λ_1 from (4.9) and (4.10) is illustrated. We see that the reconstruction is not working properly anymore, as the reconstructed source location indicated by the red filled circle lies far from the exact source, which is represented by the black cross. This implies that the accuracy of the method depends on the size of the wave number κ. This matches the observation from El Badia and Nara in [11]. They have outlined, that the accuracy depends on the wavelength compared to the distance between the points, where the Cauchy data are measured. For $\kappa = 1.85\text{m}^{-1}$ and $\kappa = 18.5\text{m}^{-1}$, they have computed the corresponding wavelengths and the number of measuring points per wavelength. By the formula $\kappa = 2\pi/\nu$, where ν denotes the wavelength, we get that $\kappa = 1.85\text{m}^{-1}$ corresponds to a wavelength $\nu \approx 3.4\text{m}$, whereas for $\kappa = 18.5\text{m}^{-1}$ the wavelength satisfies $\nu \approx 0.34\text{m}$. Thus, the wavelengths also differ by a factor of ten. Furthermore, we assume that the radius of our domain Ω is equal to 1m. We have 361 uniformly distributed points on the boundary, where the Cauchy data are measured. By computing $\sqrt{361/4\pi}$ we get that there are approximately 5.36 observation points per unit length. Multiplying this with the corresponding wavelengths ν leads to 18 observation points per wavelength for $\kappa = 1.85\text{m}^{-1}$ and to only 1.8 boundary points per wavelength for $\kappa = 18.5\text{m}^{-1}$. As a consequence, we need enough observation points on the boundary per wavelength in order to make this method work. Therefore, all the subsequent examples will use the wave number $\kappa = 1.85$.

Reconstruction of multiple point sources at a small wave number

So far we know, that the method works for a single point source, if we have enough observation points on the boundary per wavelength. Hence, in our example with 361 points on the boundary, it works for the wave number $\kappa = 1.85$. Now we are interested in the reconstruction of more point sources. We investigate how accurate the reconstruction remains if the number of point sources is increased from $n = 2$ to $n = 6$. The locations and the corresponding intensities are given in (4.9) and (4.10).

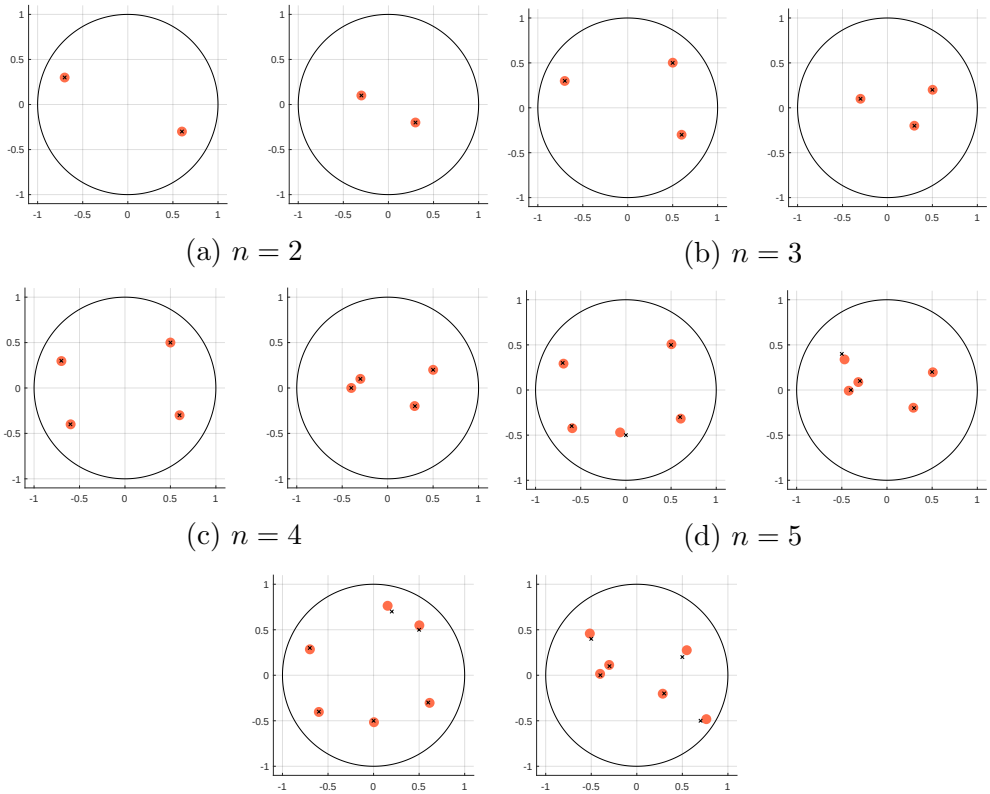

(a) $n = 2$ (b) $n = 3$

(c) $n = 4$ (d) $n = 5$

(e) $n = 6$

Figure 4.4: Reconstruction of n point sources with the wave number $\kappa = 1.85$. In each subfigure on the left the xy-plane is depicted and on the right the yz-plane is shown. The black cross indicates the exact source location and the red filled circle the reconstructed one.

Figure 4.4 shows the reconstruction of $n = 2, ..., 6$ point sources for $\kappa = 1.85$. The reconstruction up to 4 point sources is accurate. However, for $n = 5$ and $n = 6$ the reconstructed locations and the exact locations do not coincide anymore. The corresponding intensities are depicted in Table 4.2. Here we obtain the same behaviour. For $n \leq 4$ point sources the absolute error for the intensities is between 10^{-4} and 10^{-2}. Considering $n = 5$ point sources, we obtain that there occurs a significantly higher

error. Another observation is that the absolute error of the exact and reconstructed intensity is increasing with the number of point sources n.

Table 4.2: Exact and reconstructed source intensities for n point sources with the wave number $\kappa = 1.85$ from exact boundary data.

(a) $n = 2$

Source	Exact intensity	Reconstructed intensity	$\lvert\lambda_{ex} - \lambda_{rec}\rvert$
1	1.0	$0.9999557 - 0.0009375$i	$9.39e-04$
2	i	$0.0002512 + 0.9992929$i	$7.50e-04$

(b) $n = 3$

Source	Exact intensity	Reconstructed intensity	$\lvert\lambda_{ex} - \lambda_{rec}\rvert$
1	1.0	$0.9987253 - 0.0037878$i	$4.00e-03$
2	i	$-0.0041341 + 1.0040032$i	$5.75e-03$
3	$0.7071068 + 0.7071068$i	$0.7023607 + 0.6997673$i	$8.74e-03$

(c) $n = 4$

Source	Exact intensity	Reconstructed intensity	$\lvert\lambda_{ex} - \lambda_{rec}\rvert$
1	1.0	$1.0114748 - 0.0065258$i	$1.32e-02$
2	i	$0.0017758 + 0.9990397$i	$2.02e-03$
3	$0.7071068 + 0.7071068$i	$0.7093222 + 0.7071839$i	$2.22e-03$
4	-1.0	$-1.0030609 + 0.0101975$i	$1.06e-02$

(d) $n = 5$

Source	Exact intensity	Reconstructed intensity	$\lvert\lambda_{ex} - \lambda_{rec}\rvert$
1	1.0	$1.0667709 + 0.0128260$i	$6.80e-02$
2	i	$-0.0707122 + 0.9160704$i	$1.11e-01$
3	$0.7071068 + 0.7071068$i	$0.6801917 + 0.6646930$i	$5.02e-02$
4	-1.0	$-0.9257692 + 0.1888644$i	$2.03e-01$
5	$-0.50 + 0.8660254$i	$-1.0143030 + 0.8763707$i	$5.14e-01$

(e) $n = 6$

Source	Exact intensity	Reconstructed intensity	$\lvert\lambda_{ex} - \lambda_{rec}\rvert$
1	1.0	$1.0752894 - 0.0476099$i	$8.91e-02$
2	i	$0.0352419 + 0.9232421$i	$8.45e-02$
3	$0.7071068 + 0.7071068$i	$0.9325004 + 0.4996077$i	$3.06e-01$
4	-1.0	$-0.9333504 + 0.0174585$i	$6.89e-02$
5	$-0.50 + 0.8660254$i	$-0.4946991 + 0.8550565$i	$1.22e-02$
6	$0.3090170 - 0.9510565$i	$0.4346387 - 0.7714625$i	$2.12e-01$

We have obtained that in the setting of a small wave number, such as $\kappa = 1.85$, exact boundary data and an upper bound $N = 6$, the method reconstructs the source quite accurately up to $n = 4$ point sources.

Reconstruction of point sources at a small wave number from noisy boundary data

In the following we are interested in the effect of noisy boundary data on the reconstruction accuracy. To construct the noisy boundary data we compute the root mean square of the exact Cauchy data evaluated in all 361 points, scale it with the given noise level in % and multiply it with a vector of normally distributed random numbers. Adding this noise term to the exact boundary data leads to the noisy data. Furthermore, in order to make the result more reliable, we repeat the method 10 times for the same noise level. Then we compute the mean value and the standard deviations of the reconstructed source locations in each coordinate as well as the mean value of the reconstructed source intensities.
For the numerical examples we use the parameters $\kappa = 1.85$, $N = 6$ and a noise level of 1%. In order to make this method work, we again need a suitable threshold to estimate the number of point sources n first. In Figure 4.5 the singular values of the Hankel matrix H defined in (4.8) with the values α_m for $0 \leq m \leq 10$ using the noisy boundary data are plotted.

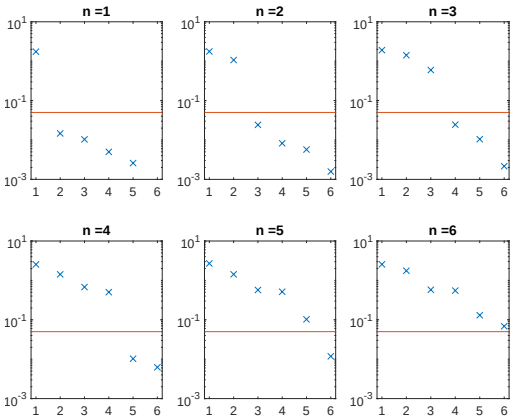

Figure 4.5: Singular values of the matrix H with $N = 6$, $\kappa = 1.85$ and a noise level of 1% for a varying number n of point sources. The threshold of $\varepsilon = 0.05$ is marked by a red line.

We see in Figure 4.5 that a threshold of $\varepsilon = 0.05$ separates the n^{th} and $(n+1)^{th}$ singular value for $n = 1, ..., 5$ point sources. While for $n \leq 4$ the gap between the n^{th} and $(n+1)^{th}$ singular value is significant, this gap is noticeably smaller for five point sources and hence, a reliable estimate of n is not possible. However, we will consider the reconstruction of five and six point sources, if the number of point sources n is known a priori.
With this consideration we can compare the results of the method with the exact quantities of our source given in (4.9) and (4.10). In Figure 4.6 the reconstruction of the locations for $n = 1, ..., 6$ point sources is illustrated with a noise level of 1%. The true point source locations are indicated by black crosses, whereas the reconstructed

source locations are represented by filled red spheres. The standard deviation of the estimated locations is illustrated by black dashed ellipses, but they are negligible small in all figures except for the figure, where 5 and 6 point sources are reconstructed. The reconstruction is still accurate for $n \leq 4$ point sources and visibly identical to the noise–free examples in Figure 4.4. The reconstructions of $n = 5$ and $n = 6$ point sources are inaccurate again as in the noise–free case. Therefore, comparing the reconstruction of the point sources from noisy boundary data in Figure 4.6 with the one from exact boundary data in Figure 4.4 we see, that these two figures are nearly the same.

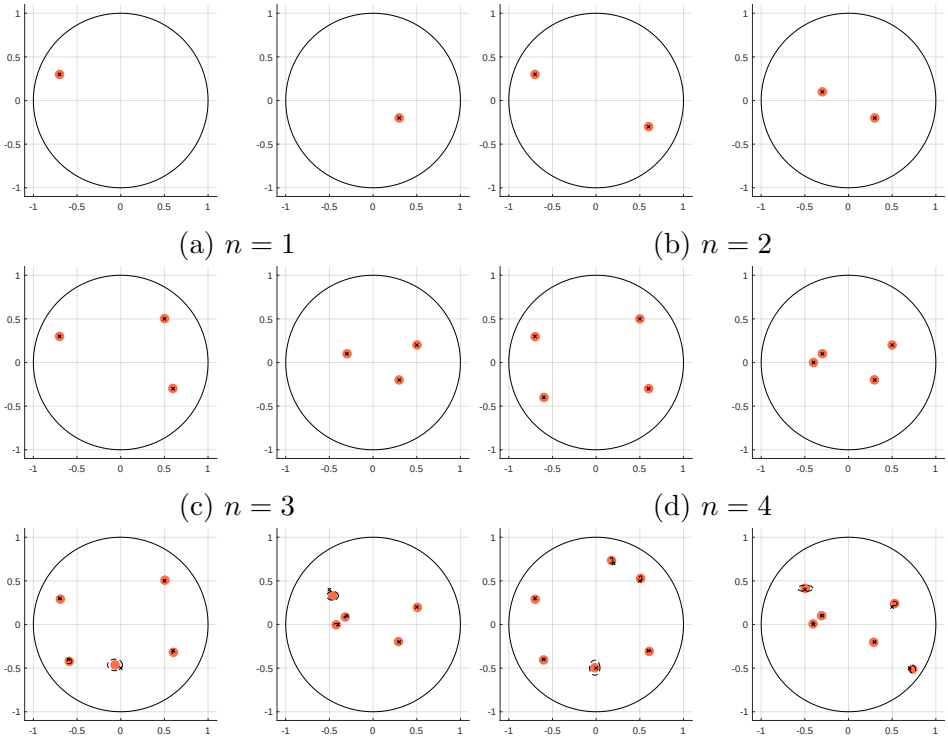

(a) $n = 1$ (b) $n = 2$

(c) $n = 3$ (d) $n = 4$

(e) $n = 5$ (f) $n = 6$

Figure 4.6: Reconstruction of n point sources with the wave number $\kappa = 1.85$, the upper bound of point sources $N = 6$ and noisy boundary data with a noise level of 1%. In each subfigure on the left the xy-plane is depicted and on the right the yz-plane is shown. The black cross indicates the exact source location and the red filled circle the reconstructed one.

Furthermore, we are also interested in the reconstructed source intensities in this setting. In Table 4.3 the exact intensities as well as the mean value of the reconstructed intensities are shown for $\kappa = 1.85$, different values for n and a noise level of 1%. Furthermore, the absolute error of the mean value and the exact intensity is depicted. We see, that the error is getting larger with increasing n. The absolute errors are very similar compared to Table 4.1 and Table 4.2, where the exact Cauchy data are used.

Table 4.3: Exact and reconstructed source intensities for n point sources with the wave number $\kappa = 1.85$ from noisy boundary data with a noise level of 1%.

(a) $n = 1$

Source	Exact intensity	Reconstructed intensity	$\lvert\lambda_{ex} - \lambda_{rec}\rvert$
1	1.0	$1.0007272 + 0.0004304i$	$8.45e-04$

(b) $n = 2$

Source	Exact intensity	Reconstructed intensity	$\lvert\lambda_{ex} - \lambda_{rec}\rvert$
1	1.0	$1.0000536 - 0.0006984i$	$7.00e-04$
2	i	$0.0018327 + 1.0005145i$	$1.90e-03$

(c) $n = 3$

Source	Exact intensity	Reconstructed intensity	$\lvert\lambda_{ex} - \lambda_{rec}\rvert$
1	1.0	$1.0024502 - 0.0010088i$	$2.65e-03$
2	i	$0.0045540 + 0.9935502i$	$7.90e-03$
3	$0.7071068 + 0.7071068i$	$0.7112667 + 0.7118119i$	$6.28e-03$

(d) $n = 4$

Source	Exact intensity	Reconstructed intensity	$\lvert\lambda_{ex} - \lambda_{rec}\rvert$
1	1.0	$1.0196328 + 0.0120561i$	$2.30e-02$
2	i	$-0.0109911 + 1.0097372i$	$1.47e-02$
3	$0.7071068 + 0.7071068i$	$0.7006884 + 0.7037799i$	$7.23e-03$
4	-1.0	$-1.0310884 + 0.0123541i$	$3.35e-02$

(e) $n = 5$

Source	Exact intensity	Reconstructed intensity	$\lvert\lambda_{ex} - \lambda_{rec}\rvert$
1	1.0	$1.0787389 + 0.0261184i$	$8.30e-02$
2	i	$-0.0615957 + 0.9200630i$	$1.01e-01$
3	$0.7071068 + 0.7071068i$	$0.6748569 + 0.6651997i$	$5.29e-02$
4	-1.0	$-0.9325405 + 0.2453722i$	$2.54e-01$
5	$-0.50 + 0.8660254$	$-1.0609109 + 0.7812015i$	$5.67e-01$

(f) $n = 6$

Source	Exact intensity	Reconstructed intensity	$\lvert\lambda_{ex} - \lambda_{rec}\rvert$
1	1.0	$1.0363171 - 0.0929758i$	$9.98e-02$
2	i	$-0.0156677 + 0.8670225i$	$1.34e-01$
3	$0.7071068 + 0.7071068i$	$0.6503753 + 0.4166501i$	$2.96e-01$
4	-1.0	$-1.0181226 - 0.0346065i$	$3.91e-02$
5	$-0.50 + 0.8660254i$	$-0.5670009 + 0.6821885i$	$1.96e-01$
6	$-0.50 + 0.50i$	$-0.2863515 + 0.3449765i$	$2.64e-01$

As for $\kappa = 1.85$ and a noise level of 1% the reconstruction is accurate for $n \leq 4$, we are interested in the effect of varying noise levels. In this setting we test with $\kappa = 1.85$ and $n = 2$ point sources. We make 100 repetitions per noise level and compute the

maximum standard deviations of the reconstructed source coordinates. Figure 4.7 illustrates the results and suggests that there is a direct proportionality between the standard deviation and the noise level in %.

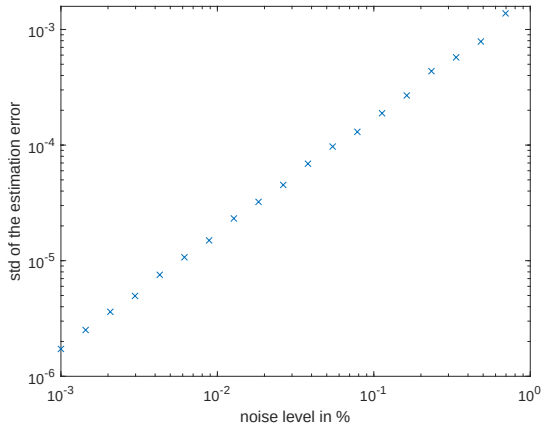

Figure 4.7: Maximum standard deviation for two point sources located in y_1 and y_2 in dependency of the noise level in %. The wave number is $\kappa = 1.85$.

Finally, we investigate the behaviour of the reconstruction accuracy when the distance between the sources is varying. In this setting we use $\kappa = 1.85$, a noise level of 1% and two point sources $y_1 = (+d, 0, 0)$ and $y_2 = (-d, 0, 0)$ with $d \in [0.1, 0.7]$. For the intensities we choose $\lambda_1 = 1.0$ and $\lambda_2 = \exp(\mathrm{i}\pi/2)$. As error computation we use the relative location error defined as

$$\mathrm{e} := \max_{j=1,2} \frac{\|\bar{y}_j - y_j\|_2}{2d}, \tag{4.11}$$

where $\bar{y}_j$ is the mean value of the reconstructed location for the j^{th} exact location. In Figure 4.8 the relative location error is plotted in dependency of the distance $2d$ between the two point sources y_1 and y_2. We obtain, that the error increases if the distance between the two point sources is getting smaller. This suggests, that the method will fail to reconstruct point sources that are close to each other.

Altogether, these numerical examples provide insights into the conditions under which the reconstruction method succeeds or fails. We have seen that the reconstruction is highly accurate for small wave numbers and a small number of sources. For large wave numbers, El Badia and Nara have pointed out in [11] that we need enough boundary observations per wavelength, which explains why the method fails for the wave number $\kappa = 18.5$. Furthermore, the reconstruction is accurate for $n \leq 4$ point sources in our setting with the upper bound $N = 6$. Moreover, the results obtained from the method for noisy boundary data with a noise level of 1% are also satisfactory for $n \leq 4$ point sources. The reconstructions are nearly identical to the ones using exact Cauchy data. In addition, we have observed that the reconstruction error

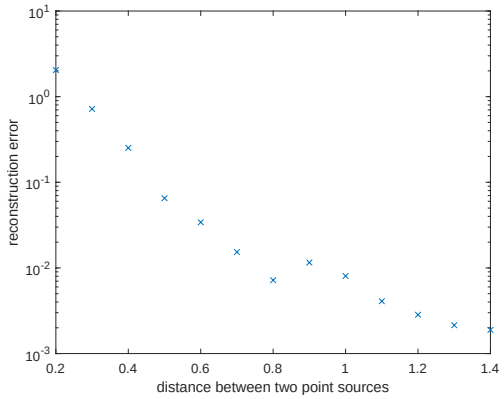

Figure 4.8: Reconstruction error defined in (4.11) in dependency of the distance between two point sources. The wave number is $\kappa = 1.85$.

depends linearly on the noise level in %. The limitations of this algebraic method are as follows. It fails if there are too few observation points on the boundary per wavelength. For instance, the method could not reconstruct a single point source for $\kappa = 18.5$. Moreover, the reconstruction becomes inaccurate when the number of point sources approaches the upper bound N, even without noise. In our example, this has been the case for $n = 5$ and $n = 6$ point sources, while the upper bound has been $N = 6$. We note that increasing the upper bound N improves the reconstruction accuracy, however, it makes the choice of a suitable threshold more difficult. Another disadvantage is that the error increases significantly if two sources are close to each other.

4.2 Numerical method for the reconstruction at several wave numbers

We have seen in Section 3.1.1 that reconstructing the source z of the inverse problem (3.1) from boundary data at a single wave number is unique only if some a priori information about the source term is known. However, in Section 3.2 we have shown that the source can be reconstructed in the L^2–sense if the boundary data are given at multiple wave numbers. Motivated by this result, we discuss in this section a numerical method, which enables the reconstruction of sources $z \in L^2(\Omega)$ when the Cauchy data are known for several wave numbers. The approach is based on solving a variational formulation using plane waves as basis functions and has been proposed by Alves et al. [3, Sec.6.2]. In [3] the authors restrict themselves to homogeneous Dirichlet datum, but this is not a necessary assumption for the numerical reconstruction. Subsequently, we provide some numerical examples for this approach. At the end of this section we briefly discuss another choice of basis functions which has been proposed in [13].

Description of the numerical method

For this section we consider a bounded Lipschitz domain $\Omega \subset \mathbb{R}^2$. The aim is to reconstruct the source $z \in L^2(\Omega)$ from given boundary data measurements for the Helmholtz equation

$$\begin{aligned} \Delta u(x) + \kappa^2 u(x) &= z(x) && \text{for } x \in \Omega, \\ u(x) &= g(x) && \text{for } x \in \partial\Omega, \\ \frac{\partial u}{\partial \underline{n}}(x) &= f(x) && \text{for } x \in \partial\Omega. \end{aligned}$$

The starting point of this method is the reciprocity gap functional defined in Definition 3.1 and the essential equation (3.3). This immediately leads to the continuous variational formulation: find $z \in L^2(\Omega)$ such that

$$\int_\Omega zv \,\mathrm{d}x = \int_{\partial\Omega} (f\gamma_0 v - g\gamma_1 v) \,\mathrm{d}s_x =: R(v) \qquad \forall v \in \mathcal{H}^1_{\Delta+\kappa^2}(\Omega) =: Y_\kappa. \tag{4.12}$$

The choice of the test space Y_κ is natural, as the reciprocity gap functional is well–defined on this space. Moreover, for any $v \in H^1(\Omega)$ with $\Delta v \in L^2(\Omega)$, the Neumann trace $\gamma_1 v$ exists by Lemma 1.8. We equip Y_κ with the norm $\|\cdot\|_{H^1(\Omega)}$. The continuous variational formulation (4.12) can equivalently be written as an operator equation: find $z \in L^2(\Omega)$ such that

$$\langle Az, v\rangle_{Y_\kappa' \times Y_\kappa} = R(v) \qquad \forall v \in Y_\kappa, \tag{4.13}$$

where $A : L^2(\Omega) \to Y_\kappa'$ is defined by

$$\langle Az, v\rangle_{Y_\kappa' \times Y_\kappa} := \int_\Omega zv \,\mathrm{d}x.$$

We want to illustrate by an example that the continuous variational formulation (4.12), respectively (4.13), is ill–posed. Therefore, we have to show that the operator A does not admit a bounded inverse, i.e., there does not exist a constant $c > 0$ such that

$$\|Az\|_{Y_\kappa'} \geq c\|z\|_{L^2(\Omega)} \qquad \forall z \in L^2(\Omega). \tag{4.14}$$

Example 4.1. We consider the one–dimensional domain $\Omega = (0, 2\pi)$ and fix $\kappa \in \mathbb{R}$. Let $z_n(x) = \exp(\mathrm{i}nx) \in L^2(\Omega)$ for $n \in \mathbb{N}$. As test functions we use the plane waves

$$v_+(x) = \exp(\mathrm{i}\kappa x), \qquad v_-(x) = \exp(-\mathrm{i}\kappa x),$$

which form a basis of Y_κ in one dimension. Hence, it is sufficient to estimate the action of Az_n on these two basis functions in order to control the dual norm. We compute

$$\begin{aligned} |\langle Az_n, v_\pm\rangle_{Y_\kappa' \times Y_\kappa}| &= \left| \int_0^{2\pi} z_n v_\pm \,\mathrm{d}x \right| = \left| \int_0^{2\pi} \exp(\mathrm{i}(n \pm \kappa)x) \,\mathrm{d}x \right| = \left| \frac{\exp(\mathrm{i}(n \pm \kappa)x)}{\mathrm{i}(n \pm \kappa)} \Big|_0^{2\pi} \right| \\ &= \left| \frac{\exp(2\pi\mathrm{i}(n \pm \kappa)) - 1}{\mathrm{i}(n \pm \kappa)} \right| \leq \frac{2}{|n \pm \kappa|} \xrightarrow{n\to\infty} 0. \end{aligned}$$

Furthermore, it holds $\|z_n\|_{L^2(0,2\pi)} = \sqrt{2\pi}$. Hence, there exists no constant $c > 0$ such that (4.14) is satisfied, which means that the operator A does not admit a bounded inverse. Consequently, the problem (4.12), respectively (4.13), is ill–posed.

In the numerical examples, we will restrict both the wave numbers κ and the Fourier modes n to bounded intervals. This ensures that the operator A admits a bounded inverse and consequently, that the problem is well–posed at the continuous level.

Discretisation via plane waves

In this section, we discretise the continuous variational formulation (4.13) using plane waves as basis functions in the test and ansatz space. To allow the reconstruction from the Cauchy data at multiple wave numbers, we introduce an open non empty interval $I \subset \mathbb{R}^+$. The goal is to find the source $z \in L^2(\Omega)$ of the Helmholtz equation for different wave numbers $\kappa_i \in I$ such that

$$\begin{aligned} \Delta u_{\kappa_i}(x) + \kappa_i^2 u_{\kappa_i}(x) &= z(x) && \text{for } x \in \Omega, \\ u_{\kappa_i}(x) &= g_{\kappa_i}(x) && \text{for } x \in \partial\Omega, \\ \frac{\partial u_{\kappa_i}}{\partial \underline{n}}(x) &= f_{\kappa_i}(x) && \text{for } x \in \partial\Omega. \end{aligned} \tag{4.15}$$

Although the operator A does not admit a bounded inverse, we can still discretise the variational formulation (4.13). Therefore, we use as basis functions the plane waves defined in (3.16) as

$$\varphi_\xi^\kappa(x) = e^{-i\kappa x\cdot\xi} \qquad \text{for } \kappa \in I, \xi \in \partial B(0,1).$$

With this consideration we define the test space

$$Y_{N,n} = \operatorname{span}\{\varphi_{\xi_j}^{\kappa_i}(x)\} \subset \mathcal{H}^1_{\Delta+\kappa_i^2}(\Omega), \quad \text{for } i = 1,...,N, \text{ and } j = 1,...,n,$$

where $\varphi_{\xi_j}^{\kappa_i}$ are plane waves with the wave number κ_i and the direction ξ_j. It is crucial that the test space $Y_{N,n}$ uses the wave numbers κ_i from the original problem as the basis functions must belong to the spaces $\mathcal{H}^1_{\Delta+\kappa_i^2}(\Omega)$. The ansatz space is defined as

$$X_{M,m} = \operatorname{span}\{\varphi_{c_k}^{\lambda_\ell}(x)\} \subset \mathcal{H}^1_{\Delta+\lambda_\ell^2}(\Omega) \subset L^2(\Omega), \quad \text{for } \ell = 1,...,M, \text{ and } k = 1,...,m,$$

where $\varphi_{c_k}^{\lambda_\ell}$ are plane waves with wave number $\lambda_\ell \in I$ and $\lambda_\ell \neq \kappa_i$ and c_k are chosen directions. Here M denotes the number of distinct wave numbers in the ansatz space and m is the number of directions. The ansatz space has to be equipped with different wave numbers to avoid that certain blocks of the system matrix would almost behave like others. We use this ansatz space $X_{M,m}$ to write a discrete approximation of our source z as

$$z_{M,m}(x) = \sum_{\ell=1}^{M}\sum_{k=1}^{m} z_{k,\ell}\varphi_k^{\lambda_\ell}(x),$$

where $z_{k,\ell}$ are coefficients, which have to be determined. Plugging this into (4.12) and using the discrete test space leads to the discrete variational formulation: find $z_{M,m} \in X_{M,m}$ such that

$$\int_\Omega z_{M,m}(x)\varphi_{\xi_j}^{\kappa_i}(x)\,\mathrm{d}x = R(\varphi_{\xi_j}^{\kappa_i}) \qquad \forall \varphi_{\xi_j}^{\kappa_i} \in Y_{N,n}. \tag{4.16}$$

Solving the discrete formulation (4.16) is equivalent to solve the system of linear equations

$$M_h \underline{z} = \underline{f},$$

where the matrix $M_h \in \mathbb{R}^{nN \times mM}$ is defined blockwise as

$$M_h := \begin{pmatrix} M_{\kappa_1,\lambda_1} & M_{\kappa_1,\lambda_2} & \cdots & M_{\kappa_1,\lambda_M} \\ M_{\kappa_2,\lambda_1} & M_{\kappa_2,\lambda_2} & \cdots & M_{\kappa_2,\lambda_M} \\ \vdots & \vdots & \ddots & \vdots \\ M_{\kappa_N,\lambda_1} & M_{\kappa_N,\lambda_2} & \cdots & M_{\kappa_N,\lambda_M} \end{pmatrix}. \tag{4.17}$$

One block in this matrix M_h is defined as

$$M_{\kappa_i,\lambda_\ell}[j,k] = \int_\Omega \varphi_{\xi_j}^{\kappa_i}(x)\varphi_{c_k}^{\lambda_\ell}(x)\,\mathrm{d}x,$$

for $j = 1, ..., n$ and $k = 1, ..., m$. The vector of the right hand side is defined as

$$\underline{f} := \begin{pmatrix} \underline{f}_{\kappa_1} \\ \underline{f}_{\kappa_2} \\ \vdots \\ \underline{f}_{\kappa_N} \end{pmatrix}, \tag{4.18}$$

whose entries are given by

$$\underline{f}_{\kappa_i}[j] = R(\varphi_{\xi_j}^{\kappa_i}),$$

for $j = 1, ..., n$.
The matrix M_h is likely to be ill–conditioned as the basis functions become nearly linearly dependent if the directions are almost collinear. Using more wave numbers does not resolve this problem. Furthermore, in [13] is outlined that the plane waves are even more linearly dependent as the wave number tends to zero. Next, we present the condition numbers of the matrix M_h for different choices of the parameters N, n, M and m. The results are illustrated in Table 4.4, where we use the wave numbers $\kappa = [1.5, 3.5, 5.5, 7.5, 9.5]$ in the test space and $\lambda = [2, 4, 6, 8, 10]$ in the ansatz space. We note that in our numerical tests we will always use the first n, respectively m

Table 4.4: The condition number of M_h for varying parameters N, n, M and m.

m	M	n	N	cond(M_h)
5	2	5	2	6.39e+01
10	2	10	2	7.92e+05
15	2	15	2	3.80e+09
10	3	10	3	1.50e+07
15	3	15	3	1.05e+11
20	3	20	3	5.65e+15
5	4	5	4	3.66e+02
10	4	10	4	1.56e+08
15	4	15	4	4.19e+11
10	5	10	5	1.21e+09
15	5	15	5	1.09e+12
20	5	20	5	8.24e+15

entries from these sets. Table 4.4 demonstrates that the condition number of the matrix M_h increases rapidly as the number of wave numbers and the number of used directions grow. Hence, the system matrix M_h is ill–conditioned.
As the system matrix M_h is not square, because in general it holds $Nn \neq Mm$, we interpret the solution in the least–squares sense, i.e.,

$$\underline{z} = \underset{\underline{w}\in\mathbb{R}^{Mm}}{\arg\min} \frac{1}{2}\|M_h\underline{w} - \underline{f}\|_2^2.$$

This is equivalent to solve the least–squares problem

$$M_h^T M_h \underline{z} = M_h^T \underline{f}.$$

As a consequence of the high condition numbers, as shown in Table 4.4, we have to regularise our least–squares problem. Therefore, we apply a Tikhonov regularisation. Introducing a regularisation parameter $\mu > 0$, we consider the minimisation problem

$$\underline{z}_\mu = \underset{\underline{w}\in\mathbb{R}^{Mm}}{\arg\min} \frac{1}{2}\|M_h\underline{w} - \underline{f}\|_2^2 + \frac{\mu}{2}\|\underline{w}\|_2^2.$$

This is equivalent to solving

$$\left(\mu I + M_h^T M_h\right)\underline{z}_\mu = M_h^T \underline{f},$$

where I denotes the identity matrix [15].
Now, the question arises how to choose the regularisation parameter μ. To this end, we consider the L–curve criterion. If the problem is over–regularised, the residual error $\|M_h\underline{w} - \underline{f}\|_2$ becomes large. On the other hand, if we regularise too weakly the

norm of the solution $\|\underline{w}\|_2$ increases significantly. Hence, for different values of $\mu > 0$ the curve $\left(\log \|\underline{w}\|_2, \log \|M_h \underline{w} - \underline{f}\|_2\right)$ is plotted, which typically exhibits an L–shaped form. To find a good trade–off between the solution norm and the residual error, one chooses the value of μ which corresponds to the corner of this curve. Hence, the optimal regularisation parameter keeps a good balance in minimising both errors [15].

Numerical examples

In this section we present two numerical examples with analytical sources to illustrate the behaviour of the proposed discretisation using plane waves and Tikhonov regularisation. In particular, we investigate the quality of the reconstruction as well as the L^2–error depending on the parameters N, n, M and m. First, we consider an example, where the Dirichlet datum is vanishing. Afterwards, we investigate a more general example with non vanishing Cauchy data. For both examples we use the domain $\Omega = (-1, 1)^2$.

Reconstruction of z_1 from exact boundary data

In the first example we consider the right hand side

$$z_1(x, y) = \sin(\pi x) \sin(\pi y), \tag{4.19}$$

which is an eigenfunction of the Laplacian on the square with homogeneous Dirichlet datum. The corresponding eigenvalue is $2\pi^2$, which will not be a wave number in the ansatz space. In Figure 4.9 the source z_1 is illustrated. The solution of the Helmholtz

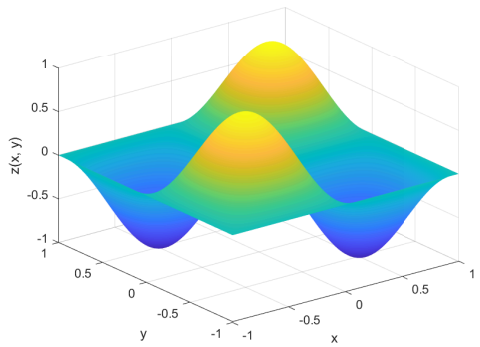

Figure 4.9: Plot of the original source $z_1(x, y)$ defined in (4.19).

equation corresponding to the source z_1 for each wave number κ_i is given by

$$u_{\kappa_i,1}(x, y) = \frac{1}{\kappa_i^2 - 2\pi^2} \sin(\pi x) \sin(\pi y) \quad \text{for } (x, y) \in \Omega,$$

admitting the Dirichlet datum $g_{\kappa_i,1} = 0$ and the Neumann datum

$$f_{\kappa_i,1}(x,y) = \frac{\pi}{\kappa_i^2 - 2\pi^2} \begin{pmatrix} \cos(\pi x)\sin(\pi y) \\ \sin(\pi x)\cos(\pi y) \end{pmatrix} \cdot \underline{n} \quad \text{for } (x,y) \in \partial\Omega.$$

In order to compute the matrix entries of M_h as well as the entries of the vector $\underline{f}$ on the right hand side, we use a quadrature rule, that integrates polynomials of degree up to 9 exactly [18]. To analyse the numerical behaviour of the proposed method we consider different combinations of basis functions in the test and ansatz space. This can be done by varying the number of wave numbers N and the number of directions n in the test space. Moreover, in the ansatz space the number of wave numbers M and the number of directions m will be varied. The regularisation parameter is obtained using the L–curve criterion.
For the reconstructions of the source z_1 shown in Figures 4.10–4.12 we first choose the wave numbers in the test space as $\kappa = [1.5, 3.5, 5.5, 7.5]$ and those in the ansatz space as $\lambda = [2, 4, 6, 8]$. For $n = 10$ directions in the test space and $m = 5$ directions in the ansatz space the L–curve and the corresponding reconstruction are shown in Figure 4.10.

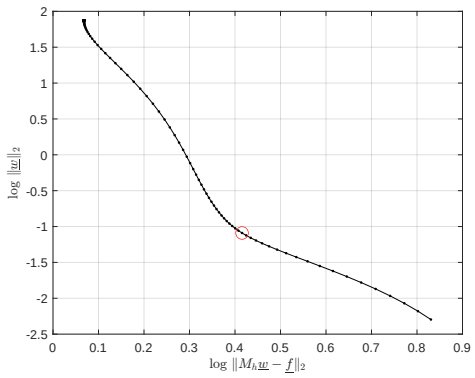

(a) L–curve

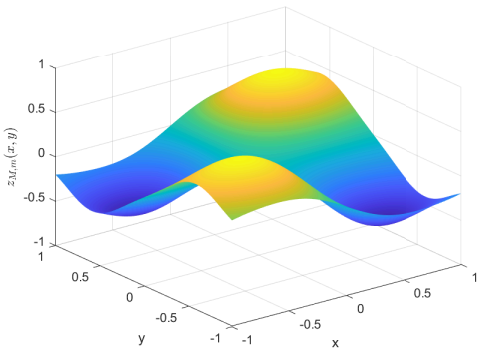

(b) Reconstruction of $z_1(x,y)$ with regularisation parameter $\mu = 5.19$

Figure 4.10: Reconstruction results for $\kappa = [1.5, 3.5, 5.5, 7.5]$ and $n = 10$ in the test space and $\lambda = [2, 4, 6, 8]$ and $m = 5$ in the ansatz space.

The regularisation parameter corresponding to the red circle in the L–curve in Figure 4.10 is $\mu = 5.19$. This relatively large value is necessary as smaller values lead to a large solution norm. In the reconstruction plot we observe that the symmetry of the source is captured, but the reconstruction is inaccurate. Thus, we are interested in the accuracy if we change the number of directions in both spaces. In Figure 4.11 we see the reconstruction of z_1 using $n = 17$ directions in the test space and $m = 13$ directions in the ansatz space.

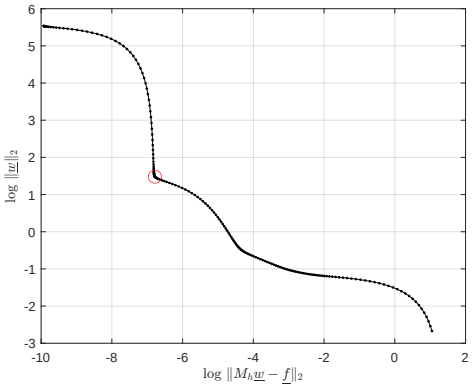

(a) L–curve

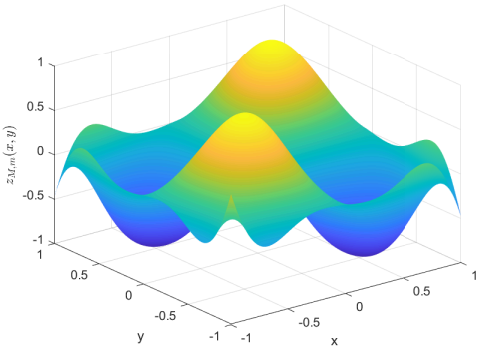

(b) Reconstruction of $z_1(x, y)$ with regularisation parameter $\mu = 4.89e - 08$

Figure 4.11: Reconstruction results for $\kappa = [1.5, 3.5, 5.5, 7.5]$ and $n = 17$ in the test space and $\lambda = [2, 4, 6, 8]$ and $m = 13$ in the ansatz space.

In this case, the regularisation parameter is set to $\mu = 4.89e - 08$ and the reconstruction accuracy of the source z_1 is improved. Nevertheless, the reconstruction still deviates significantly from the original source near the boundary of the domain $\Omega = (-1, 1)^2$. Increasing the parameters further to $n = 30$ directions in the test space and $m = 20$ directions in the ansatz space leads to a reconstruction, where no difference to the original source z_1 is visible. Hence, the shape as well as the values on the boundary are recovered well, as illustrated in Figure 4.12. The corresponding regularisation parameter is $\mu = 4.50e - 10$.

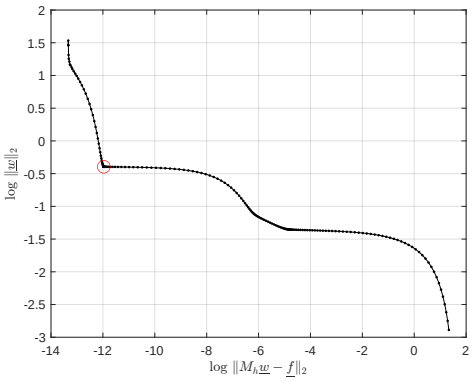

(a) L–curve

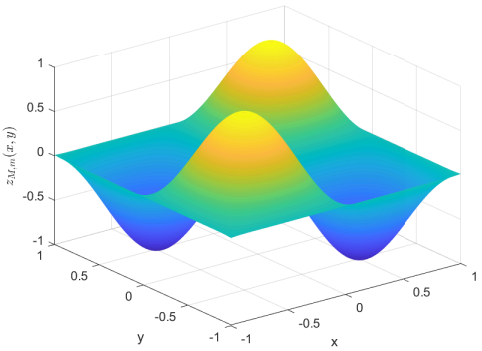

(b) Reconstruction of $z_1(x, y)$ with regularisation parameter $\mu = 4.50e - 10$

Figure 4.12: Reconstruction results for $\kappa = [1.5, 3.5, 5.5, 7.5]$ and $n = 30$ in the test space and $\lambda = [2, 4, 6, 8]$ and $m = 20$ in the ansatz space.

Error analysis in dependency of the discretisation parameters

To give a qualitative error analysis, we test the numerical method for different combinations of wave numbers and directions in the test and ansatz space. The goal is to see the capabilities and limitations of this method. In Table 4.5 the reconstruction error $\|z_1 - z_{M,m}\|_{L^2((-1,1)^2)}$ is presented in dependency of the number of wave numbers $N = M$. The number of directions is fixed in both spaces at $n = m = 15$. As wave numbers we use in the test space $\kappa = [1.5, 3.5, 5.5, 7.5, 9.5, 11.5]$ and in the ansatz space $\lambda = [2, 4, 6, 8, 10, 12]$. In the case of N wave numbers we use the first N entries of κ. We do this analogously for M and λ.

Table 4.5: L^2–error $\|z_1 - z_{M,m}\|_{L^2((-1,1)^2)}$ for different values of wave numbers $N = M$ in test and ansatz space using $n = m = 15$ directions. The regularisation parameter μ obtained from the L–curve is also given.

m	M	n	N	$\|z_1 - z_{M,m}\|_{L^2((-1,1)^2)}$	μ
15	2	15	2	5.43e-02	4.87e-11
15	3	15	3	4.62e-02	5.95e-05
15	4	15	4	1.82e-02	1.56e-06
15	5	15	5	8.03e-03	4.92e-08

Table 4.5 confirms the expectation, that the error decreases if we increase the number of wave numbers. This shows the advantage of choosing more wave numbers in the test and ansatz space for a fixed number of basis functions per wave number.
We further investigate the reconstruction error when the only free parameter is N, which is the number of used wave numbers in the test space. We consider two examples, where the number of directions is fixed at $n = m = 15$. In the first example we use $M = 2$ with $\lambda = [2, 4]$ and in the second example we set $M = 3$ with $\lambda = [2, 4, 6]$. Both examples are shown in Table 4.6, where the error $\|z_1 - z_{M,m}\|_{L^2((-1,1)^2)}$ is depicted in dependency of N.

Table 4.6: L^2–error $\|z_1 - z_{M,m}\|_{L^2((-1,1)^2)}$ for different values of wave numbers N in the test space. $M = 2$ and $M = 3$ are considered. The number of directions is $n = m = 15$. The optimal regularisation parameter μ is also given.

M	N	$\|z_1 - z_{M,m}\|_{L^2((-1,1)^2)}$	μ	M	N	$\|z_1 - z_{M,m}\|_{L^2((-1,1)^2)}$	μ
2	2	5.43e-02	4.87e-11	–	–	–	–
2	3	5.78e-02	2.54e-04	3	3	4.62e-02	5.95e-05
2	4	5.87e-02	5.61e-03	3	4	8.29e-03	1.30e-06
2	5	5.71e-02	6.73e-03	3	5	9.10e-03	7.14e-05
2	6	5.67e-02	8.08e-03	3	6	8.31e-03	1.77e-04

Table 4.6 shows that increasing the number of wave numbers N in the test space does not necessarily improve the reconstruction accuracy. In the case $M = 2$, the

L^2–error remains almost identical as N increases. In contrast, for $M = 3$ a significant reduction of the reconstruction error is observed when increasing N from 3 to 4, after which the error nearly stagnates. This suggests that adding a wave number in the test space can make the system matrix more ill–conditioned.
Now we focus on the effects of the L^2–error for varying N and n in the test space while keeping the ansatz space fixed. We analyse two examples, where the results are given in Table 4.7 and Table 4.8. In the first example the ansatz space is fixed with $m = 10$ and $M = 3$ for $\lambda = [2, 4, 6]$.

Table 4.7: L^2–error $\|z_1 - z_{M,m}\|_{L^2((-1,1)^2)}$ for different combinations of used wave numbers N and directions n in the test space. The ansatz space is fixed with $\lambda = [2, 4, 6]$ and $m = 10$. Furthermore, the regularisation parameter μ obtained from the L–curve is given.

m	M	n	N	$\|z_1 - z_{M,m}\|_{L^2((-1,1)^2)}$	μ
10	3	15	2	1.89e-01	8.39e-09
10	3	20	2	1.65e-01	8.57e-07
10	3	25	2	1.65e-01	1.14e-06
10	3	30	2	1.65e-01	1.23e-06
10	3	10	3	1.06e-01	3.70e-07
10	3	15	3	1.30e-01	3.00e-03
10	3	20	3	1.30e-01	3.61e-03
10	3	10	4	1.11e-01	1.59e-03
10	3	15	4	1.11e-01	3.70e-02
10	3	10	5	1.10e-01	3.27e-02
10	3	12	5	1.48e-01	9.17e-02
10	3	10	6	1.09e-01	3.27e-02

We note that in Table 4.7 cases with $N = 1$ or $n < m$ are not depicted, because they do not yield a meaningful L–curve. This indicates that these parameter choices are insufficient to balance both the residual norm and the solution norm. As a consequence, we restrict our considerations to sufficiently large values of N and n in the test space. Taking more wave numbers in the test space is advantageous, as it covers a broader spectrum. Moreover, we will always use at least as many basis functions in the test space as in the ansatz space. From Table 4.7 we observe that for fixed N, increasing the number of directions n does not influence the L^2–error significantly. Moreover, for comparable values of n, increasing the number of basis functions N in the test space decreases the L^2–error or leaves it essentially unchanged.
In the second example, for which the results are presented in Table 4.8 we fix the ansatz space by $\lambda = [2, 4, 6, 8]$ and $m = 15$ directions. As explained for Table 4.7, in this example choosing $N \leq 3$ does not yield a meaningful L–curve and is therefore omitted. We observe from Table 4.8 that for $N = 4$ and $N = 6$ the error decreases if we increase the number of directions n. Moreover, for fixed $n = 25$, increasing the

Table 4.8: L^2–error $\|z_1 - z_{M,m}\|_{L^2((-1,1)^2)}$ for different combinations of used wave numbers N and directions n in the test space. The ansatz space is fixed with $\lambda = [2, 4, 6, 8]$ and $m = 15$. Furthermore, the regularisation parameter μ obtained from the L–curve is given.

m	M	n	N	$\|z_1 - z_{M,m}\|_{L^2((-1,1)^2)}$	μ
15	4	15	4	1.82e-02	1.56e-06
15	4	20	4	1.27e-02	6.56e-08
15	4	25	4	2.37e-03	2.15e-07
15	4	15	5	2.88e-03	4.92e-08
15	4	20	5	6.01e-03	6.44e-06
15	4	25	5	2.90e-03	1.25e-05
15	4	15	6	3.57e-03	1.30e-06
15	4	20	6	3.30e-03	2.33e-05
15	4	25	6	3.01e-03	3.15e-05

number of wave numbers N does not result in a further improvement of the L^2–error, which remains of order 10^{-3}.

Reconstruction of z_1 from noisy boundary data

Next, we investigate how sensitive the L^2–error is when reconstructing the source z_1 from noisy boundary data. This is more realistic for practical applications. The noisy datum is computed as the maximum of the absolute value of the corresponding exact boundary datum multiplied with a uniformly distributed random vector. It is then scaled by the noise level, which is given in % and added to the exact datum. If the exact datum is zero a uniformly distributed random vector is used as noisy datum. The setting for the example with noisy boundary data is the same as in Figure 4.10. Hence, we use four wave numbers $\kappa = [1.5, 3.5, 5.5, 7.5]$ in the test space and four wave numbers $\lambda = [2, 4, 6, 8]$ in the ansatz space. Furthermore, the test space is equipped with $n = 10$ directions and the ansatz space with $m = 5$ directions. The noise level which is applied to the Cauchy data is 1%.

In Figure 4.13 the reconstruction of z_1 from noisy boundary data is shown. Compared to the reconstruction in Figure 4.10, obtained using the same test and ansatz space with exact boundary data, no visible difference can be observed. This suggests that the Tikhonov regularisation yields a stable reconstruction with noisy boundary data at this noise level.

Now, we investigate the L^2–error as a function of the noise level. In Table 4.9 we consider the same settings as in the reconstructions shown in Figures 4.10–4.12. Each test is repeated 25 times for each noise level and the mean value of the resulting L^2–errors is presented. Table 4.9 shows that for fixed discretisation parameters, the L^2–error increases as the noise level grows. In the case $N = M = 4$, $m = 5$ and $n = 10$ the

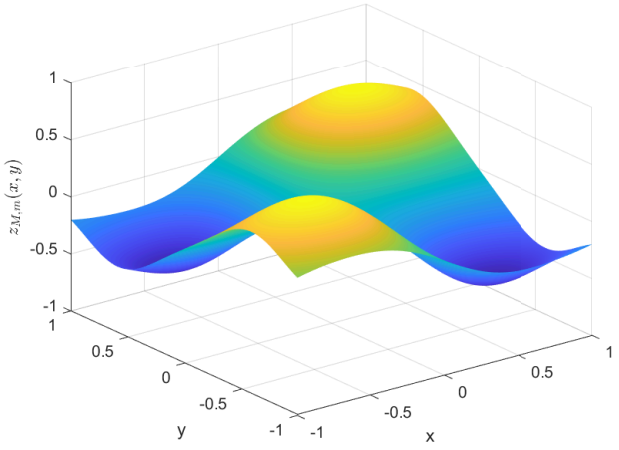

Figure 4.13: Plot of the reconstruction of $z_1(x, y)$ for $\kappa = [1.5, 3.5, 5.5, 7.5]$ and $n = 10$ in the test space and $\lambda = [2, 4, 6, 8]$ and $m = 5$ in the ansatz space and a noise level of 1%. The regularisation parameter obtained from the L–curve is $\mu = 5.19$.

Table 4.9: L^2–error $\|z_1 - z_{M,m}\|_{L^2((-1,1)^2)}$ for different values of noise level δ in %. The ansatz space is equipped with $M = 4$, and the test space with $N = 4$. The parameters n and m are varying.

m	M	n	N	δ	$\|z_1 - z_{M,m}\|_{L^2((-1,1)^2)}$
5	4	10	4	0	4.88e-01
5	4	10	4	1	4.89e-01
5	4	10	4	5	4.91e-01
5	4	10	4	10	4.97e-01
13	4	17	4	0	4.94e-02
13	4	17	4	1	6.77e-02
13	4	17	4	5	1.19e-01
13	4	17	4	10	1.77e-01
20	4	30	4	0	1.71e-03
20	4	30	4	1	6.25e-02
20	4	30	4	5	1.01e-01
20	4	30	4	10	1.40e-01

error remains almost unchanged for each noise level since the reconstruction error for the exact data is already worse. In contrast, for richer test and ansatz spaces the reconstruction error grows significantly as the noise level δ increases.
Next, we are interested in the behaviour of the L^2–error $\|z_1 - z_{M,m}\|_{L^2((-1,1)^2)}$ in dependency of the noise level given in %. We use for the test space $\kappa = [1.5, 3.5, 5.5, 7.5]$ and $n = 17$ and for the ansatz space $\lambda = [2, 4, 6, 8]$ and $m = 13$. In order to make a reliable plot, we have made 100 repetitions for each noise level and then computed the mean value of the L^2–errors. This is presented in Figure 4.14. As expected, the plot indicates that the L^2–error grows with increasing noise level. Moreover, the plot suggests that $\|z_1 - z_{M,m}\|_{L^2((-1,1)^2)}$ depends linearly on the noise level in %.

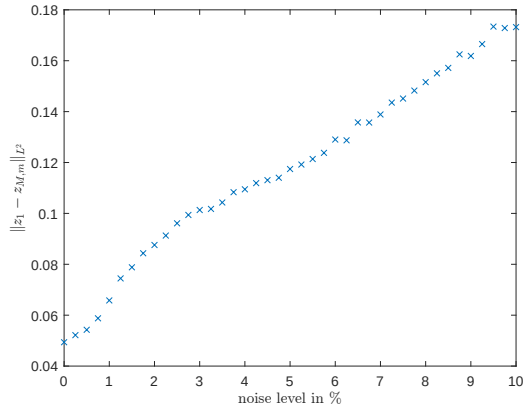

Figure 4.14: Plot of the error $\|z_1 - z_{M,m}\|_{L^2((-1,1)^2)}$ in dependency of the noise level in % using $\kappa = [1.5, 3.5, 5.5, 7.5]$ and $n = 17$ in the test space and $\lambda = [2, 4, 6, 8]$ and $m = 13$ in the ansatz space. The regularisation parameter is obtained by the L–curve.

Reconstruction of z_2 from exact boundary data

As already mentioned at the beginning of this section it is not a necessary assumption to have homogeneous Dirichlet datum. Therefore, we study a second example, where the Dirichlet datum is non–vanishing. We consider the source

$$z_2(x, y) = \cos(\pi x) \sin(\pi y), \tag{4.20}$$

which is an eigenfunction of the Laplacian on the square with mixed boundary conditions. On the top and bottom of the square it fulfils zero Dirichlet datum, whereas on the left and right side the Neumann datum is vanishing. The corresponding eigenvalue is $2\pi^2$, which will not be a wave number in the ansatz space. In Figure 4.15 the source z_2 is shown. The corresponding solution of the Helmholtz equation for each wave number κ_i is

$$u_{\kappa_i,2}(x, y) = \frac{1}{\kappa_i^2 - 2\pi^2} \cos(\pi x) \sin(\pi y) \quad \text{for } (x, y) \in \Omega.$$

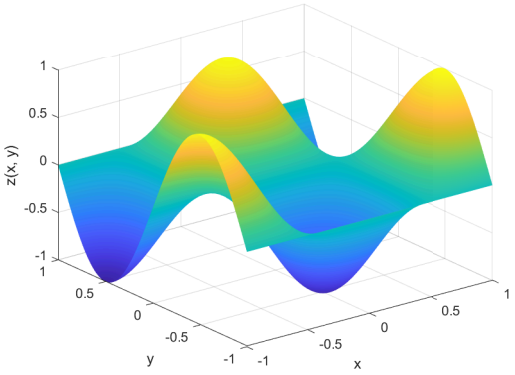

Figure 4.15: Plot of the original source $z_2(x, y)$ defined in (4.20).

Evaluating this for $(x, y) \in \partial\Omega$ leads to the Dirichlet datum, which is not zero on the whole boundary $\partial\Omega$. Moreover, the Neumann datum can be computed as

$$f_{\kappa_i,2}(x, y) = \frac{\pi}{\kappa_i^2 - 2\pi^2} \begin{pmatrix} -\sin(\pi x)\sin(\pi y) \\ \cos(\pi x)\cos(\pi y) \end{pmatrix} \cdot \underline{n} \quad \text{for } (x, y) \in \partial\Omega.$$

Hence, the main difference from the first example is that the normal derivatives of our basis functions are required, since in the reciprocity gap functional

$$R(v) = \int_{\partial\Omega} (f\gamma_0 v - g\gamma_1 v)\, \mathrm{ds}_x, \qquad \forall v \in \mathcal{H}^1_{\Delta+\kappa^2}(\Omega),$$

the Dirichlet datum g is non–vanishing.
For the reconstructions of the source z_2 shown in Figures 4.16–4.18 we choose the wave numbers $\kappa = [1.5, 3.5, 5.5, 7.5]$ in the test space and $\lambda = [2, 4, 6, 8]$ in the ansatz space. The number of directions is changing throughout the figures in both spaces. For $n = 10$ directions in the test space and $m = 5$ directions in the ansatz space the L–curve and the corresponding reconstruction are shown in Figure 4.16. The obtained regularisation parameter is $\mu = 3.18e - 01$. The reconstruction plot hardly has similarities with the original source z_2. One can argument, that at least the symmetry is reconstructed.

For the reconstruction shown in Figure 4.17, the number of directions is increased to $n = 17$ in the test space and $m = 13$ in the ansatz space. We obtain the regularisation parameter $\mu = 3.03e - 04$. The reconstruction of the source z_2 is quite accurate with visible differences near the boundary of the domain $(-1, 1)^2$.

Increasing the parameters further to $n = 30$ directions in the test space and $m = 20$ directions in the ansatz space leads to a reconstruction, where no difference to the original source z_2 is visible. Hence, the shape as well as the values on the boundary are recovered well, as illustrated in Figure 4.18. The corresponding regularisation parameter is $\mu = 2.15e - 07$.

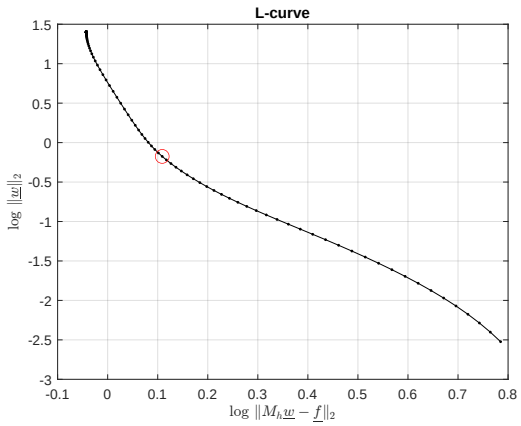

(a) L–curve

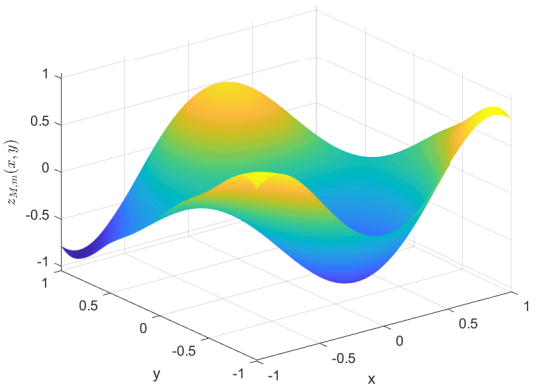

(b) Reconstruction of $z_2(x, y)$ with regularisation parameter $\mu = 3.18e - 01$

Figure 4.16: Reconstruction results for $\kappa = [1.5, 3.5, 5.5, 7.5]$ and $n = 10$ in the test space and $\lambda = [2, 4, 6, 8]$ and $m = 5$ in the ansatz space.

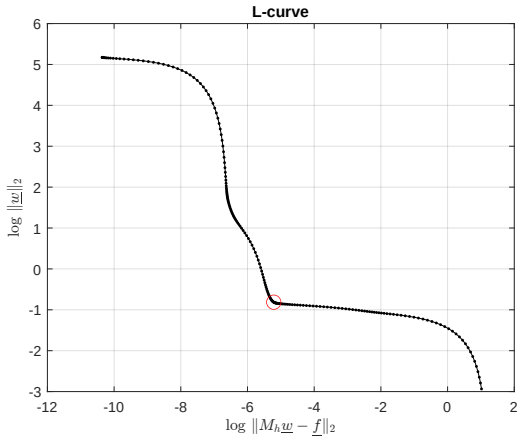

(a) L–curve

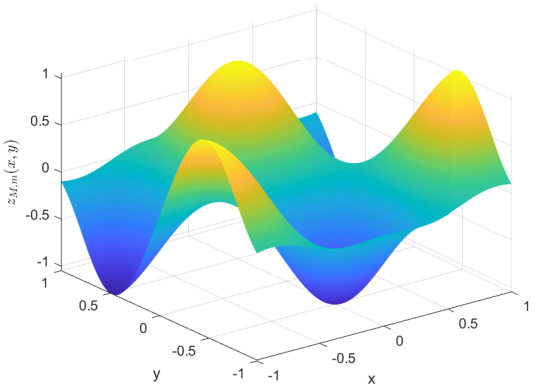

(b) Reconstruction of $z_2(x, y)$ with regularisation parameter $\mu = 3.03e - 04$

Figure 4.17: Reconstruction results for $\kappa = [1.5, 3.5, 5.5, 7.5]$ and $n = 17$ in the test space and $\lambda = [2, 4, 6, 8]$ and $m = 13$ in the ansatz space.

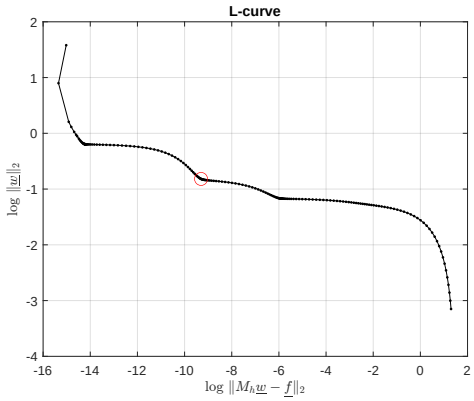

(a) L–curve

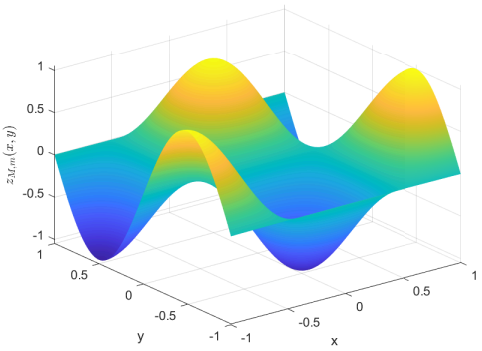

(b) Reconstruction of $z_2(x, y)$ with regularisation parameter $\mu = 2.15e-07$

Figure 4.18: Reconstruction results for $\kappa = [1.5, 3.5, 5.5, 7.5]$ and $n = 30$ in the test space and $\lambda = [2, 4, 6, 8]$ and $m = 20$ in the ansatz space.

Error analysis in dependency of the discretisation parameters

Now we will focus on the behaviour of the L^2–error as a function of the parameters defining the basis functions in the ansatz and test space. In Table 4.10 the reconstruction error $\|z_2 - z_{M,m}\|_{L^2((-1,1)^2)}$ is presented in dependency of the number of used wave numbers $N = M$. The number of directions is fixed in both spaces at $n = m = 15$. The wave numbers in the test space are chosen as $\kappa = [1.5, 3.5, 5.5, 7.5, 9.5, 11.5]$, while in the ansatz space we use $\lambda = [2, 4, 6, 8, 10, 12]$. We observe from Table 4.10 a different behaviour than in the first example shown in Table 4.5, because the error does not decrease if we increase the number of wave numbers beyond $N = M = 3$. This suggests that for this setting using more than 3 wave numbers in both spaces does not lead to a further improvement of the reconstruction accuracy.

Table 4.10: L^2–error $\|z_2 - z_{M,m}\|_{L^2((-1,1)^2)}$ for different values of wave numbers $N = M$ in test and ansatz space using $n = m = 15$ directions. Furthermore, the regularisation parameter obtained from the L–curve is given.

m	M	n	N	$\|z_2 - z_{M,m}\|_{L^2((-1,1)^2)}$	μ
15	2	15	2	7.28e-02	2.86e-05
15	3	15	3	1.68e-02	2.37e-08
15	4	15	4	2.12e-02	1.76e-07
15	5	15	5	4.58e-02	9.65e-06

In the next step we investigate the reconstruction error $\|z_2 - z_{M,m}\|_{L^2((-1,1)^2)}$ when the only free parameter is the number of used wave numbers N in the test space. Two examples are considered, where the number of directions is fixed at $n = m = 15$. In the

first example we use $M = 2$ with $\lambda = [2, 4]$ and in the second example we set $M = 3$ with $\lambda = [2, 4, 6]$. The results of both numerical tests are presented in Table 4.11. For $M = 2$, increasing the number of wave numbers N in the test space leads to an error reduction. For $M = 3$, the error is not strictly decreasing, as it can be seen in the step from $N = 4$ to $N = 5$. Furthermore, comparing the results for $M = 2$ and $M = 3$ we observe that increasing the number of wave numbers in the ansatz space leads to a significant reduction of the L^2–error.

Table 4.11: L^2–error $\|z_2 - z_{M,m}\|_{L^2((-1,1)^2)}$ for different values of wave numbers N in the test space. It is considered for $M = 2$ and $M = 3$ with $n = m = 15$ directions. The optimal regularisation parameter μ is also given.

M	N	$\|z_2 - z_M\|_{L^2((-1,1)^2)}$	μ	M	N	$\|z_2 - z_{M,m}\|_{L^2((-1,1)^2)}$	μ
2	2	7.28e-02	2.86e-05	–	–	–	–
2	3	6.50e-02	6.27e-07	3	3	1.68e-02	2.37e-08
2	4	5.07e-02	6.32e-04	3	4	1.15e-02	6.64e-09
2	5	4.78e-02	1.09e-03	3	5	1.31e-02	5.58e-06
2	6	4.65e-02	1.57e-03	3	6	8.95e-03	9.64e-06

In the following example we analyse how the L^2–error depends on the choice of different test spaces, by varying N and n. The ansatz space is fixed with $m = 10$ directions and the wave numbers $\lambda = [2, 4, 6]$, which means $M = 3$. We note that in Table 4.12 cases with $N \leq 2$ are not presented, since they do not yield a meaningful L–curve. The observed behaviour is identical to the results presented in Table 4.7. For fixed N, increasing n does not influence the error significantly. Furthermore, for comparable n, increasing the number of wave numbers N leaves the L^2–error essentially unchanged.

Table 4.12: L^2–error $\|z_2 - z_{M,m}\|_{L^2((-1,1)^2)}$ for different combinations of used wave numbers N and directions n in the test space. The ansatz space is fixed with $\lambda = [2, 4, 6]$ and $m = 10$. Furthermore, the regularisation parameter from the L–curve is given.

m	M	n	N	$\|z_2 - z_{M,m}\|_{L^2((-1,1)^2)}$	μ
10	3	10	3	2.65e-01	3.20e-04
10	3	15	3	2.90e-01	1.35e+00
10	3	20	3	2.90e-01	1.73e+00
10	3	10	4	2.77e-01	2.32e-01
10	3	15	4	2.64e-01	7.89e-01
10	3	10	5	2.72e-01	8.05e-01
10	3	12	5	2.66e-01	1.12e+00
10	3	10	6	2.72e-01	8.05e-01

In the second example we fix the ansatz space by $\lambda = [2, 4, 6, 8]$ and $m = 15$ directions. Table 4.13 demonstrates that for fixed N increasing the number of directions n reduces the error.

Table 4.13: L^2–error $\|z_2 - z_{M,m}\|_{L^2((-1,1)^2)}$ for different combinations of used wave numbers N and directions n in the test space. The ansatz space is fixed with $\lambda = [2, 4, 6, 8]$ and $m = 15$. Furthermore, the regularisation parameter from the L–curve is given.

m	M	n	N	$\|z_2 - z_{M,m}\|_{L^2((-1,1)^2)}$	μ
15	4	15	4	2.12e-02	1.76e-07
15	4	20	4	1.11e-02	4.93e-07
15	4	25	4	8.54e-03	1.64e-06
15	4	15	5	4.58e-02	9.65e-06
15	4	20	5	7.62e-03	5.82e-05
15	4	25	5	6.02e-03	1.15e-04
15	4	15	6	2.77e-02	5.29e-04
15	4	20	6	4.88e-03	7.59e-04
15	4	25	6	4.56e-03	1.05e-03

Reconstruction of z_2 from noisy boundary data

Subsequently, we consider the reconstruction of the source z_2 from noisy boundary data. We again employ noisy boundary data generated in the same way as for the source z_1. Hence, it is computed as the maximum of the absolute value of the corresponding boundary data multiplied with a uniformly distributed random vector. It is then scaled by the noise level, which is given in %. We use the same setting as in Figure 4.16. Therefore, we are using the wave numbers $\kappa = [1.5, 3.5, 5.5, 7.5]$ in the test space and $\lambda = [2, 4, 6, 8]$ in the ansatz space as well as $n = 10$ and $m = 5$ directions in the corresponding spaces. The noise level for this example is 1%. In Figure 4.19 the reconstruction is very similar to the noise free example in Figure 4.16, obtained using the same test and ansatz space. However, compared to the original source z_2 it is not accurate at all.
Now, we investigate the L^2–error as a function of the noise level. In Table 4.14 we consider the same settings as in the reconstructions shown in Figures 4.16–4.18. Each test is repeated 25 times for each noise level and the mean value of the resulting L^2–errors is presented. Table 4.14 demonstrates that for fixed discretisation parameters, the L^2–error increases as the noise level grows. In the next step we are interested in the behaviour of the L^2–error $\|z_2 - z_{M,m}\|_{L^2((-1,1)^2)}$ in dependency of the noise level given in %. We have made 100 repetitions for each noise level and then computed the mean value of the L^2–errors. This is presented in Figure 4.20, where $\kappa = [1.5, 3.5, 5.5, 7.5]$ and $\lambda = [2, 4, 6, 8]$ with each 15 directions are used.

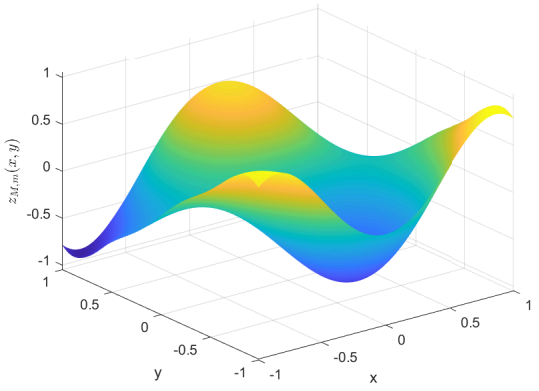

Figure 4.19: Plot of the reconstruction of $z_2(x, y)$ for $\kappa = [1.5, 3.5, 5.5, 7.5]$ and $n = 10$ in the test space and $\lambda = [2, 4, 6, 8]$ and $m = 5$ in the ansatz space. The noise level is 1%. The regularisation parameter obtained from the L–curve is $\mu = 3.18e - 01$.

Table 4.14: L^2–error $\|z_2 - z_{M,m}\|_{L^2((-1,1)^2)}$ for different values of noise level δ in %. The ansatz space is equipped with $M = 4$, and the test space with $N = 4$. The parameters m and n are varying.

m	M	n	N	δ	$\|z_2 - z_{M,m}\|_{L^2((-1,1)^2)}$
5	4	10	4	0	4.88e-01
5	4	10	4	1	5.36e-01
5	4	10	4	5	5.36e-01
5	4	10	4	10	5.37e-01
13	4	17	4	0	4.64e-02
13	4	17	4	1	4.76e-02
13	4	17	4	5	5.45e-02
13	4	17	4	10	6.23e-02
20	4	30	4	0	5.85e-03
20	4	30	4	1	3.74e-02
20	4	30	4	5	4.34e-02
20	4	30	4	10	4.65e-02

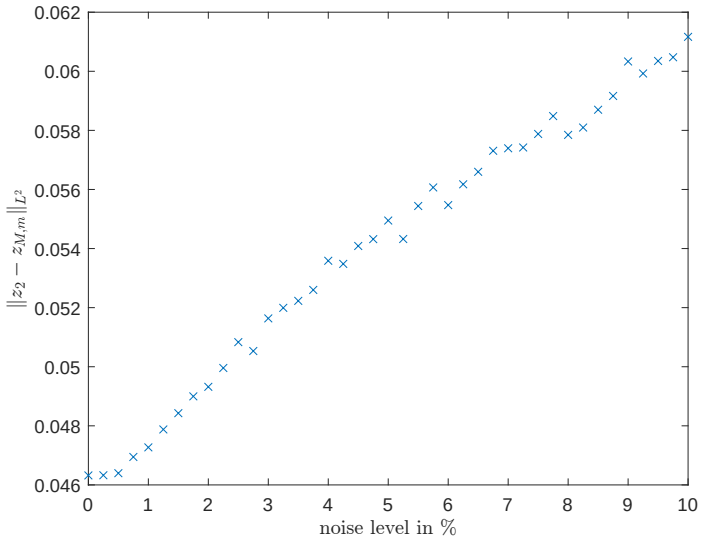

Figure 4.20: Plot of the error $\|z_2 - z_{M,m}\|_{L^2((-1,1)^2)}$ in dependency of the noise level in % using $\kappa = [1.5, 3.5, 5.5, 7.5]$, $\lambda = [2, 4, 6, 8]$, $n = 17$ and $m = 13$. The regularisation parameter is obtained by the L– curve.

As expected, the plot indicates that the L^2–error grows with increasing noise level. Furthermore, we obtain a linear dependency between the L^2–error and the noise level in %.

Alternative discretisation approach

In this section we consider an alternative discretisation approach, as the use of plane waves has undesirable properties. As discussed by Gittelson et al. [13] in the context of plane wave discontinuous Galerkin methods for solving the forward Helmholtz problem, the plane wave basis becomes unstable for small wave numbers. Moreover, plane waves may become nearly linearly dependent if their directions are collinear. As a consequence, Gittelson et al. introduce an alternative basis, which remains stable for small wave numbers. An additional advantage of this basis is, that its elements are orthogonal for a fixed wave number. This basis will be used in the following instead of the plane wave basis.
We recall the continuous variational formulation (4.12): find $z \in L^2(\Omega)$ such that

$$\int_\Omega zv \,\mathrm{d}x = \int_{\partial\Omega} (f\gamma_0 v - g\gamma_1 v) \,\mathrm{d}s_x =: R(v) \qquad \forall v \in \mathcal{H}^1_{\Delta+\kappa^2}(\Omega).$$

In order to discretise this variational formulation we introduce a suitable test and ansatz space. Therefore, we use the stable basis functions from [13], which are defined

in polar coordinates (r, θ) by

$$\psi_1 = J_0(\kappa r) \text{ and } \psi_j = \begin{cases} \kappa^{-\frac{j}{2}} \Re \left[J_{\frac{j}{2}}(\kappa r) \exp(\mathrm{i}\tfrac{j}{2}\theta) \right] & \text{for even } j, \\ \kappa^{-\frac{j-1}{2}} \Im \left[J_{\frac{j-1}{2}}(\kappa r) \exp(\mathrm{i}\tfrac{j-1}{2}\theta) \right] & \text{for odd } j \neq 1, \end{cases} \tag{4.21}$$

where J_k is the Bessel function of order k. One can show, that these basis functions belong to $H^1(\Omega)$ and solve the homogeneous Helmholtz equation. Hence, it holds that $\psi_j \in \mathcal{H}^1_{\Delta+\kappa^2}(\Omega)$ for every $j \in \mathbb{N}$. In Figure 4.21 the first four basis functions for the wave number $\kappa = 5.5$ on the domain $(-1, 1)^2$ are illustrated.

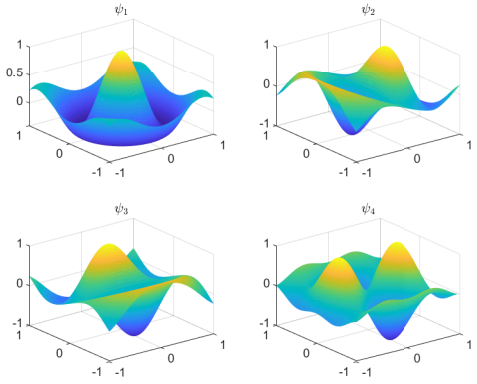

Figure 4.21: Plot of the first four basis functions as defined in (4.21) with $\kappa = 5.5$ on the domain $(-1, 1)^2$.

Since we allow the use of multiple wave numbers, we define the test space as

$$\widetilde{Y}_{N,n} = \operatorname{span}\{\psi_j^{\kappa_i}(x)\} \subset \mathcal{H}^1_{\Delta+\kappa_i^2}(\Omega), \quad \text{for } i = 1, ..., N, \text{ and } j = 1, ..., n,$$

where $\kappa_i \in I$. Analogously, the ansatz space is given by

$$\widetilde{X}_{M,m} = \operatorname{span}\{\psi_k^{\lambda_\ell}(x)\} \subset \mathcal{H}^1_{\Delta+\lambda_\ell^2}(\Omega) \subset L^2(\Omega), \quad \text{for } \ell = 1, ..., M, \text{ and } k = 1, ..., m,$$

with $\lambda_\ell \in I$ and $\lambda_\ell \neq \kappa_i$. It is crucial that the test space $\widetilde{Y}_{N,n}$ uses the wave numbers κ_i from the original problem as the basis functions must belong to the corresponding spaces $\mathcal{H}^1_{\Delta+\kappa_i^2}(\Omega)$. In contrast, the ansatz space has to be equipped with different wave numbers. If identical wave numbers are used in both spaces, the system matrix would consist of blocks built from basis functions satisfying the same Helmholtz equation. This would cause certain blocks to become nearly redundant, which may produce linear dependencies in the system matrix. The remaining derivation is analogous to the plane wave approach. Thus, we only state the relevant results. The discrete version of our source z in the ansatz space $\widetilde{X}_{M,m}$ is given by

$$\tilde{z}_{M,m}(x) = \sum_{\ell=1}^{M} \sum_{k=1}^{m} \tilde{z}_{k,\ell} \psi_k^{\lambda_\ell}(x).$$

Table 4.15: Condition numbers of the matrix A_h for a single wave number and varying parameters n and m. Here, κ and λ denote the wave number in the test and ansatz space, respectively.

m	λ	n	κ	cond(A_h)
5	1.5	5	1.5	2.42e+02
10	1.5	10	1.5	2.10e+07
15	1.5	15	1.5	3.76e+11
5	1e-04	5	1e-04	3.60e+02
10	1e-04	10	1e-04	3.53e+07
15	1e-04	15	1e-04	6.62e+11
5	1e-10	5	1e-10	3.60e+02
10	1e-10	10	1e-10	3.53e+07
15	1e-10	15	1e-10	6.62e+11

Plugging the discrete representation of our source into (4.12) leads to the discrete variational formulation: find $\tilde{z}_{M,m} \in \widetilde{X}_{M,m}$ such that

$$\int_\Omega \tilde{z}_{M,m}(x)\psi_j^{\kappa_i}(x)\,\mathrm{d}x = R(\psi_j^{\kappa_i}) \qquad \forall \psi_j^{\kappa_i} \in \widetilde{Y}_{N,n}.$$

Solving the discrete variational formulation is equivalent to solving the system of linear equations

$$A_h \underline{\tilde{z}} = \underline{\tilde{f}},$$

where $A_h \in \mathbb{R}^{nN \times mM}$ has the same block structure as the matrix defined in (4.17). One block of the matrix is defined by

$$A_{\kappa_i,\lambda_\ell}[j,k] = \int_\Omega \psi_j^{\kappa_i}(x)\psi_k^{\lambda_\ell}(x)\,\mathrm{d}x,$$

for $j = 1, ..., n$ and $k = 1, ..., m$. The vector of the right hand side has the same structure as the one in (4.18). The entries of the right hand side are given by

$$\underline{\tilde{f}}_{\kappa_i}[j] = R(\psi_j^{\kappa_i}),$$

for $j = 1, ..., n$. We first investigate the condition number of A_h for a single wave number in the test and ansatz space, denoted by κ and λ, respectively, for varying numbers of basis functions n and m. The results are presented in Table 4.15. It is evident that the condition number increases rapidly if the number of basis functions $n = m$ exceeds 5. For $n = m \leq 5$, the matrix A_h is well–conditioned for all wave numbers and a diagonal matrix. However, for larger $n = m$, this behaviour changes as some off–diagonal entries in A_h become comparable in magnitude to the diagonal

entries. Hence, A_h is no longer diagonal. One contributing factor for the high condition number is that the basis functions are not normalised. However, normalising them leads to a failed reconstruction, for reasons that are currently unclear.
In the next step we investigate the condition number as well as the extremal singular values of A_h, denoted by $\sigma_{\min}$ and $\sigma_{\max}$, for several wave numbers. This analysis is carried out for different choices of the parameters N, n, M and m. The corresponding results are presented in Table 4.16, where we employ the wave numbers $\kappa = [1.5, 3.5, 5.5, 7.5, 9.5]$ in the test space and $\lambda = [2, 4, 6, 8, 10]$ in the ansatz space. We note that, in each experiment, the first N, respectively M entries of these sets are used. Moreover, we compare the condition numbers with those obtained from the approach using plane waves, where the system matrix is denoted by M_h. Thus, the number of directions in the plane wave approach and the number of basis functions per wave number in the alternative approach are denoted by n and m, respectively, in the corresponding spaces. Taking the same values of n, respectively m, makes the two approaches comparable. Table 4.16 demonstrates that the condition number of the

Table 4.16: Comparison of the condition numbers obtained from the original approach using the matrix M_h and the alternative approach using the matrix A_h with varying parameters N, n, M and m. Moreover, the maximal and minimal singular value of A_h are given.

m	M	n	N	$\text{cond}(M_h)$	$\text{cond}(A_h)$	$\sigma_{\max}(A_h)$	$\sigma_{\min}(A_h)$
5	2	5	2	6.39e+01	1.21e+04	1.54e+00	1.28e-04
10	2	10	2	7.92e+05	3.34e+09	1.54e+00	4.61e-10
15	2	15	2	3.80e+08	9.92e+13	1.54e+00	1.55e-14
10	3	10	3	1.50e+07	1.81e+11	1.54e+00	8.52e-12
15	3	15	3	1.05e+11	1.16e+16	1.54e+00	1.33e-16
20	3	20	3	5.65e+15	1.63e+22	1.54e+00	9.47e-23
5	4	5	4	3.66e+02	1.41e+06	1.54e+00	1.09e-06
10	4	10	4	1.56e+08	4.34e+12	1.54e+00	3.56e-13
15	4	15	4	4.19e+11	5.71e+17	1.54e+00	2.71e-18
10	5	10	5	1.21e+09	6.15e+13	1.54e+00	2.51e-14
15	5	15	5	1.09e+12	1.89e+19	1.54e+00	8.17e-20
20	5	20	5	8.24e+15	6.85e+24	1.54e+00	2.25e-25

matrix A_h using the basis from (4.21) is significantly larger than the condition number of the matrix M_h obtained with plane waves. This is an interesting observation, as it was mentioned in [13] that the basis from (4.21) is more stable than the plane wave basis for solving forward problems. However, Table 4.16 indicates that using the basis defined in (4.21) leads to a higher condition number of the system matrix. Thus, this basis does not lead to better stability than the basis of plane waves for inverse problems of the Helmholtz equation at all.

Since the matrix A_h is in general not a square matrix and ill–conditioned, we consider the regularised least–squares problem. Therefore, we introduce a regularisation parameter μ and solve the system

$$\left(\mu I + A_h^T A_h\right) \underline{\tilde{z}} = A_h^T \underline{\tilde{f}},$$

where I denotes the identity matrix.

Numerical example

We consider the same source as in the first numerical example of the plane wave approach, given by

$$z_1(x, y) = \sin(\pi x) \sin(\pi y).$$

The corresponding boundary data are $g_{\kappa_i,1} = 0$ and

$$f_{\kappa_i,1}(x, y) = \frac{\pi}{\kappa_i^2 - 2\pi^2} \begin{pmatrix} \cos(\pi x) \sin(\pi y) \\ \sin(\pi x) \cos(\pi y) \end{pmatrix} \cdot \underline{n} \quad \text{for } (x, y) \in \partial\Omega.$$

As we are familiar with the L–curve, which has been briefly explained in the method using plane waves, we apply this, to select the optimal regularisation parameter μ. For two different choices of parameters the plot of the L–curve is illustrated in Figure 4.22. However, we observe, that the plots do not yield a meaningful L–curve.

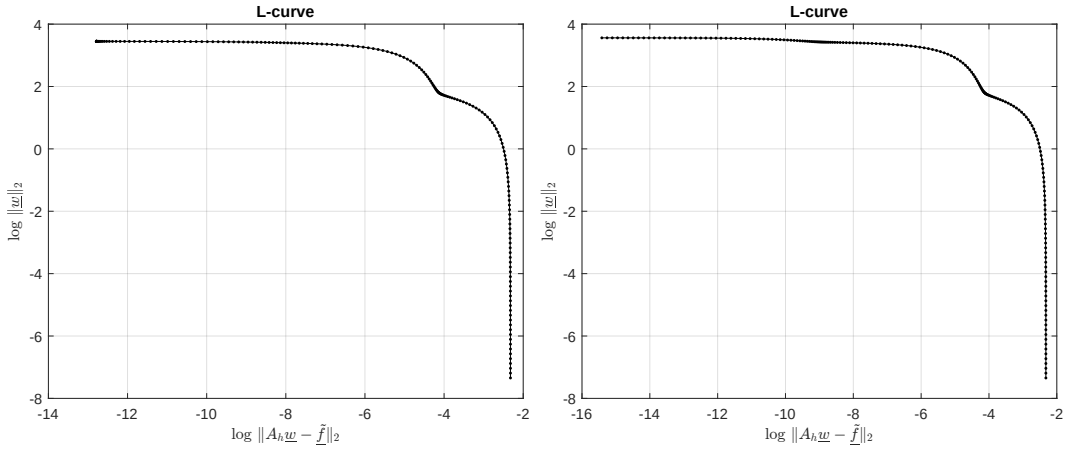

(a) $\kappa = [1.5, 3.5, 5.5]$, $n = 20$, $\lambda = [2, 4, 6]$, $m = 15$

(b) $\kappa = [1.5, 3.5, 5.5, 7.5]$, $n = 10$, $\lambda = [2, 4, 6, 8]$, $m = 5$

Figure 4.22: Failure of the L–curve plot using varying parameters N, n, M and m and the basis from (4.21).

This indicates that choosing the regularisation parameter with the L–curve criterion fails for the discretisation using the basis functions in (4.21). In particular, although

the basis is a good choice using a single wave number, it does not improve the stability when multiple wave numbers are used. While this basis is known to be stable for forward problems, numerical experiments show that it leads to significantly worse condition numbers in the setting of several wave numbers. Consequently, the alternative discretisation does not lead to an advantage compared with the plane wave approach for inverse Helmholtz problems using multiple wave numbers.

5 Conclusions and outlook

In this thesis, we studied the inverse problem of the Helmholtz equation to reconstruct the source term from boundary data measurements, at both a single wave number and multiple wave numbers, in a bounded Lipschitz domain. In general, it is not possible to reconstruct the source of an inverse problem from a single pair of Cauchy data uniquely. Hence, the aim was to provide an overview of uniqueness results for different types of sources at a single wave number as well as at multiple wave numbers. In order to gain deeper insights into source reconstruction it was crucial to discuss unique solvability of the Dirichlet and Neumann boundary value problem for the Helmholtz equation as well as the boundary value problem for a Bi–Helmholtz–type equation first. Afterwards, we proved uniqueness results for the inverse problem at a single wave number under the condition that the source is a linear combination of point sources. However, for Dirac distributions supported on spheres and for characteristic functions on hollow or solid balls in $\mathbb{R}^3$ the source can not be determined uniquely, as we obtained an expression including the radius of the domain and the intensity of the source. To prove these results we applied the reciprocity gap functional and the mean value theorem for the Helmholtz equation. For more general source terms we considered another approach by introducing two operators, mapping the source onto the Neumann datum and the Dirichlet datum, respectively. Analysing the mapping properties, especially their kernels, orthogonal complements and ranges, led to uniqueness results but with restrictions on the Cauchy data. Furthermore, we discovered that without additional assumptions only the harmonic part of the source can be recovered uniquely. Using a Bi–Helmholtz–type equation and assuming that the source z satisfies $(\Delta - \kappa^2)z = F$ for $F \in L^2(\Omega)$ results in uniqueness of the inverse problem in a subspace of $L^2(\Omega)$ without restrictions on the boundary data. In contrast, when the boundary data are known for multiple wave numbers, the inverse problem is uniquely solvable in the L^2–sense.

From a numerical point of view, we implemented an algebraic method to reconstruct point sources from the Cauchy data at a single wave number. This approach reconstructed the source accurately for small wave numbers, since the accuracy of this method depends on the number of observation points per wavelength. Moreover, we discussed a method to reconstruct $L^2(\Omega)$–sources from the boundary data at several wave numbers. This method is based on the reciprocity gap functional and on solving a discrete variational formulation. The numerical examples demonstrated that $L^2(\Omega)$–sources are reconstructed accurately when using a Tikhonov regularisation and the L–curve criterion to select the optimal regularisation parameter. Moreover, the

method also reconstructs the sources accurately if noisy boundary data are used. Since regularisation was introduced only on the discrete level in this work, an important direction for future work is the incorporation of regularisation already on the continuous level. In this setting, the optimality system can be derived by formulating the regularised continuous optimisation problem and computing its first–order optimality condition using variational methods. The derivation is briefly outlined below. Being consistent with the operator framework in (4.13), and applying Tikhonov regularisation with a regularisation parameter $\mu > 0$ on the continuous level leads to the following optimisation problem: find $z \in L^2(\Omega)$ minimising the functional

$$J(w) := \frac{1}{2}\|Aw - R\|^2_{Y_\kappa'} + \frac{\mu}{2}\|w\|^2_{L^2(\Omega)}, \quad \text{for } w \in L^2(\Omega),$$

where $R \in Y_\kappa'$ denotes the reciprocity gap functional. Introducing the Riesz–operator $R_{Y_\kappa} : Y_\kappa' \to Y_\kappa$ and its inverse $R^{-1}_{Y_\kappa} : Y_\kappa \to Y_\kappa'$ leads to the equality

$$\|Aw - R\|^2_{Y_\kappa'} = \|R_{Y_\kappa}(Aw - R)\|^2_{Y_\kappa}.$$

The first–order optimality condition is then

$$0 = \delta J(z; v) = (R_{Y_\kappa} Az, R_{Y_\kappa} Av)_{Y_\kappa} - (R_{Y_\kappa} Av, R_{Y_\kappa} R)_{Y_\kappa} + \mu(z, v)_{L^2(\Omega)}, \quad \forall v \in L^2(\Omega),$$

or equivalently

$$\langle Az, R_{Y_\kappa} Av\rangle_{Y_\kappa' \times Y_\kappa} + \mu(z, v)_{L^2(\Omega)} = \langle R, R_{Y_\kappa} Av\rangle_{Y_\kappa' \times Y_\kappa}, \quad \forall v \in L^2(\Omega).$$

Defining $p := R_{Y_\kappa}(R - Az) \in Y_\kappa$ the previous equation is equivalent to the system

$$\begin{aligned} (p, q)_{Y_\kappa} + \langle Az, q\rangle_{Y_\kappa' \times Y_\kappa} &= \langle R, q\rangle_{Y_\kappa' \times Y_\kappa}, && \forall q \in Y_\kappa, \\ \langle Av, p\rangle_{Y_\kappa' \times Y_\kappa} - \mu(v, z)_{L^2(\Omega)} &= 0, && \forall v \in L^2(\Omega). \end{aligned}$$

Hence, the resulting system to be solved is: find $(p, z) \in Y_\kappa \times L^2(\Omega)$ such that

$$\begin{aligned} (\nabla p, \nabla q)_{L^2(\Omega)} + (p, q)_{L^2(\Omega)} + (z, q)_{L^2(\Omega)} &= \langle R, q\rangle_{Y_\kappa' \times Y_\kappa}, && \forall q \in Y_\kappa, \\ (p, v)_{L^2(\Omega)} - \mu(z, v)_{L^2(\Omega)} &= 0, && \forall v \in L^2(\Omega), \end{aligned}$$

which can then be discretised and analysed in future work. Further directions for future research include the derivation of error estimates for the source reconstruction at multiple wave numbers, the consideration of more complex domains for the numerical reconstruction and the analysis of the inverse problem for the time dependent wave equation instead of the Helmholtz equation.

Bibliography

[1] R. A. Adams. *Sobolev Spaces*. Pure and Applied Mathematics. Academic Press, New York, 1975.

[2] C. J. S. Alves, M. J. Colaco, V. M. A. Leitão, N. F. M. Martins, H. R. B. Orlande, and N. C. Roberty. Recovering the source term in a linear diffusion problem by the method of fundamental solutions. *Inverse Problems in Science and Engineering*, 16(8):1005–1021, 2008.

[3] C. J. S. Alves, N. F. M. Martins, and N. C. Roberty. Full identification of acoustic sources with multiple frequencies and boundary measurements. *Inverse Problems and Imaging*, 3(2):275–294, 2009.

[4] J. Bak and D. J. Newman. *Complex analysis*. Springer, New York, 3 edition, 2010.

[5] J. Behrndt, F. Gesztesy, and M. Mitrea. Sharp boundary trace theory and schrödinger operators on bounded lipschitz domains. 307(1550), 2025.

[6] J. Behrndt and T. Micheler. Elliptic differential operators on Lipschitz domains and abstract boundary value problems. *Journal of Functional Analysis*, 267(10):3657–3709, 2014.

[7] X. Chen and R. Womersley. Spherical t-design with $d = (t + 1)^2$ points. `http://www.polyu.edu.hk/ama/staff/xjchen/sphdesigns.html`, 2004. Accessed: 24.09.2025.

[8] D. Colton and R. Kress. *Inverse Acoustic and Electromagnetic Scattering Theory*. Springer, New York, 3 edition, 2013.

[9] A. El Badia and T. Ha-Duong. Some remarks on the problem of source identification from boundary measurements. *Inverse Problems*, 14(4):883, 1998.

[10] A. El Badia and T. Ha-Duong. An inverse source problem in potential analysis. *Inverse Problems*, 16(3):651, 2000.

[11] A. El Badia and T. Nara. An inverse source problem for Helmholtz's equation from the Cauchy data with a single wave number. *Inverse Problems*, 27(10):105001, 2011. `doi:10.1088/0266-5611/27/10/105001`.

[12] I. M. Gelfand and N. Y. Vilenkin. *Generalized Functions, Vol. 4: Applications of Harmonic Analysis*. Academic Press, New York London, 1964.

[13] C. J. Gittelson, R. Hiptmair, and I. Perugia. Plane wave discontinuous galerkin methods: Analysis of the h-version. *ESAIM: Mathematical Modelling and Numerical Analysis*, 43(2):297–331, 2009.

[14] P. Grisvard. *Elliptic Problems in Nonsmooth Domains*. SIAM, 2011.

[15] P. C. Hansen and D. P. O'Leary. The use of the l-curve in the regularization of discrete ill-posed problems. *SIAM*, 14(6):1487–1503, 1993.

[16] L. Hörmander. *Linear Partial Differential Operators*. Springer, 1963.

[17] V. Isakov. *Inverse Problems for Partial Differential Equations*. Applied Mathematical Sciences. Springer, New York, 2 edition, 1998.

[18] J. Kemetmüller. Git Repository. `https://github.com/knedlsepp`, 2013. Accessed: 13.10.2025.

[19] N. Kuznetsov. Mean value properties of solutions to the helmholtz and modified helmholtz equations. *Journal of Mathematical Sciences*, 257(5):673–683, 2021.

[20] R. E. Langer. An inverse problem in differential equations. *Bulletin of the American Mathematical Society*, 39(10):814–820, 1933.

[21] S. Larsson and V. Thomée. *Partial Differential Equations with Numerical Methods*. Springer, Berlin Heidelberg, 2003.

[22] W. McLean. *Strongly Elliptic Systems and Boundary Integral Equations*. Cambridge University Press, 2000.

[23] OpenAI. Chatgpt. `https://chatgpt.com`, 2025. Accessed: 30.11.2025.

[24] R. P. Porter and A. J. Devaney. Holography and the inverse source problem. *Optical Society of America*, 72(3):327–330, 1982. `doi:10.1364/JOSA.72.000327`.

[25] M. Reed and B. Simon. *Methods of modern mathematical physics, Vol. 1: Functional analysis*. Academic Press, San Diego, 1980.

[26] O. Steinbach. *Numerical approximation methods for elliptic boundary value problems*. Springer, New York, 2008.

[27] H. Weber. Über einige bestimmte Integrale. *Journal für die reine und angewandte Mathematik*, 1868(69):222–237, 1868. `doi:10.1515/crll.1868.69.222`.

[28] D. Werner. *Funktionalanalysis*. Springer, Berlin Heidelberg, 7 edition, 2011.